

## ABSTRACT

Title of Document: NANOSTRUCTURE INVESTIGATION OF  
POLYMER SOLUTIONS, POLYMER GELS,  
AND POLYMER THIN FILMS

Wonjoo Lee, Doctor of Philosophy, 2009

Directed By: Professor, Robert M. Briber, Materials Science  
and Engineering

This thesis discusses two systems. One is structured hydrogels which are hydrogel systems based on crosslinked poly((2-dimethylamino)ethyl methacrylate) (PDMAEMA) containing micelles which form nanoscale pores within the PDMAEMA hydrogel. The other is nanoporous block copolymer thin films where solvent selectivity is exploited to create nanopores in PS-b-P4VP thin films. Both of these are multicomponent polymer systems which have nanoscale porous structures.

1. Small angle neutron scattering of micellization of anionic surfactants in water, polymer solutions and hydrogels

Nanoporous materials have been broadly investigated due to the potential for a wide range of applications, including nano-reactors, low-K materials, and membranes. Among those, molecularly imprinted polymers (MIP) have attracted a large amount of interest because these materials resemble the “lock and key” paradigm of enzymes.

MIPs are created by crosslinking either polymers or monomers in the presence of template molecules, usually in water. Initially, functional groups on the polymer or the monomer are bound either covalently or noncovalently to the template, and crosslinking results in a highly crosslinked hydrogel. The MIPs containing templates are immersed in a solvent (usually water), and the large difference in the osmotic pressure between the hydrogel and solvent removes the template molecules from the MIP, leaving pores in the polymer network containing functionalized groups. A broad range of different templates have been used ranging from molecules to nanoscale structures including stereoisomers, virus, and micelles. When micelles are used as templates, the size and shape before and after crosslinking is an important variable as micelles are thermodynamic objects whose structure depends on the surfactant concentration of the solution, temperature, electrolyte concentration and polymer concentration. In our research, the first goal is to understand the micellization of anionic surfactants in polymer solutions and the corresponding hydrogels using small angle neutron scattering (SANS). SANS has been widely used to investigate structures ranging from sub-nanometer to sub-micrometer. Since the scattering lengths of H and D atoms are quite different, the scattering contrast can be enhanced (and varied) through isotopic labeling. It is possible to investigate the structure of micelles in polymer solutions and hydrogels using H/D contrast matching methods with SANS. For this aim, water-soluble and chemically crosslinkable poly((2-dimethylamino)ethyl methacrylate) (PDMAEMA) was synthesized using group transfer polymerization. In order to control the size and shape of micelles, the degree of quaternization of the polymer was also controlled through the reaction of

PDMAEMA with methyl iodide. The micellization of deuterated sodium dodecylsulfate (d-SDS) in (quaternized) PDMAEMA solutions and the corresponding hydrogels was then observed using SANS and the size and shape of d-SDS micelles was obtained by modeling.

## 2. Nanopatterning using block copolymer/homopolymer blends

Block copolymers are well-known to self-assemble into meso- and nano-scale structures. The use of block copolymers for nanostructured patterns has attracted increasing attention due to their potential use as templates and scaffolds for the fabrication of functional nanostructures. In order to realize the potential of these materials, it is necessary to be able to control the orientation of the nanoscale pattern in a precise manner. Numerous methods such as manipulation of the interfacial surface energies, use of electric fields, and controlling the rate of solvent evaporation have developed to control orientation. In addition, it has been shown that nanopores within cylindrical domains oriented normal to the substrate can be generated by several methods. For example, one component can be degraded by UV exposure, or the homopolymer in a block copolymer/homopolymer blend can be extracted in a selective solvent. In our work, polystyrene-*b*-poly(4-vinylpyridine) (PS-*b*-P4VP)/poly(4-vinylpyridine) (P4VP) films on silicon substrates were prepared using spincoating. The homopolymer was then extracted in ethanol generating pores perpendicular to the substrate. It is noted that the pore size and density were readily controlled by the amount of P4VP homopolymer in the PS-*b*-P4VP/P4VP solutions,

giving simple control of the film structure. It was also possible to make pores more uniform and ordered by annealing in solvent vapor before extracting the homopolymer.

NANOSTRUCTURE INVESTIGATION OF POLYMER SOLUTIONS, POLYMER  
GELS, AND POLYMER THIN FILMS

By

Wonjoo Lee

Dissertation submitted to the Faculty of the Graduate School of the  
University of Maryland, College Park, in partial fulfillment  
of the requirements for the degree of  
Doctor of Philosophy  
2009

Advisory Committee:  
Professor Robert M. Briber, Chair  
Professor Peter Kofinas  
Professor Mohamad Al-Sheikhly  
Professor Joonil Seog  
Professor Srinivas R. Raghavan

© Copyright by  
Wonjoo Lee  
2009

## Dedication

To my wife, Jungsoon Choi, to my son, Junghyun Lee, and to my parents

## Acknowledgements

Most of all, I would like to thank my wife, Jungsoon Choi. She has sacrificed her life for me to get a Ph. D degree. Without her dedication and patience, I might not have reached at this moment.

I would like to thank my advisor, Prof. Robert M. Briber. It was my honor to have had chance to learn about not only science but also attitude as scientist. I hope to be remembered as one of his proud students.

I would like to thank my committee members, Prof. Peter Kofinas, Prof. Srinivas R. Raghavan, Prof. Mohamad Al-Sheikhly, and Prof. Joonil Seog for their valuable advice.

I would like to thank Xin Zhang, Sanghak Shin and Chris Metting for helping my SANS experiments at NCNR. Also, I would like to thank our group members and Prof. Kofinas group members for the helpful group meetings.

Last, I would like to thank my parents for having supported me until now. Although they were not educated in school, they were, are, and will be my heroes as their love and their diligence are the assets I would like to hand over to my son. Whenever I was in desperation, they encouraged me to challenge again. I hope I could be such a great and warm father to my son, Junghyun Lee.

# Table of Contents

Dedication.....	ii
Acknowledgements.....	iii
Table of Contents.....	iv
List of Tables .....	vii
List of Figures.....	viii
Chapter 1: Significance and Background .....	1
1.1 Singnificance.....	1
1.2 Theoretical Background.....	3
1.2.1 Group transfer polymerization.....	3
1.2.2 Small angle neutron scattering.....	6
1.2.3 Block copolymer.....	16
Chapter 2: Small angle neutron scattering study of deuterated sodium dodecylsulfate micellization in a dilute poly((2-dimethylamino)ethyl methacrylate) solution .....	19
2.1 Introduction.....	19
2.2 Experimental.....	21
2.3 Results.....	22
2.3.1 PDMAEMA synthesis .....	22
2.3.2 Polymer characterization .....	23
2.3.3 SANS results.....	27
2.4 Conclusions.....	46
Chapter 3: Small angle neutron scattering study of deuterated sodium dodecylsulfate micellization in concentrated poly((2-dimethylamino)ethyl methacrylate) solutions	48
3.1 Introduction.....	48
3.2 Experimental.....	51
3.3 Theory.....	52

3.4 Results.....	57
3.4.1 Concentrated PDMAEMA solutions with 100 mM h-SDS or d-SDS.....	57
3.4.2 A model fit of 100 mM d-SDS in PDMAEMA solutions.....	63
3.5 Conclusions.....	77
Chapter 4: Construction of structured hydrogels with anionic micelles.....	79
4.1 Introduction.....	79
4.2 Experimental.....	81
4.3 Results.....	83
4.4 Conclusions.....	90
Chapter 5: The effect of the degree of quaternization of poly((2-dimethylamino)ethyl methacrylate) on deuterated sodium dodecylsulfate micellization.....	92
5.1 Introduction.....	92
5.2 Experimental.....	94
5.3 Results.....	95
5.3.1 Quaternization of PDMAEMA and characterization.....	95
5.3.2 SANS of quaternized PDMAEMA solutions/hydrogels with 100 mM d-SDS.....	99
5.4 Conclusions.....	108
Chapter 6: A simple method for creating oriented nanopores in block-copolymer thin films.....	110
6.1 Introduction.....	110
6.2 Experimental.....	112
6.3 Results.....	113
6.4 Conclusions.....	123
Chapter 7: Conclusions and Suggestion.....	124
7.1 Conclusions.....	124

7.2 Suggestion for future work .....	126
Bibliography .....	129

## List of Tables

Table 3.1. Volumes of chemical groups ( $V$ ) and hydration numbers ( $\omega$ ) used in the data analysis.....	56
Table 3.2. Neutron scattering length densities of the molecules used in this work.....	59
Table 3.3. Scattering lengths, volumes and neutron scattering length densities of chemical groups.....	69
Table 3.4. Optimized parameters from model fits.....	71
Table 5.1. Degree of quaternization obtained from $^1\text{H-NMR}$ results.....	98
Table 5.2. Optimized parameters from model fits.....	105

## List of Figures

Figure 1.1. Group transfer polymerization of (meth)acrylic monomers.....	5
Figure 1.2. A schematic of the coordinate system showing a pair of scatterers that belong to two different particles.....	9
Figure 1.3. Morphologies and phase diagrams for diblock copolymers.....	18
Figure 2.1. <sup>1</sup> H-NMR of synthesized PDMAEMA in CDCl <sub>3</sub> .....	25
Figure 2.2. (a) GPC results of standard PMMAs and synthesized PDMAEMA: PMMAs and PDMAEMA and (b) A plot of molecular weight versus retention time: PMMAs and PDMAEMA.....	26
Figure 2.3. SANS of 10 mg/ml PDMAEMA solutions in pure D <sub>2</sub> O and acidified D <sub>2</sub> O.....	28
Figure 2.4. SANS of 10 mg/ml PDMAEMA solutions with d-SDS in pure D <sub>2</sub> O (0 to 1.3 mM d-SDS).....	32
Figure 2.5. SANS of 10 mg/ml PDMAEMA solutions with d-SDS in pure D <sub>2</sub> O (3 to 48 mM d-SDS).....	35
Figure 2.6. A change of the SANS peak position ( $q^*$ ) and the calculated distance between charged micelles ( $d$ ) as a function of the ratio of moles of d-SDS to the moles of PDMAEMA chain.....	37
Figure 2.7. (a) SANS of 10 mg/ml PDMAEMA solutions with d-SDS in pure D <sub>2</sub> O (60 to 150 mM d-SDS) .....	40
Figure 2.8. SANS intensity of 10 mg/ml PDMAEMA solutions with d-SDS in pure D <sub>2</sub> O subtracted by a power law, $I(q) = kq^{-1.3}$ .....	43

Figure 2.9. SANS intensity of a 10 mg/ml PDMAEMA solution with 100 mM d-SDS where PDMAEMA was contrast-matched to 80% H <sub>2</sub> O and 20% D <sub>2</sub> O.....	45
Figure 3.1. A schematic of a spherical core-shell micelle of mean radii $R_1$ and $R_3$ ...	53
Figure 3.2. SANS of PDMAEMA solutions with 100 mM h-SDS in pure D <sub>2</sub> O.....	58
Figure 3.3. SANS of PDMAEMA solutions with 100 mM d-SDS in pure D <sub>2</sub> O.....	62
Figure 3.4. SANS of PDMAEMA solutions with 100 mM d-SDS in a mixture of 80% H <sub>2</sub> O and 20% D <sub>2</sub> O.....	64
Figure 3.5. A schematic of the mixed micelle of mean radii $R_1$ and $R_3$ in PDMAEMA solutions.....	66
Figure 3.6. The scattering length densities of core and shell obtained from the model fit.....	73
Figure 3.7. The form factors of d-SDS micelles in PDMAEMA solutions at the condition that PDMAEMA was contrast matched to a mixture of 80% H <sub>2</sub> O and 20% D <sub>2</sub> O.....	74
Figure 3.8. The structure factors of d-SDS micelles in PDMAEMA solutions. PDMAEMA contrast match point (80%H <sub>2</sub> O/20%D <sub>2</sub> O) .....	76
Figure 4.1. A scheme of the crosslinking reaction between PDMAEMA and BIEE..	82
Figure 4.2. SANS intensity of a 200 mg/ml PDMAEMA solution with 100 mM d-SDS in D <sub>2</sub> O and its corresponding hydrogels.....	84
Figure 4.3. SANS intensity of a 200 mg/ml PDMAEMA solution with 100 mM d-SDS and its corresponding hydrogels in a mixture of 80% H <sub>2</sub> O and 20% D <sub>2</sub> O.....	87
Figure 5.1. <sup>1</sup> H-NMR of (quaternized) PDMAEMAs in D <sub>2</sub> O.....	97

Figure 5.2. SANS intensity of a 200 mg/ml PDMAEMA solution and a 290 mg/ml 51% quaternized PDMAEMA solution in D <sub>2</sub> O.....	100
Figure 5.3. SANS intensity of (quaternized) PDMAEMA solutions with 100 mM d-SDS in a mixture of 80% H <sub>2</sub> O and 20% D <sub>2</sub> O .....	102
Figure 5.4. SANS intensity of a 290 mg/ml 51% quaternized PDMAEMA solutions with 100 mM d-SDS and its corresponding hydrogel with 0.04 crosslinking ratio in a mixture of 80% H <sub>2</sub> O and 20% D <sub>2</sub> O.....	107
Figure 6.1. AFM height images of an as-spun PS/P4VP blend film with 0.35 of P4VP weight fraction and the PS/P4VP blend film after immersed in ethanol for 3 hours.....	115
Figure 6.2. AFM height images of as-spun PS-b-P4VP/P4VP blend films as a function of P4VP weight fraction in the polymer solutions and TEM image of PS-b-P4VP/P4VP film with 0.45 of P4VP weight fraction after iodine staining.....	117
Figure 6.3. AFM height images of as-spun PS-b-P4VP/P4VP blend films with 0.45 of P4VP weight fraction as a function of relative humidity.....	119
Figure 6.4. AFM height images of PS-b-P4VP/P4VP blend films after soaked in ethanol for 3 hours.....	122

# Chapter 1: Significance and Background

Molecularly imprinted polymers (MIP) are formed in the presence of template species, which are extracted after network formation, thus leaving complementary pores behind. The MIP shows a chemical affinity for the original template species, so they can be used to fabricate sensors, catalysts or separation materials. We are interested in creating and analyzing structured hydrogels containing micelles as templates using small angle neutron scattering (SANS). This required the synthesis of a water-soluble and chemically crosslinkable polymer, poly((2-dimethylamino)ethyl methacrylate) (PDMAEMA). We will present group transfer polymerization (GTP) used to synthesize PDMAEMA, and SANS using to measure the size and shape of the micelles. Finally work on a separate topic will be presented where we developed a simple way to create nanoporous films using a diblock copolymer.

## 1.1 Significance

MIPs are created by crosslinking either polymers or monomers in the presence of templates, usually in water.<sup>1-9</sup> Initially, functional groups on the polymer are bound either covalently or noncovalently to the template, and then crosslinking results in a highly crosslinked hydrogel. The MIPs containing templates are immersed in water, and the large difference in the osmotic pressure between the hydrogel and water drives the templates out of the MIP, leaving pores in the polymer network containing functionalized groups. It is argued that these pores are complementary in size and

shape to the template molecules, resembling the “lock and key” paradigm of enzymes and the functional groups of the polymer are positioned to rebind to the template molecule, so that this material has potential to be used for applications in separation, drug delivery, biosensors, etc. There is also interest in creating nanoporous hydrogels using micelles as templates which could be used as separation materials,<sup>10-13</sup> similar to MIPs although micelles are at larger size scale than single molecules. In order to understand the proposed mechanism of MIPs, it is necessary to compare the resultant pores to the original templates with respect to size and shape.

When micelles are used as templates, the size and shape before and after crosslinking needs to be studied because micelles are thermodynamic structures which depend on the surfactant concentration of the solution, temperature, electrolyte concentration and polymer concentration. SANS has been widely used to investigate structures ranging from sub-nanometer to sub-micrometer.<sup>14-16</sup> Because the scattering lengths of H and D atoms are very different, the scattering contrast can be enhanced (and varied) through isotopic labeling. It is possible to investigate the structure of micelles in polymer solutions and hydrogels using H/D contrast matching methods with SANS. The size and the shape of the pores in comparison to size and shape of the original micelles can be investigated using SANS. The first goal of this work is to control the size and shape of micelles in polymer solutions and the corresponding hydrogels to understand the mechanism of MIP formation.

Although many articles have been published which describe the behavior of MIPs, some basic questions still need to be addressed to improve MIPs, such as the size and the shape of the pores, the effect of swelling and deswelling of the MIPs on the pores, and the dynamics of polymer chains in the MIP. Among these, a difficulty in directly observing the change of pores during swelling and deswelling of MIPs comes from the fact that pores exist inside MIPs.

In order to overcome the restriction, we used the self-assembly of polystyrene-*b*-poly(4-vinyl pyridine) (PS-*b*-P4VP)/poly(4-vinyl pyridine) (P4VP) blend films to generate pores penetrating the entire PS-*b*-P4VP/P4VP blend film after extracting P4VP homopolymers in a selective solvent. Since P4VP can be chemically modified to have charges and PS is non-soluble in water, a similar structure to MIPs is expected to be created to allow us to observe the pores using atomic force microscope in pure water and electrolyte solutions.

## **1.2 Theoretical Background**

### **1.2.1 Group transfer polymerization**

Group transfer polymerization (GTP) is a Michael-type catalyzed addition reaction.<sup>17-20</sup> A silyl ketene acetal is often used as the initiator. Figure 1.1 illustrates the polymerization of methyl methacrylates with dimethylketene methyl trimethylsilyl acetal as initiator. The silane group is transferred to the growing end after the addition of each monomer unit. Thus, the chain end remains active until the

complete consumption of the monomer. This is a living polymerization, and the molecular weight of the polymer synthesized can be predetermined from the ratio the monomer to the initiator used. Also, sequential addition of different monomers can give block copolymers. This type of polymerization reaction has been widely applied to the polymerization of (meth)acrylic monomers at room temperature, in the presence of a variety of side groups, which are sensitive to ionic or radical polymerization reactions. GTP is relatively tolerant to functionalities such as tertiary amines, epoxides, styrenic, and allylic groups. Monomers with functionalities such as  $-OH$  and  $-COOH$  can be polymerized after protection with appropriate groups. Deprotection after polymerization gives access to hydrophilic polymers. The use of anionic or Lewis acid catalysts, in conjunction with the initiator, improves the polymerization because these catalysts coordinate with the silicon atom or the monomer, and facilitate group transfer.

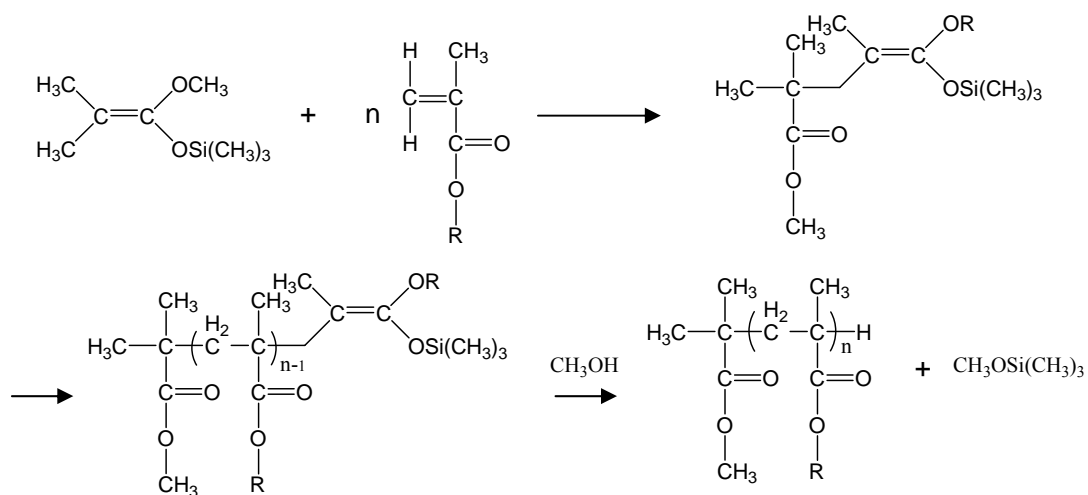


Figure 1.1. Group transfer polymerization of (meth)acrylic monomers

### 1.2.2 Small angle neutron scattering

SANS is a powerful technique to provide detailed structural information on a size scale of  $\sim 5$  to  $100$  nm.<sup>14-16</sup> For scattering from nanoscale particles in a very dilute solution (such as colloids or micelles), it is possible to measure only intra-particle scattering. However, in most cases the inter-particle scattering contributes to the intensity, especially at low scattering vector  $q$ , and to a greater extent as the concentration increases. The scattering vector  $q$  is related to the scattering angle and wavelength by

$$q = \frac{4\pi}{\lambda} \sin\left(\frac{\theta}{2}\right) \quad (1.1)$$

Here,  $\lambda$  is the wavelength of the incident light and  $\theta$  is the scattering angle.

The coherent scattering cross section of a system made of  $n$  nuclei is proportional to the density-density correlation function as follows.

$$\frac{d\sum(q)}{d\Omega} = b^2 \sum_{i=1}^n \sum_{j=1}^n \left\langle \exp\left(-i\vec{q} \cdot (\vec{r}_i - \vec{r}_j)\right) \right\rangle \quad (1.2)$$

where  $b$  represents the sum of all the coherent scattering lengths of the nuclei of a single particle and  $r_i$  defines the distance of the  $i$ th atom from the observer. It is useful to replace the discrete sum of equation (1.2) with an integral by defining the local density of molecules by the expression

$$n(\vec{r}) = \sum_{j=1}^n \delta(\vec{r} - \vec{r}_j) \quad (1.3)$$

where  $n(\vec{r})$  is the density of molecules at any point  $r$ . Since

$$\int_V f(\vec{r}) \delta(\vec{r} - \vec{r}_k) d\vec{r} = f(\vec{r}_k) \quad (1.4)$$

The equation (1.1) is written into

$$\frac{d\Sigma(q)}{d\Omega} = b^2 \int_V \int_{V'} \exp(-i\vec{q}(\vec{r} - \vec{r}')) \langle n(\vec{r}) n(\vec{r}') \rangle d\vec{r} d\vec{r}' \quad (1.5)$$

Now, consider a two species mixture, with  $n_1$  molecules of scattering length  $b_1$  and with  $n_2$  molecules of scattering length  $b_2$  occupying the sample volume  $V$ . Collecting the terms belonging to each species and those of the cross terms together, the coherent cross section is given by

$$\begin{aligned} \frac{d\Sigma(q)}{d\Omega} &= \frac{b_1^2}{V} \sum_{i_1=1}^{n_1} \sum_{j_1=1}^{n_1} \langle \exp(-i\vec{q} \cdot (\vec{r}_{i_1} - \vec{r}_{j_1})) \rangle + 2 \frac{b_1 b_2}{V} \sum_{i_1=1}^{n_1} \sum_{j_2=1}^{n_2} \langle \exp(-i\vec{q} \cdot (\vec{r}_{i_1} - \vec{r}_{j_2})) \rangle \\ &+ \frac{b_2^2}{V} \sum_{i_2=1}^{n_2} \sum_{j_2=1}^{n_2} \langle \exp(-i\vec{q} \cdot (\vec{r}_{i_2} - \vec{r}_{j_2})) \rangle \end{aligned} \quad (1.6)$$

or

$$\begin{aligned} \frac{d\Sigma(q)}{d\Omega} &= \frac{b_1^2}{V} \int_V \int_{V'} \exp(-i\vec{q}(\vec{r} - \vec{r}')) \langle n_1(\vec{r}) n_1(\vec{r}') \rangle d\vec{r} d\vec{r}' + \\ &2 \frac{b_1 b_2}{V} \int_V \int_{V'} \exp(-i\vec{q}(\vec{r} - \vec{r}')) \langle n_1(\vec{r}) n_2(\vec{r}') \rangle d\vec{r} d\vec{r}' + \frac{b_2^2}{V} \int_V \int_{V'} \exp(-i\vec{q}(\vec{r} - \vec{r}')) \langle n_2(\vec{r}) n_2(\vec{r}') \rangle d\vec{r} d\vec{r}' \end{aligned} \quad (1.7)$$

where  $n_i(\vec{r})$  is the local density of constituent  $i$ . The molecular volumes  $v_1$  and  $v_2$

and scattering length densities  $\rho_1 = \frac{b_1}{v_1}$  and  $\rho_2 = \frac{b_2}{v_2}$  are defined for the molecules,

respectively. For convenience, the following partial structure factors are defined:

$$S_{ij}(q) = \frac{v_i v_j}{V} \int_V \int_{V'} \exp(-i\vec{q}(\vec{r} - \vec{r}')) \langle n_i(\vec{r}) n_j(\vec{r}') \rangle d\vec{r} d\vec{r}' \quad (1.8)$$

And, the scattering cross section becomes

$$\frac{d\sum(q)}{d\Omega} = \rho_p^2 S_{PP}(q) + \rho_s^2 S_{SS}(q) + 2\rho_p\rho_s S_{PS}(q) \quad (1.9)$$

In an incompressible system, the following is satisfied.

$$S_{PP}(q) = S_{SS}(q) = -S_{PS}(q) \quad (1.10)$$

This simplifies the cross section to the following form:

$$\frac{d\sum(q)}{d\Omega} = (\rho_1 - \rho_2)^2 S_{11}(q) = (\rho_1 - \rho_2)^2 S_{22}(q) = -(\rho_1 - \rho_2)^2 S_{12}(q) \quad (1.11)$$

The above equation implies that the scattering of a two component system depends only on one of these components and is independent of the other.

Consider a system consisting of N particles with a particle volume occupying volume V, like a colloid solution. Each particle comprises n molecules of volume v each so that the particle volume is  $v_p = nv$ . Schematic representation of the coordinate system showing a pair of scatterers that belonging to two different particles is shown in Figure 1.2. In a particle, the fact that the relative positions of certain sets of atoms in the sample are constrained by the requirement that they form a particle is taken advantage of.

The scattering cross section is

$$\begin{aligned} \frac{d\sum(q)}{d\Omega} &= \Delta\rho^2 \frac{v^2}{V} \left[ \sum_{I,J}^N \sum_{i,j}^n \left\langle \exp(-i\vec{q} \cdot (\vec{r}_{Ii} - \vec{r}_{Jj})) \right\rangle \right] = \\ &\Delta\rho^2 \frac{v^2}{V} \left[ \sum_{I=J}^N \sum_{i,j}^n \left\langle \exp(-i\vec{q} \cdot (\vec{r}_{Ii} - \vec{r}_{Ij})) \right\rangle + \sum_{I \neq J}^N \sum_{i,j}^n \left\langle \exp(-i\vec{q} \cdot (\vec{r}_{Ii} - \vec{r}_{Jj})) \right\rangle \right] \end{aligned} \quad (1.12)$$

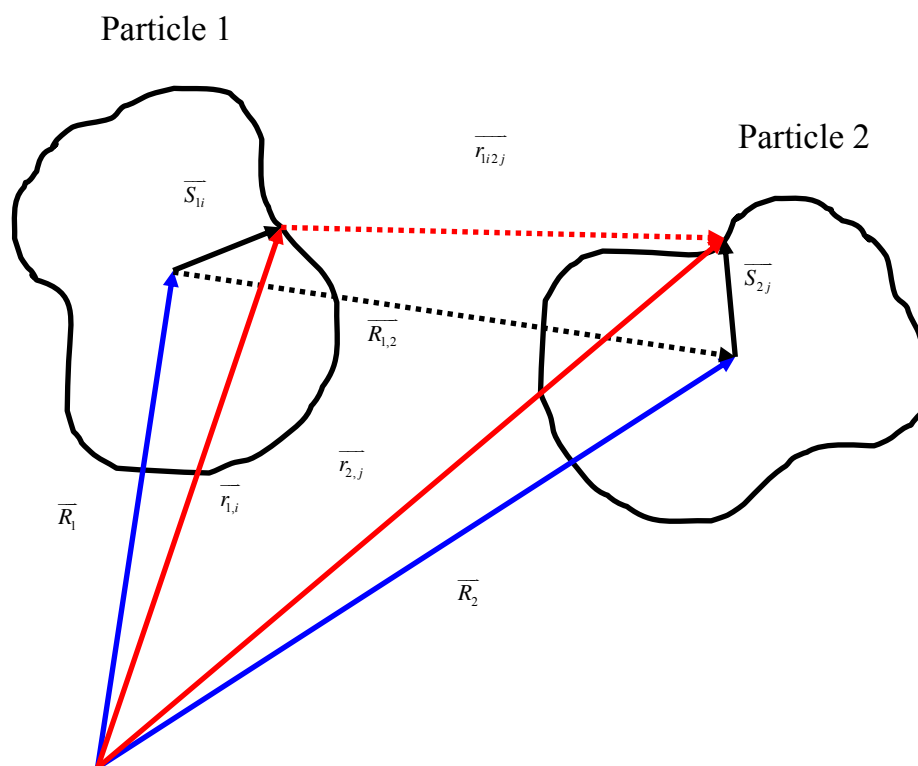


Figure 1.2. A schematic of the coordinate system showing a pair of scatterers that belong to two different particles

where  $li$  indicates the  $i$ th atom in the  $l$ th particle. So the equation is separated out the intra-particle ( $I = J$ ) and the inter-particle ( $I \neq J$ ) terms in the scattering cross section. It is assumed for the sake of clarity that all particles have the same shape and size. Therefore,

$$\frac{d\sum(q)}{d\Omega} = \Delta\rho^2 \frac{v^2}{V} \left[ N \sum_{i,j} \langle \exp(-i\bar{q} \cdot (\bar{r}_{ii} - \bar{r}_{jj})) \rangle + N(N-1) \sum_{i,j} \langle \exp(-i\bar{q} \cdot (\bar{r}_{ii} - \bar{r}_{jj})) \rangle \right] \quad (1.13)$$

The inter-distance between the scattering pair  $\bar{r}_{ij}$  can be expressed as  $\bar{r}_{ij} = -\bar{s}_{ii} + \bar{s}_{jj} + \bar{R}_{ij}$ , and the inter-particle average can be split into the following parts:

$$\langle \exp(-i\bar{q} \cdot (\bar{r}_{ii} - \bar{r}_{jj})) \rangle = \langle \exp(i\bar{q} \cdot \bar{s}_{ii}) \rangle \langle \exp(-i\bar{q} \cdot \bar{s}_{jj}) \rangle \langle \exp(-i\bar{q} \cdot \bar{R}_{ij}) \rangle \quad (1.14)$$

The first two averages are within single particles and the third average is across particles.

The summations become

$$\sum_{i,j} \langle \exp(-i\bar{q} \cdot (\bar{r}_{ii} - \bar{r}_{jj})) \rangle = \langle \exp(-i\bar{q} \cdot \bar{R}_{ij}) \rangle \sum_i \langle \exp(i\bar{q} \cdot \bar{s}_{ii}) \rangle \sum_j \langle \exp(-i\bar{q} \cdot \bar{s}_{jj}) \rangle \quad (1.15)$$

The form factor amplitude is defined as

$$F(q) = \frac{1}{n} \sum_i \langle \exp(-i\bar{q} \cdot \bar{s}_{ii}) \rangle = \frac{1}{n} \sum_j \langle \exp(-i\bar{q} \cdot \bar{s}_{jj}) \rangle \quad (1.16)$$

The single-particle form factor is defined as

$$P(q) = \frac{1}{n^2} \sum_{i,j} \langle \exp(-i\bar{q} \cdot \bar{s}_{ij}) \rangle \quad (1.17)$$

An inter-particle structure factor is defined as

$$S(q) = \frac{1}{N} \sum_{I,J} \langle \exp(-i\vec{q} \cdot \vec{R}_{IJ}) \rangle \quad (1.18)$$

The cross section can therefore be written as follows

$$\frac{d\Sigma(q)}{d\Omega} = \Delta\rho^2 \frac{v^2 n^2 N}{V} \left[ P(q) + |F(q)|^2 (S(q) - 1) \right] \quad (1.19)$$

Uniform density scatterers such as particles are characterized by  $P(q) = |F(q)|^2$ , so

that

$$\frac{d\Sigma(q)}{d\Omega} = \Delta\rho^2 \frac{v^2 n^2 N}{V} P(q) S(q) \quad (1.20)$$

Defining a particle's volume fraction  $\phi = Nnv/V$ , the following result is obtained

$$\frac{d\Sigma(q)}{d\Omega} = \Delta\rho^2 vn\phi P(q) S(q) \quad (1.21)$$

A few examples of the form factor are described below.

### **Form factor for a uniform sphere**

Consider a sphere of radius R and uniform density. The single particle form factor  $P(q)$  involves integrations over the volume  $V_P$  of the sphere.

$$P(q) = \int dr \int dr' \frac{\langle n(r)n(r') \rangle}{n^2} \exp(-iq \cdot (\vec{r} - \vec{r}')) \quad (1.22)$$

Since the scattering elements are not correlated, the average of the product  $\langle n(r)n(r') \rangle$  is equal to the product of the average  $\langle n(r) \rangle \langle n(r') \rangle$ . Therefore,

$$P(q) = |F(q)|^2 \quad (1.23)$$

The amplitude of the form factor  $F(q)$  is defined as

$$F(q) = \int dr \frac{\langle n(r) \rangle}{n} \exp[-i\vec{q} \cdot \vec{r}] \quad (1.24)$$

For uniform density,

$$\langle n(r) \rangle = \frac{n}{V_P} \quad \text{for } r \leq R \quad (1.25)$$

$$\langle n(r) \rangle = 0 \quad \text{for } r > R \quad (1.26)$$

Therefore,

$$F(q) = \frac{3}{4\pi R^3} \int_0^R r^2 dr \int_{-1}^1 d\mu \exp(-iqr\mu) \int_0^{2\pi} d\phi = \frac{3}{R^3} \int_0^R r^2 dr \frac{\sin(qr)}{qr} = \frac{3j_1(qR)}{qR} \quad (1.27)$$

Here, the spherical Bessel function  $j_1(x)$  is defined as

$$j_1(x) = \frac{\sin x}{x^2} - \frac{\cos x}{x} \quad (1.28)$$

Therefore, the form factor for the sphere is

$$P(q) = \left[ \frac{3j_1(qR)}{qR} \right]^2 = \left[ \frac{3}{qR} \left( \frac{\sin qR}{qR^2} - \frac{\cos qR}{qR} \right) \right]^2 \quad (1.29)$$

### Form factor for a spherical shell

Following the same procedure, the form factor for a spherical shell between radii  $R_1$  and  $R_2$  (and hollow for  $r < R_1$ ) can be calculated as follows:

$$\begin{aligned}
F(q) &= \frac{3}{4\pi(R_2^3 - R_1^3)} \int_{R_1}^{R_2} r^2 dr \int_{-1}^1 d\mu \exp(-iqr\mu) \int_0^{2\pi} d\phi \\
&= \frac{1}{(R_2^3 - R_1^3)} \left[ \left( \frac{3j_1(qR_2)}{qR_2} \right) R_2^3 - \left( \frac{3j_1(qR_1)}{qR_1} \right) R_1^3 \right]
\end{aligned} \tag{1.30}$$

And, the form factor for the shell is

$$P(q) = |F(q)|^2 \tag{1.31}$$

### Structure Factor

The structure factor contains all of the information about the spatial arrangement of the particles relative to an arbitrary origin. For the case of an isotropic solution, the average can be calculated around a centrally located sphere. The orientational average can be calculated as

$$S(q) = 1 + 4\pi n_p \int_0^\infty [g(r) - 1] \frac{\sin qr}{qr} r^2 dr \tag{1.32}$$

The pair correlation function,  $g(r)$ , can be calculated using liquid state theory, and thus the structure factor can be calculated. The pair correlation function is related to thermodynamic properties of the fluid such as pressure or compressibility. To obtain information from systems of interacting colloids, it is necessary to model the scattered intensity by calculating the form and structure factors.

For particles of known morphology, it is often desirable to determine the unknown interparticle potential. This is done by proposing an interaction potential, using statistical mechanics to calculate  $S(q)$ , and fitting the model to the data. The

interaction potential determines the equilibrium arrangement of particles,  $g(r)$ , from which  $S(q)$  can be calculated. For a homogeneous, isotropic fluid of spheres, the Ornstein-Zernike equation is

$$h(r) = g(r) - 1 = c(r) + n \int c(|\bar{r} - \bar{x}|) h(x) d\bar{x} \quad (1.33)$$

and states that the total correlation,  $h(r)$ , between two particles is the sum of the direct correlations,  $c(r)$ , and the sum of all other correlations which are felt indirectly through all other particles. The structure factor  $S(q)$  depends directly on  $c(r)$ . Unfortunately,  $c(r)$  and  $h(r)$  are both unknown functions and the Ornstein-Zernike equation can only be solved if there is available an additional relationship between them. The additional equation is an approximation, called a closure relation, which relates  $c(r)$  and  $h(r)$ . The simplest of these closure relations is the Percus-Yevick closure,

$$c(r) = g(r) \left[ 1 - e^{\beta U(r)} \right] \quad (1.34)$$

which provides a good description of fluids with very short ranged interactions. For the simplest case of hard sphere interactions with a radius,  $a$

$$U(r) = \infty \text{ for } r \leq 2a \quad (1.35)$$

$$U(r) = 0 \text{ for } r > 2a \quad (1.36)$$

where  $r$  is a center-to-center distance.

The screened Coulomb interaction is a good description of macroions in solution.

$$U(r) = \infty \text{ for } r \leq 2a \quad (1.37)$$

$$U(r) = \frac{z_m^2}{4\pi\epsilon_0\epsilon(1+\kappa a)^2} \exp[-\kappa(r-2a)]/r \quad \text{for } r > 2a \quad (1.38)$$

where  $r$  is a center-to-center distance.  $z_m$  is the charge on the micelle,  $\epsilon_0$  is the permittivity of free space,  $\epsilon$  is the dielectric constant of the solvent, and  $\kappa$  is the Debye-Hückel inverse screening length. Since the screened Coulomb repulsion is much longer ranged than hard sphere interactions, a different, more appropriate closure relation will take this into account.

### 1.2.3 Block copolymer

Block copolymers contain two or more different polymer chains linked together. Usually the blocks become less miscible as the temperature is lowered, i.e. the system exhibits an upper critical ordering temperature (UCOT). Below the UCOT, phase separation occurs. However, in contrast to blends of polymers, the length-scale for phase separation in block copolymers is restricted by the connectivity of the blocks. It is typically 10-100 nm, depending on the radius of gyration of the blocks. Hence the process of phase separation for block copolymers is termed microphase separation.<sup>21-</sup>

<sup>24</sup> The transition from an ordered microphase to the homogeneous polymer melt at high temperatures occurs at the order-disorder transition (ODT). Microphase separation leads to the formation of a variety of ordered structures, illustrated in Figure 1.3, which shows an idealized phase diagram for a diblock copolymer. Different structures are stable for block copolymers with different compositions, specified as the volume fraction of one block  $f$ . Block copolymer phase diagrams are parameterized by  $f$  and  $\chi N$ . Here  $\chi$  is the Flory-Huggins interaction parameter associated with the enthalpy of mixing of segments and  $N$  is the degree of polymerization. The stability of the block copolymer microphases results from a balance between the enthalpy penalty for curvature of the interface between microdomains, the entropy associated with localizing junctions between the blocks at the interface and the entropy associated with maintaining a uniform density, which leads to the stretching of chains to fill space. Again, considering diblock copolymers as the simplest case, in a symmetric diblock ( $f = 0.5$ ) there is no tendency for the interface to curve, so upon microphase separation, a lamellar phase is formed. As the

asymmetry of the diblock increases, the mean interfacial curvature increases, leading to the formation of phases of hexagonal-packed cylinders or spheres of the minority block in the majority matrix. Between the hexagonal-packed cylinder and lamellar phase, a gyroid phase is formed.

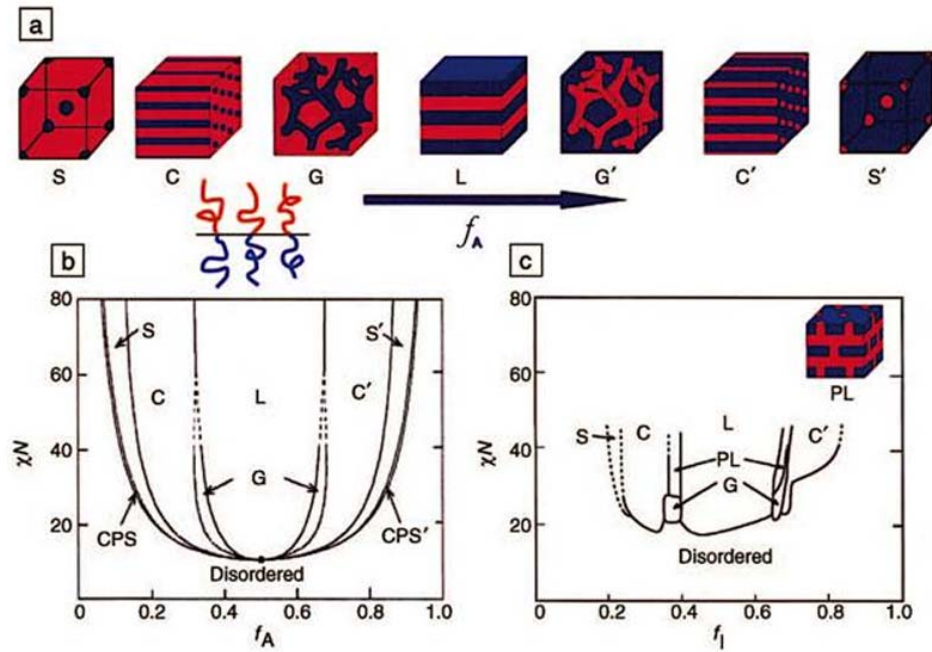


Figure 1.3. (a) Morphologies such as spheres (S), cylinders (C), gyroid (G), and lamellar (L) are controlled by  $f$  and  $\chi N$  (b) Theoretical and (c) experimental polystyrene-*b*-polyisoprene phase diagrams for diblock copolymers (Frank S Bates, *MRS Bulletin*, **2005**, 30, 525-532)

## **Chapter 2: Small angle neutron scattering study of deuterated sodium dodecylsulfate micellization in dilute poly((2-dimethylamino)ethyl methacrylate) solutions**

In order to create hydrogels containing micelles, it was required to synthesize a water-soluble and chemically crosslinkable polymer. In this chapter, we will present the synthesis and characterization of poly((2-dimethylamino)ethyl methacrylate) (PDMAEMA) using group transfer polymerization (GTP). The effect of sodium dodecylsulfate (SDS) on PDMAEMA chain conformation in water is investigated using small angle neutron scattering (SANS).

### **2.1 Introduction**

Interactions between polymers and surfactants in water have been widely investigated because of their potential applications as detergents,<sup>25</sup> rheology modifiers,<sup>26</sup> and gelation agents.<sup>27, 28</sup> The surfactants are typically charged, while the polymers are generally neutral or oppositely charged with respect to the surfactants. Depending on whether the polymers are neutral or oppositely charged, mixtures of polymers and surfactants in water show different behavior.<sup>29, 30</sup> In cases where anionic surfactants were added to a dilute neutral polymer solution, such as poly(ethylene oxide) (PEO), poly(vinyl pyrrolidone) (PVP) or poly(vinyl alcohol) in water, the spherical surfactant micelles were wrapped by the polymer chains, which is

termed a necklace-like structure, and is formed above the critical aggregation concentration (CAC), which is lower than the critical micelle concentration (CMC) of the surfactant in pure water. This continues until the polymers are saturated with micelles.<sup>29, 31</sup> Many factors, such as molecular weight, amount, flexibility and hydrophobicity of the polymer all influence the association between the polymer and the surfactant. It has been shown that in dilute or semidilute PEO water solutions, necklace-like PEO/SDS complexes are formed when the PEO molecular mass is high enough.<sup>29, 31-34</sup> Spherical micelles wrapped by polymers in semi-dilute solutions can be used to create a templated hydrogel if the polymer is crosslinkable. PDMAEMA is a water-soluble polymer which can be cationic or neutral depending on pH,<sup>35, 36</sup> and can be chemically crosslinked using 1,2-bis(2-iodoethoxy)ethane (BIEE) in water.<sup>37, 38</sup> Recently, binding of SDS surfactants to short PDMAEMA (8000 g/mol) chains was observed using SANS by Cosgrove, et al. at pH 9.1 where the polymer is considered neutral.<sup>39</sup> It is notable that the interactions between PDMAEMA with a small degree of polymerization (~50) and SDS surfactants occur, since the value of 50 is comparable to the degree of polymerization of PVP (~36) which has the highest reactivity for anionic surfactants among the neutral polymers.<sup>29</sup> In the SANS data by Cosgrove, et al. a peak was observed in the  $q$  range 0.04-0.06  $\text{\AA}^{-1}$ , and  $q^{-4}$  power law behavior at low  $q$  was observed in dilute PDMAEMA solutions with either deuterated SDS (d-SDS) or hydrogenated SDS (h-SDS) in  $D_2O$ . They attributed the peak in the scattering to the formation of PDMAEMA/SDS complexes and suggested several short PDMAEMA chains are associated with each micelle, as chains used in their research had an averaged degree of polymerization of only about 50, which is lower

than expected for the necklace-like structure where several spherical micelles are connected by a single polymer chain.<sup>29, 32-34, 40</sup> Since a necklace-like structure is one of the prerequisites to create a structured PDMAEMA hydrogel templated with SDS micelles, in this work we synthesized 60,000 g/mol PDMAEMA (approximately, ~395 degree of polymerization) using GTP<sup>19</sup>, and the structure of PDMAEMA/SDS complexes in dilute PDMAEMA solutions was investigated using SANS and H/D contrast matching methods.

## 2.2 Experimental

All reagents were purchased from Aldrich, unless otherwise stated. The monomer, ((2-dimethylamino)ethyl methacrylate) (DMAEMA) from Polysciences, Inc, was passed through a basic alumina column to remove the inhibitor and was dried by stirring over calcium hydride for 24 hrs. The monomer was vacuum-distilled at 45 °C before use. Tetrahydrofuran (THF) from Fisher was refluxed over sodium and benzophenone for 3 days and then distilled. The dried THF was transferred to the reaction flask via a double-tipped needle. The initiator, 1-methoxy-1-trimethylsiloxy-2-methyl-1-propene (MTS), was distilled and stored in a graduated Schlenk flask before use. Tetrabutylammonium bibenzoate catalyst (TBABB) was prepared by the method of Dicker et al.<sup>20</sup> For the SANS measurements, D<sub>2</sub>O and d-SDS were purchased from Cambridge Isotope Laboratories, Inc. To observe the effect of pH on the SANS intensity of the PDMAEMA solutions, PDMAEMA was dissolved in pure D<sub>2</sub>O or acidified D<sub>2</sub>O. Acidified D<sub>2</sub>O was prepared by adding small amount of a 35 wt% DCl solution in D<sub>2</sub>O to pure D<sub>2</sub>O. Also, a series of 10 mg/ml PDMAEMA

solutions in pure D<sub>2</sub>O with the desired d-SDS concentrations were prepared by mixing a 20 mg/ml PDMAEMA solution with various concentrated d-SDS solutions in order to investigate the change of PDMAEMA chain conformation resulting from the interactions between PDMAEMA and d-SDS. The size and shape of the micelles in a 10 mg/ml PDMAEMA solution with 100 mM d-SDS was observed under the conditions where PDMAEMA was contrast-matched to a mixture of 80% H<sub>2</sub>O and 20% D<sub>2</sub>O. Each solution was measured in a demountable titanium cell with a 1 mm or 2 mm path length for the SANS experiments, depending on the solvent. SANS experiments were carried out at the Center for Neutron Research at the National Institute of Standards and Technology on the 30 m NIST-NG7 instrument.<sup>41</sup> The raw data were corrected for scattering from the empty cell, incoherent scattering, detector dark current, detector sensitivity, sample transmission, and thickness. Following these corrections the data were placed on an absolute scale using direct beam measurement and circularly averaged to produce I(q) versus q plots where I(q) is the scattered intensity and q is the scattering vector ( $q=4\pi\sin\theta/\lambda$ ). The q range was 0.0046–0.40 Å<sup>-1</sup> and the neutron wavelength was 6 Å with a wavelength spread  $\Delta\lambda/\lambda = 0.11$ .

## **2.3 Results**

### **2.3.1 PDMAEMA synthesis**

PDMAEMA was synthesized using GTP as described by Armes et al.<sup>35, 42</sup> All glassware was heated overnight at 130 °C before use. In order to eliminate surface moisture, the assembled glassware was heated under vacuum. 100 ml of dry, distilled

THF was transferred into a flask via a double-tipped needle. 5 mg TBABB (2mol % based on initiator) was dissolved in small amount of the dried THF and the solution was transferred into the flask via a double-tipped needle. Then, 0.1 ml MTS was added to the flask. 25 ml of DMAEMA monomer was added dropwise via a double-tipped needle to the solution. The reaction causes the temperature of the solution increase as it is an exothermic reaction. A thermocouple was used to monitor the temperature of the solution during the polymerization. The solution was stirred without heating until the solution temperature returned to room temperature. The polymerization was terminated by addition of 10 ml methanol and the solvent was removed using a rotary evaporator at 45 °C. The synthesized polymer was further dried in a vacuum oven for at least 3 days at 45 °C.

### **2.3.2 Polymer characterization**

#### **2.3.2.1 Proton nuclear magnetic resonance spectroscopy (<sup>1</sup>H-NMR)**

The chemical structure of synthesized PDMAEMA, as shown in Figure 2.1, was confirmed using a Bruker 400 MHz <sup>1</sup>H-NMR and using CDCl<sub>3</sub> with 1% TMS as solvent. The NMR signal at  $\delta$  0.8-1.1, assigned to the methyl group in the main chain, indicates the vinyl group of the monomers polymerized.

#### **2.3.2.2 Gel permeation chromatography (GPC)**

GPC was used to determine a PMMA equivalent molecular weight and molecular weight distribution of the synthesized PDMAEMA. A series of near-monodisperse poly(methyl methacrylate) (PMMA) from Polymer Laboratories were used as

calibration standards. (Figure 2.2) The eluent was HPLC grade THF with 2 vol% triethylamine at a flow rate of 1 ml/min. Here, the molecular weight is reported as PMMA equivalent. Based on the calibration curve, the number-average molecular weight of the synthesized PDMAEMA was 60,000 g/mol with 1.12 PDI which is close to the target molecular weight of 50,000 g/mol. The difference between the measured and the target molecular weight is probably due to the hydrodynamic volume of PDMAEMA being larger than the PMMA used as calibration standards.

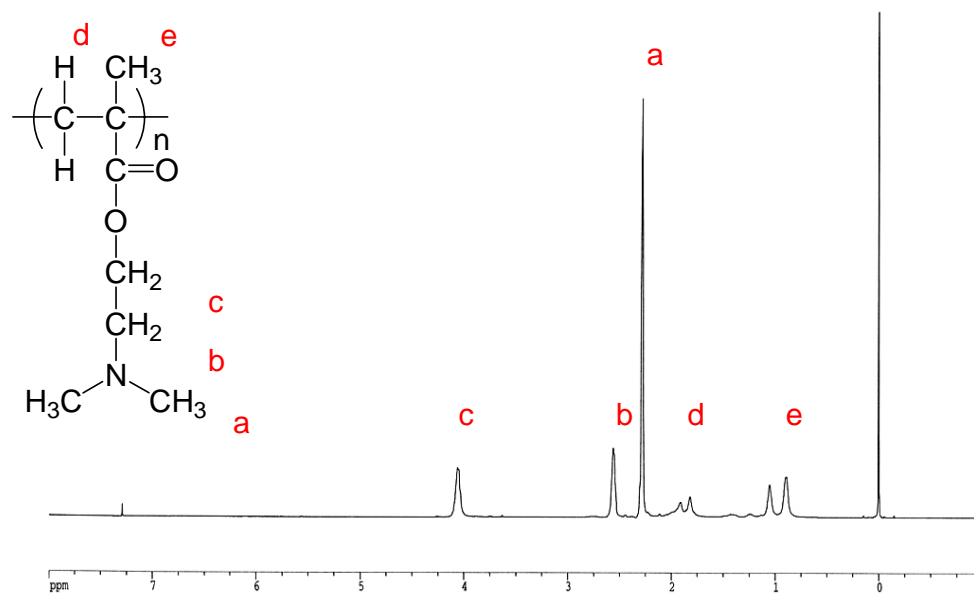
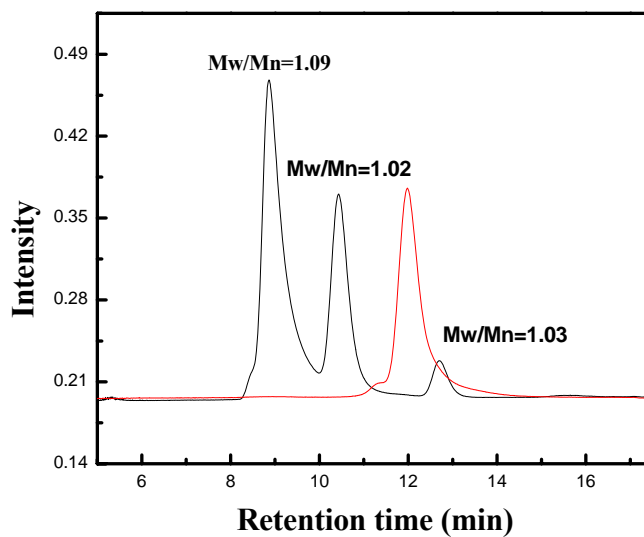
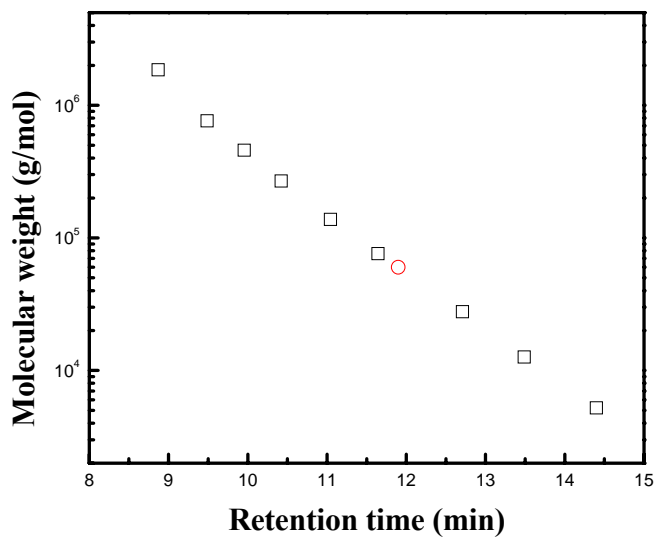


Figure 2.1. <sup>1</sup>H-NMR of synthesized PDMAEMA in CDCl<sub>3</sub>



(a)



(b)

Figure 2.2. (a) GPC results of standard PMMAs and synthesized PDMAEMA: PMMAs (black line) and PDMAEMA (red line) and (b) A plot of molecular weight versus retention time: PMMAs (black squares) and PDMAEMA (red circle)

### 2.3.3 SANS results

#### 2.3.3.1 Dilute PDMAEMA solutions

The binding of SDS to PDMAEMA has been investigated as a function of SDS concentration in dilute polymer solution by several authors.<sup>39, 43</sup> It was found that three different transitions occur during the binding process, e.g., (1) at very low concentrations, a non-cooperative PDMAEMA monomer/SDS binding, (2) above the CAC, there is hydrophobically driven cooperative formation of PDMAEMA/SDS micelles, and (3) the onset of formation of free SDS micelles at the saturation concentration.<sup>43</sup> In transition (2), the structure of PDMAEMA/SDS micelles has been studied using SANS.<sup>39</sup> In that work, PDMAEMA in water was regarded as a neutral polymer at a pH of 8.6<sup>43</sup> or 9.1<sup>39</sup>. PDMAEMA can be charged in water depending on pH. Several authors have investigated the charge behavior of PDMAEMA using proton titrations.<sup>35, 36</sup> They found that the conjugate acid of the tertiary amine of PDMAEMA has a  $pK_a \sim 7$ . In Figure 2.3, black squares and red circles represent SANS intensity of 10 mg/ml PDMAEMA solutions in pure D<sub>2</sub>O at the natural pH 8.5 and acidified D<sub>2</sub>O at pH 5.9. At pH 8.5 and pH 5.9, the portion of charged amines per PDMAEMA chain was about 3% and 92 %, calculated from the Henderson-Hasselbalch equation<sup>44</sup> using a  $pK_a$  of 7. The SANS intensity of both polymer solutions decreases in the  $q$  region below  $0.03 \text{ \AA}^{-1}$  resulting in a peak at about  $q \sim 0.03 \text{ \AA}^{-1}$ . The measured SANS intensity in the low  $q$  region deviates from a Debye function (which describes the form factor of a neutral linear polymer in a dilute polymer solution).<sup>16, 45</sup>

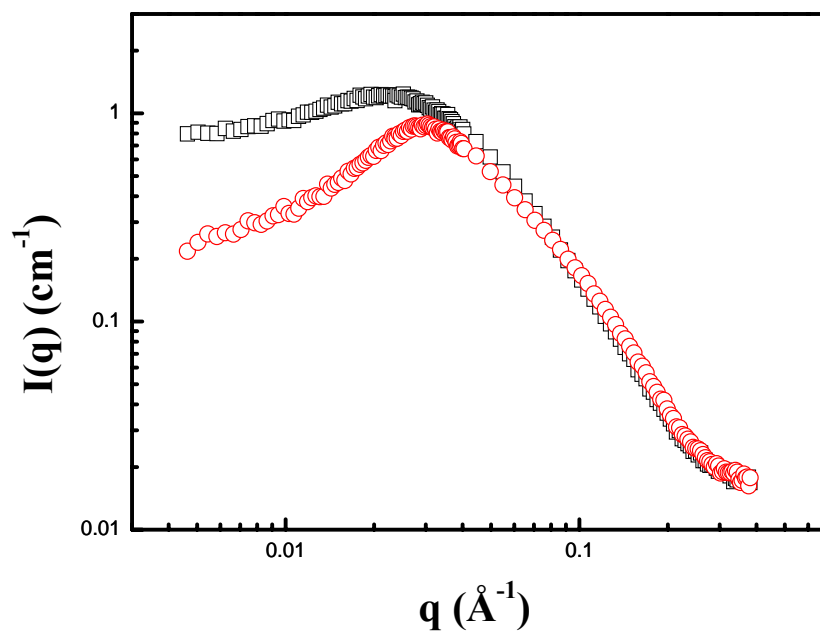


Figure 2.3. SANS of 10 mg/ml PDMAEMA solutions in pure  $\text{D}_2\text{O}$  (black squares) and acidified  $\text{D}_2\text{O}$  (red circles)

The broad peak in the scattered intensity is characteristic of polyelectrolyte solutions and the peak position is generally a function of polymer concentration.<sup>46-48</sup> In general, the scattering peak is thought to result from strong interactions of unscreened charges along the polyelectrolyte chain such that the dynamics are dominated by intra and inter-chain electrostatic interactions.<sup>47</sup>

In contrast to the measured SANS intensity for 10 mg/ml PDMAEMA solutions in pure D<sub>2</sub>O at pH 8.5 and acidified D<sub>2</sub>O at pH 5.9, the SANS intensity of Cosgrove, et al.<sup>39</sup> (for 15,500 ppm PDMAEMA solution in pure D<sub>2</sub>O at pH 9.1 and acidified D<sub>2</sub>O at pH 2.0) showed monotonically decreasing scattering and were fit using a Debye function. From their fits, it was concluded that the size of the charged polymer in acidic D<sub>2</sub>O is nearly twice that measured in pure D<sub>2</sub>O due to repulsive electrostatic interactions expanding the charged polymer. Many parameters such as PDMAEMA concentration, the solubility of CO<sub>2</sub> in pure D<sub>2</sub>O, the quality of D<sub>2</sub>O and so on<sup>44</sup>, can affect pH of PDMAEMA solution, resulting variable charge density of the PDMAEMA in pure D<sub>2</sub>O. However, the effect is minimized at acidic D<sub>2</sub>O. Despite of the lower charge density for PDMAEMA at pH 5.9 compared to PDMAEMA at pH 2.0, our SANS intensity shows a peak characteristic of polyelectrolyte solutions. One possible explanation for this discrepancy might be the fact that our q range is extended to significantly lower q compared to the data of Cosgrove et al. They only published data to  $q_{\min} \sim 0.02 \text{ \AA}^{-1}$  which may not have allowed them to observe the scattering peak.

### 2.3.3.2 Dilute PDMAEMA solutions with d-SDS ( $0.0 \text{ mM} \leq [\text{d-SDS}] \leq 1.3 \text{ mM}$ )

Figure 2.4 shows the SANS intensity of 10 mg/ml PDMAEMA solutions with d-SDS in pure D<sub>2</sub>O as a function of d-SDS concentration. As d-SDS concentration increases, the SANS intensity in the low q region increases, but does not change in the high q region. When 1.3 mM d-SDS was added to a 10 mg/ml PDMAEMA solution, the SANS intensity changed to a monotonic decreasing function of angle. Since the portion of charged amines per PDMAEMA chain in D<sub>2</sub>O at pH 8.5 is 3 %, ~1.9 mM amine groups in 10 mg/ml PDMAEMA solution are charged. The value is very close to 1.3 mM d-SDS, causing the broad peak in the SANS intensity of 10 mg/ml PDMAEMA solution in D<sub>2</sub>O to disappear. This observation that the change in SANS intensity was induced by the electrolyte nature of d-SDS was confirmed by measuring the SANS intensity of a 10 mg/ml PDMAEMA solution in D<sub>2</sub>O containing 3 mM NaCl. The broad peak disappeared, as shown as sky blue stars in Figure 2.4. Our finding is the same as reported by Amis et al<sup>48</sup> who measured a similar system based on poly(2-vinylpyridine) (P2VP). In their work, P2VP was partially quaternized with dimethyl sulfate in dimethylformamide. Three separate polymer solutions in deuterated ethylene glycol were measured using SANS: a neutral polymer solution, a polyelectrolyte solution without added electrolyte, and a polyelectrolyte solution with an excess of electrolyte. They found that a broad peak in the SANS for a polyelectrolyte solution without electrolyte disappeared by adding excess electrolyte and the observed scattering profile was nearly identical to the neutral polymer, and concluded that the unusual scattering found in the SANS of polyelectrolyte solutions is electrostatic in nature. Our SANS results indicate that

PDMAEMA at our experimental conditions is weakly charged in pure D<sub>2</sub>O and that the added d-SDS surfactant acts as an electrolyte, which effectively screens the long range electrostatic interactions between charged PDMAEMA monomers. Additional evidence of the weak charge density of PDMAEMA in pure D<sub>2</sub>O is that all solutions studied within the d-SDS concentration were optically transparent which is in contrast to most polycationic/anionic surfactant mixtures. In general, when anionic surfactants are added to strongly charged polycationic solutions, a number of thermodynamic states are observed depending on the ratio of the total charge of anionic surfactants to the total charge of the polyelectrolyte.<sup>49</sup> As the ratio increases, the clear solution turns cloudy due to the formation of large polyelectrolyte/surfactant aggregates. When the ratio is close to 1, precipitates due to charge neutralization are generally observed. As an excess of the anionic surfactant is added, the solution then appears transparent again. The SANS intensity measured after the charge screening did not fit the Debye function as D<sub>2</sub>O is not a theta solvent for PDMAEMA at 25 °C, which is consistent with the power law dependence of I(q) vs q deviating from -2.0<sup>16, 45</sup> (observed -2.13). Among the binding mechanisms of SDS and PDMAEMA in 0.2% w/v solutions with SDS at pH 8.6, it has been suggested by Holzwarth et al,<sup>43</sup> that a non-cooperative process results in PDMAEMA/SDS complexes containing unassociated dodecylsulfate (DS<sup>-</sup>) ions attached to the PDMAEMA chain below the CAC (~2.5 mM). It is pointed out that the major change in SANS data in Figure 2.4 are observed at a similar concentration of d-SDS although the authors attributed the non-cooperative binding to charge-dipole interactions with entropic effects as they ignored the charge density of PDMAEMA.

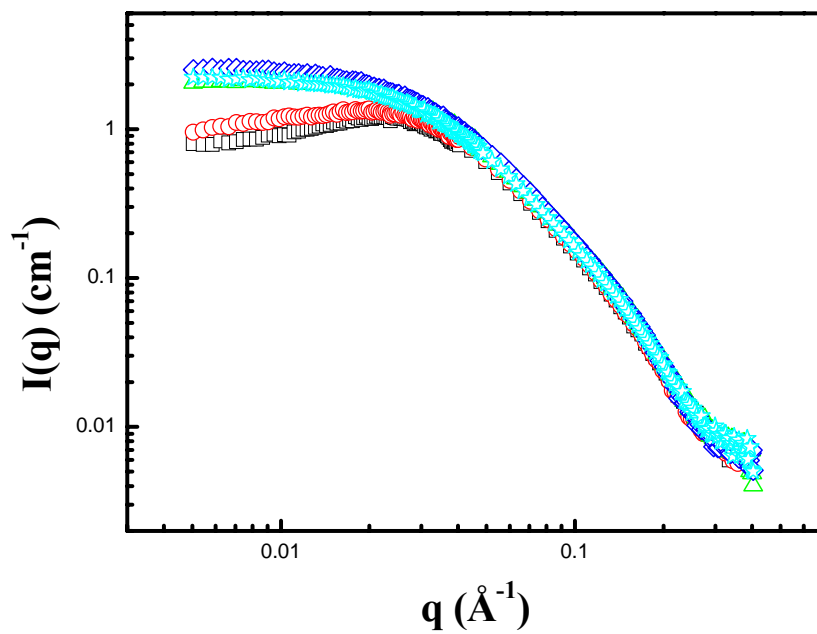


Figure 2.4. SANS of 10 mg/ml PDMAEMA solutions with d-SDS in pure D<sub>2</sub>O: 0.0 mM d-SDS (black squares), 0.15 mM d-SDS (red circles), 0.4 mM d-SDS (green triangles), 1.3 mM d-SDS (blue diamonds), and 3 mM NaCl (sky blue stars)

However, we believe the binding of PDMAEMA/d-SDS below 1.3 mM d-SDS is ascribed to charge-charge interactions, as shown in the SANS intensity. To observe the effect of the surfactant binding on the PDMAEMA chain conformation, the radius of gyration ( $R_g$ ) of a neutral PDMAEMA chain in  $D_2O$ , resulting from adding d-SDS or NaCl, was determined from Guinier analysis of the SANS data.<sup>14, 16</sup> There was a negligible difference in the  $R_g$  of the screened PDMAEMA chain ( $\sim 45 \text{ \AA}$  vs.  $41 \text{ \AA}$ ) in the presence of d-SDS or NaCl, meaning that the total amount of bound  $DS^{-1}$  is too small to induce a large change of PDMAEMA chain conformation.

### **2.3.3.3 Dilute PDMAEMA solutions with d-SDS ( $3 \text{ mM} \leq [\text{d-SDS}] \leq 48 \text{ mM}$ )**

An important property of ionic surfactants compared to other electrolytes is the hydrophobic effect which causes the surfactants to form micelles above their CMC in pure water. In general, during the micellization of surfactants in water, water molecules which are bound to the long hydrophobic tail of a free surfactant molecule are released, leading to increase in the entropy of the system. However, the formation of micelles is opposed due to unfavorable interactions of the charged headgroups which are in close proximity in a micelle. Micellization accompanies the generation of an interface between the hydrophobic core of the micelle and water. In addition, the micellization results in the polar head groups of the surfactants being brought into close proximity of one another at the micelle-water interface. This gives rise to steric repulsions among the head groups. Therefore, the formation of micelles is controlled by the interplay of these thermodynamic relationships. In case of ionic surfactants, the repulsive forces between charged headgroups additionally oppose their micellization.

As a result, ionic surfactants usually have higher CMCs compared to nonionic surfactants with the same length of alkyl chains, often by several orders of magnitude in concentration.<sup>50</sup>

It is often observed that when anionic surfactants are added to a neutral polymer solution in water and the polymer interacts with the surfactants, micelles are wrapped by the polymer chains.<sup>29, 32-34</sup> Nagarajan proposed two favorable energy terms for the formation of polymer/SDS complexes: a decrease in the hydrophobic interface of the micelle exposed to water, and the removal of the hydrophobic parts of the polymer and its transfer to a hydrophobic surface of the micellar core.<sup>51-53</sup> In order to investigate the effect of d-SDS around its CMC on PDMAEMA chain conformation, we further increased the d-SDS concentration. SANS intensity of 10 mg/ml PDMAEMA solutions in D<sub>2</sub>O with d-SDS between 3 mM and 48 mM is shown in Figure 2.5. The overall SANS intensity decreased as the d-SDS concentration increases, with the decrease of intensity in the low q range being larger, resulting in a peak in the SANS intensity. The change in the SANS intensity indicates that the added d-SDS induced a large change in the PDMAEMA conformation. Since the neutron scattering length density of d-SDS surfactant ( $6.736 \text{ \AA}^{-2} \cdot 10^{-6}$ )<sup>54</sup> is close to the neutron scattering length density of D<sub>2</sub>O ( $6.34 \text{ \AA}^{-2} \cdot 10^{-6}$ ), d-SDS micelles in D<sub>2</sub>O polymer solutions are invisible to neutrons.<sup>33, 34, 39, 55, 56</sup> However, it is unclear whether d-SDS micelles in D<sub>2</sub>O polymer solutions remain contrast matched when d-SDS micelles incorporate hydrogenated polymer segments, as it can cause a large change in the neutron scattering length density of the resultant mixed micelles.

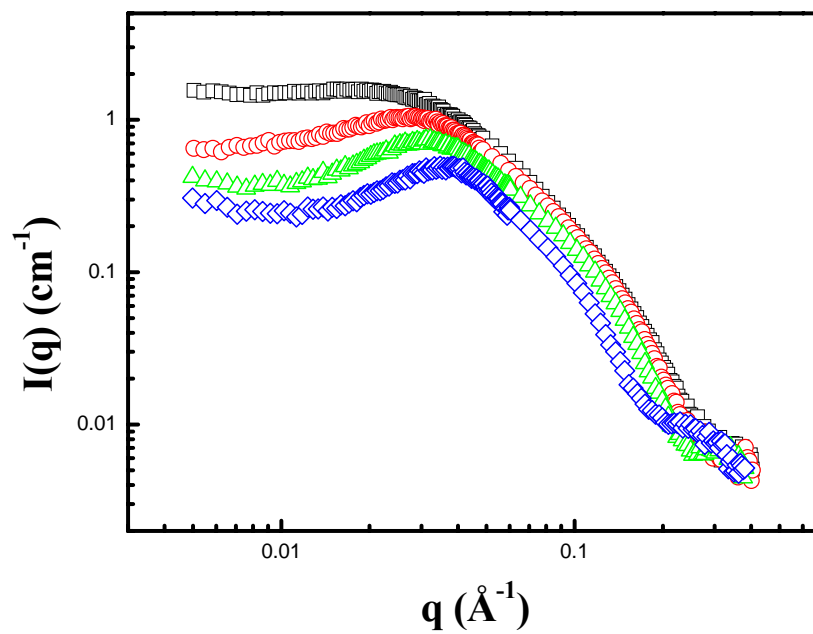


Figure 2.5. SANS of 10 mg/ml PDMAEMA solutions with d-SDS in pure  $\text{D}_2\text{O}$ : 3.0 mM d-SDS (black squares), 6.0 mM d-SDS (red circles), 12 mM d-SDS (green triangles), and 48 mM d-SDS (blue diamonds)

Although we cannot clearly distinguish whether PDMAEMA segments wrapping d-SDS micelles or mixed micelles containing PDMAEMA segments cause the observed peak in the SANS intensity in Figure 2.5, we can conclude that PDMAEMA interacts with d-SDS micelles since both scenarios require the participation of PDMAEMA segments in the d-SDS micellization process. Due to the surface charge of the micelle, the micelles interact through long-range electrostatic repulsive interactions which results in a relatively regular distance between micelles. The peak in the SANS intensity reflects this ordering of charged micelles coupled with the PDMAEMA chains. It is emphasized that the characteristic peak begins to appear at 10 mg/ml PDMAEMA solution and 3 mM d-SDS, which is less than the normal SDS CMC (ca. 8.3 mM<sup>31</sup>). The result also means that PDMAEMA interacts with d-SDS to make micellization more favorable. Since the peak position shifts to higher  $q$  region as the added d-SDS concentration increases, more micelles seem to be formed along PDMAEMA chains. A change of the peak position ( $q^*$ ) is plotted in Figure 2.6 as a function of the true moles of d-SDS (= the  $[d\text{-SDS}] - [\text{CAC}]$ ) to the moles of PDMAEMA chain. Here, the CAC uses was 2.5 mM as measured by Holzwarth et al.<sup>43</sup> With the assumption that d-SDS surfactants are evenly distributed among the PDMAEMA chains, the ratio represents the number of d-SDS surfactants per PDMAEMA chain. The ratio is also helpful to understand how micellization occurs in PDMAEMA/d-SDS solutions, since the ratio can give information about the number of micelles per PDMAEMA chain when the ratio is divided by the aggregation number of d-SDS per micelle.

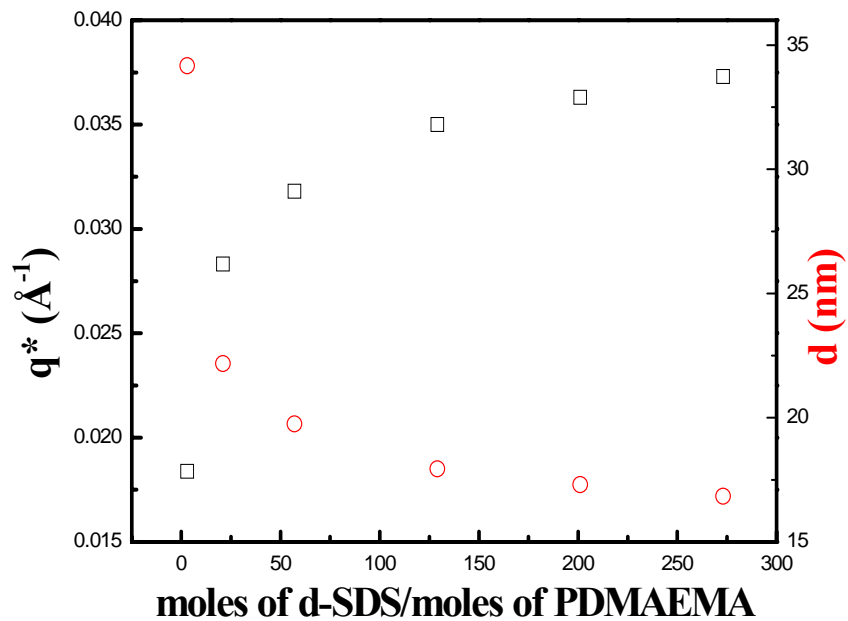


Figure 2.6. A change of the SANS peak position ( $q^*$ ) (black squares) and the calculated distance between charged micelles ( $d$ ) (red circles) as a function of the ratio of moles of d-SDS to moles of PDMAEMA chain

As mentioned before, the origin of the peak is a liquid-like ordering of charged micelles due to electrostatic repulsive interactions between charged micelles. From the peak position, the average distance of micelles ( $d$ ), using a relationship of  $q^* = 2\pi/d$ , can be estimated. It is interesting that when the ratio is 3, the peak was observed at  $q^* = 0.018 \text{ \AA}^{-1}$  which corresponds to 34 nm. It is not reasonable that only 3 d-SDS molecules can form a micelle, which implies that d-SDS surfactants are not evenly distributed among the PDMAEMA chains. Rather, d-SDS surfactants are localized to some PDMAEMA chains in order to form complete micelles, as micelles are energetically favorable compared to individual d-SDS surfactants due to the shielding of the non-polar hydrocarbons from water. Since  $d$  is much larger than  $R_g$  of a neutral PDMAEMA chain in  $D_2O$ , the scattering peak represents the interparticle scattering from PDMAEMA/d-SDS complexes. The observed peak position shifts to higher  $q$  until the ratio reaches 273, which is well-above the aggregation number of d-SDS per micelle in water<sup>34</sup> of  $\sim 70$ . At a ratio of 273, every PDMAEMA chain can contain  $\sim 3.9$  d-SDS micelles if we assume that the aggregation number of d-SDS per micelle in the PDMAEMA solution is comparable to that in water. Figure 2.6 shows that the interparticle distance between micelles, calculated from the measured peak positions, decreases as the number of charged micelles increases, similar to a spherical charged particle solutions where  $q$  follows the scaling law,  $q^* \sim N_p^{-n}$ , with  $n = 1/3$ , where  $N_p$  is the number of particles in solutions. This corresponds to a simple volume expansion of the interparticle distance with decreasing particle number.<sup>46, 57-59</sup> However, this distance scale should not be over-interpreted for our case as the scattering from the free PDMAEMA chain segments connecting micelles

overlaps in the  $q$  region. Nevertheless, it is pointed out that the spacing between charged micelles in the solution is much larger than the  $R_g$  of a neutral PDMAEMA chain in  $D_2O$ . This result indicates that as charged micelles are formed along a PDMAEMA chain, the occupied volume of the polymer changes to minimize electrostatic repulsive interactions between charged micelles.

#### **2.3.3.4 Dilute PDMAEMA solutions with d-SDS ( $60 \text{ mM} \leq [\text{d-SDS}] \leq 150 \text{ mM}$ )**

Power law behavior at low  $q$  region has been observed by SANS for the PEO/SDS system<sup>33, 34</sup> and for star-shaped poly(ethylene glycol)/SDS solutions<sup>55</sup> due to repulsive interactions between charged micelles bound to polymer chains. In this work we were interested in examining the PDMAEMA chain conformation as a function of increasing d-SDS concentration. Figure 2.7 shows the SANS intensity of 10 mg/ml PDMAEMA solutions in  $D_2O$  at d-SDS concentration between 60 mM and 150 mM. At 60 mM d-SDS, an upturn appeared in the low  $q$  region and a correlation peak is observed. Above 100 mM d-SDS, the low  $q$  upturn becomes more pronounced and the correlation peak shape is partially hidden. The low  $q$  upturn is probably associated with a change of PDMAEMA chain conformation. It is notable that the SANS intensity shows a power law behavior in both the low  $q$  and high  $q$  regions. In the high  $q$  region, the power law behavior is consistent with a polymer chain in solvent.<sup>14, 16</sup> For example, the exponent should be  $-5/3$  for a fully swollen chain and  $-2$  for a Gaussian chain. When monomers are strongly repulsive, as in polyelectrolytes, the exponent is expected to be  $-1$ .

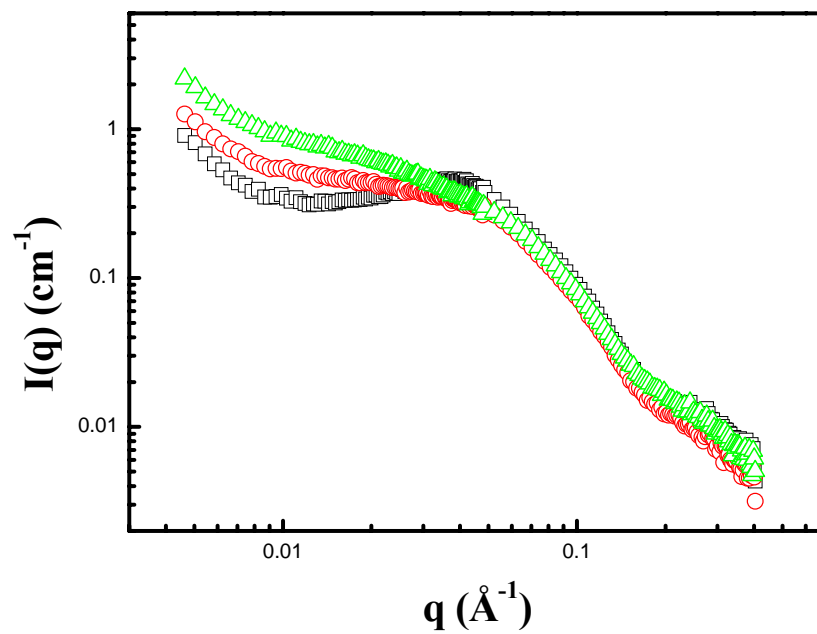


Figure 2.7. (a) SANS of 10 mg/ml PDMAEMA solutions with d-SDS in pure  $\text{D}_2\text{O}$ : 60 mM d-SDS (black squares), 100 mM d-SDS (red circles), and 150 mM d-SDS (green triangles)

The measured exponent in the high  $q$  region is -1.3, between -1 and -5/3 and is quite different from the exponent measured in PDMAEMA solutions without d-SDS (-2.13). It is clear that charged micelles formed along the PDMAEMA chains, where changes the conformation of the chain due to the surface charges on the micelles. Since forming micelles along a PDMAEMA chain is more favorable than free d-SDS micelles, the number of the charged micelles per PDMAEMA chain increases as the d-SDS concentration increases. However, as more micelles are formed, the repulsive interactions between the charged micelles get stronger as the interaction potential between charged surfaces is an exponentially decreasing function with distance.<sup>60-63</sup> The fact that the same exponent is observed in the low  $q$  region indicates that the PDMAEMA chains show the same fractal behavior. In PDMAEMA/SDS solutions, PDMAEMA chains expand as evidenced by the measured exponent. This expansion minimizes the unfavorable interactions between charged micelles and allows the accommodation of more micelles. In PEO/water solutions with ionic surfactants, when micelles are connected by a single PEO chain, an increase in viscosity is observed with increasing surfactant concentration until the polymer chains are saturated with micelles. This can be explained by the expansion of the PEO chains due to electrostatic repulsion between the SDS micelles.<sup>64, 65</sup> In order to understand why the scattering peak seems to disappear above 100 mM d-SDS, the measured SANS intensity was subtracted by  $I(q) = kq^{-1.3}$ . The function was chosen as it is consistent with the scattering in the low  $q$  and high  $q$  regions.  $k$  was selected to minimize the difference in the high  $q$  region. As shown in Figure 2.8, all subtracted

SANS data show a peak. Although the peak gets broader as the d-SDS concentration increases, it should be noted that the shape is dependent on the value of  $k$ .

#### **2.3.3.5 A model fit of 100 mM d-SDS in a 10 mg/ml PDMAEMA solution**

In order to investigate the structure of the micelles, a mixture of 80% H<sub>2</sub>O and 20% D<sub>2</sub>O was used as solvent to contrast match the PDMAEMA chains. The measured SANS intensity of 100 mM d-SDS in 10 mg/ml PDMAEMA solution is shown as black squares in Figure 2.9. Since the correlation peak between the micelles is still observed when PDMAEMA is contrast matched, this supports that the peak in Figure 2.7 was smeared due to the scattering from the PDMAEMA chains interconnecting the micelles. The size and shape of the micelles in solution was obtained by fitting a model for the scattering. Generally, the size of ionic micelles in water is determined by a balance between the area of the micelle-water interface per surfactant molecule and the charged headgroup repulsion per surfactant molecule.<sup>63</sup> The former decreases as the aggregation number of surfactant per micelle increases and favors growth of the micelle. However, the latter increases with an increase in the aggregation number, opposing a growth of the micelle. When electrolytes or polyelectrolytes are added to spherical ionic micelle solutions, the added electrolyte molecules screen the electrostatic repulsions between charged headgroups, leading to the transformation of spherical micelles into ellipsoidal or worm-like micelles.<sup>49, 66, 67</sup> Since PDMAEMA is very weakly charged at normal pH, the SANS intensity was fit to a spherical core-shell model with the rescaled mean spherical approximation (MSA) closure.<sup>60-62</sup> The fit result is shown as a black line in Figure 2.9.

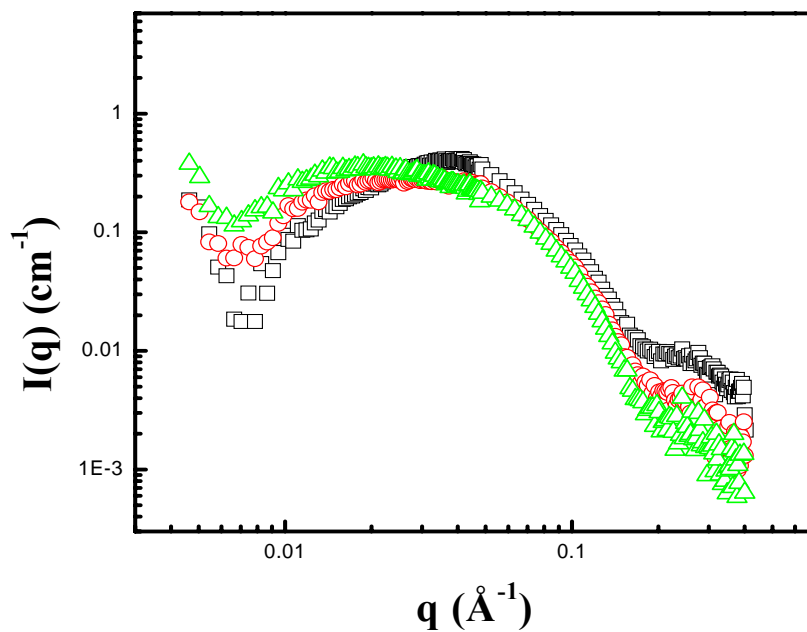


Figure 2.8. SANS intensity of 10 mg/ml PDMAEMA solutions with d-SDS in pure  $\text{D}_2\text{O}$  subtracted by a power law,  $I(q) = kq^{-1.3}$ : 60 mM d-SDS (black squares), 100 mM d-SDS (red circles), and 150 mM d-SDS (green triangles)

The form factor and the structure factor were separated using the model, and are shown as a red and green line, respectively. In the fitting process, the core radius of the micelle was constrained to be less than 16.7 Å, which is the length of a fully extended dodecyl chain of SDS<sup>68</sup>, and the neutron scattering length densities of the core and solvent were fixed at  $6.97 \times 10^{-6} \text{ \AA}^{-2}$  and  $8.2 \times 10^{-7} \text{ \AA}^{-2}$ , respectively. The neutron scattering length density of the core was calculated, assuming that the core is composed of methyl, and methylene groups in d-SDS.<sup>54, 68</sup> However, the scattering length density of the shell was left as a floating parameter to allow the participation of PDMAEMA segments in the micelles. This accounts for PDMAEMA segments incorporated into the shell. In calculating a structure factor, 2.5 mM CAC was used.<sup>43</sup> The core radius and the shell thickness of a spherical SDS micelle wrapped by PDMAEMA obtained from the fit were  $16.7 \pm 0.1 \text{ \AA}$  and  $6.0 \pm 0.1 \text{ \AA}$ , respectively. The scattering length density of the shell was  $3.72 \times 10^{-6} \pm 0.1 \times 10^{-6}$ , implying that water and PDMAEMA segments are incorporated into the shell. The surface charge per micelle was  $15.8 \pm 0.1$ , less than the value of 25 for free SDS micelles in water.

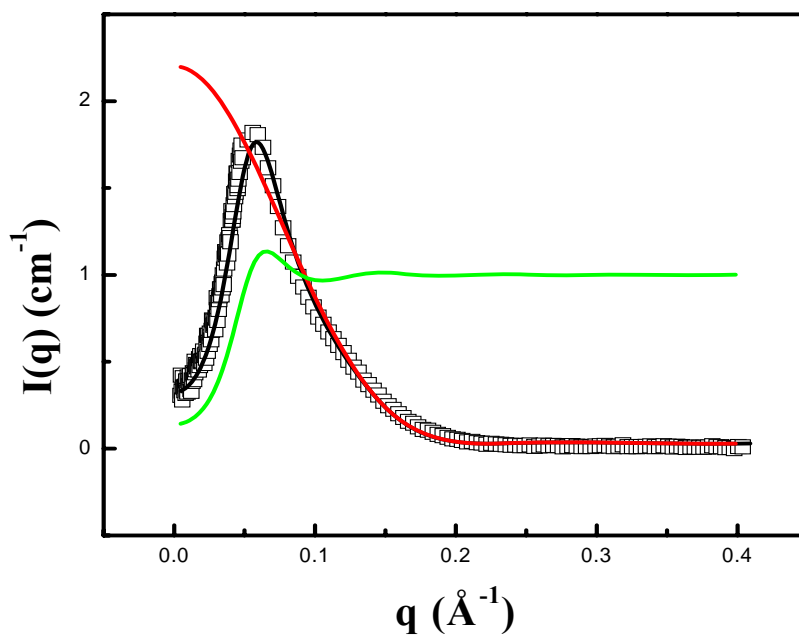


Figure 2.9. SANS intensity of a 10 mg/ml PDMAEMA solution with 100 mM d-SDS where PDMAEMA was contrast-matched to 80% H<sub>2</sub>O and 20% D<sub>2</sub>O (black squares). The black line represents the fit to a core-shell model with the rescaled MSA closure. The form factor and the structure factor are shown as a red line and a green line, respectively.

## 2.4 Conclusions

PDMAEMA with 60,000 g/mol and a narrow polydispersity, 1.12, was synthesized using GTP. The conformation of the synthesized polymer in PDMAEMA/d-SDS solution was investigated as function of d-SDS concentration using SANS. It was observed that when PDMAEMA was dissolved in D<sub>2</sub>O or in acidified D<sub>2</sub>O, the polymer shows polyelectrolyte behavior as the tertiary amines in the chain are charged. The polyelectrolyte behavior can be screened by adding 1.3 mM d-SDS or 3 mM NaCl in the solution, which balances 1.9 mM charged amine groups in a 10 mg/ml PDMAEMA solution. The result indicates that the added d-SDS acts as electrolyte, screening the charges and a neutral PDMAEMA chain conformation is restored. Above 3 mM d-SDS, SANS intensity shows correlation peaks from charged micelles formed along the PDMAEMA chains. d-SDS micellization in the PDMAEMA solution starts below the normal SDS CMC, which indicates that the PDMAEMA chains provide favorable interactions towards d-SDS micellization. As the d-SDS concentration is increased, the observed scattering peak position shifted to high  $q$ , indicating more charged micelles are associating per PDMAEMA chain. This is balanced by the closer the distance between the charged micelles and the resultant stronger repulsive interactions. In spite of the unfavorable repulsive interactions, the charged micelles associate with the PDMAEMA chains in preference to free d-SDS micelles as the unfavorable interactions are relieved by stretching of the PDMAEMA chain, as evidenced by the power law behavior in SANS scattering. The structure of charged micelles in a PDMAEMA/d-SDS solution was investigated at the condition where PDMAEMA was contrast-matched. It was found through a model fit that

spherical micelles are formed in the solution and the neutron scattering length density of the shell calculated from the fit shows that the PDMAEMA segments are incorporated into the micelle to provide shielding to reduce the hydrophobic interface of the micelle exposed to water.

# **Chapter 3: Small angle neutron scattering study of deuterated sodium dodecylsulfate micellization in concentrated poly((2-dimethylamino)ethyl methacrylate) solutions**

In order to create poly((2-dimethylamino)ethyl methacrylate) (PDMAEMA) hydrogels containing micelles, the polymer solution should be semi-dilute before crosslinking. Since micelles are thermodynamic objects, the size and shape of micelles needs to be investigated as a function of PDMAEMA concentration as it is related to the size and shape of the pores generated after removing micelles in the corresponding hydrogel. In this chapter, we will present small angle neutron scattering (SANS) results of sodium dodecylsulfate (SDS) micellization in PDMAEMA solutions using H/D contrast variation method and the model fit results will be discussed.

## **3.1 Introduction**

When ionic surfactants are added to a polymer solution in water, polymer/surfactant complexes are formed due to specific interactions between the components. The structure of these complexes is highly dependent on whether the polymer is neutral or charged.<sup>29, 30</sup> For a mixture of neutral polymer and ionic surfactant in solution, such as the poly(ethylene oxide) (PEO)/SDS system, spherical micelles are formed along

the polymer chain, which is called a necklace-like structure.<sup>29, 32-34, 40, 64</sup> Since the micellization is assisted by polymer segments, the polymer conformation is governed by the micelles, causing the polymer chains to expand due to electrostatic repulsive interactions between charged micelles.<sup>33, 34, 40, 64</sup> When a positively charged polyelectrolyte solution is mixed with an anionic surfactant, growth of anionic micelles from spheres to cylinders or lamellae is observed as the positive charge of polyelectrolyte screen the electrostatic repulsion between the anionic head groups in the micelles.<sup>69-72</sup> Although a growth of spherical micelles is also induced by the addition of an electrolyte to anionic micelle solutions,<sup>66, 67, 73, 74</sup> the micelles in the polyelectrolyte solution are connected to each other by polyelectrolyte chains, resulting in various hierarchical structures. Sometimes, the complexes precipitate from the solution when the charges are neutralized. It has been suggested to create structured hydrogels where are templated using micelles by crosslinking monomers or polymers in monomer/surfactant solutions or in polymer/surfactant solutions for applications as separation materials.<sup>10-13</sup> PDMAEMA is one of promising polymers to achieve this goal since it is possible to crosslink the polymer in water through the Menshutkin reaction between a dihalide and two tertiary amines.<sup>37, 38</sup> We have demonstrated that in a dilute PDMAEMA solution, SDS interacts with PDMAEMA to form the necklace-like structure, (similar to PEO/SDS), as PDMAEMA is only weakly charged in pure D<sub>2</sub>O. In order to create a structured hydrogel templated using micelles, the solution should be semidilute before crosslinking. It has been reported that the micellization of SDS in PEO solutions is affected by the PEO concentration and the SDS concentration as three different regions exist in the phase diagram.<sup>29, 31</sup>

As visualized in the phase diagram developed by Cabane and Duplexsix<sup>33</sup>, starting from a pure PEO solution, the first SDS surfactants added dissociate into free unassociated dodecylsulfate ( $DS^{-1}$ ) and  $Na^{+}$  ions and remain unassociated below the critical aggregation concentration (CAC), which is insensitive to polymer concentration. At the CAC, the chemical potential of the isolated  $DS^{-1}$  ions becomes equal to that of  $DS^{-1}$  ions in PEO/SDS complexes. The SDS added beyond the CAC form PEO/SDS complexes. This association continues until the PEO chains are saturated with SDS micelles. After this point, the additional SDS surfactant again dissociates into free ions until it reaches the critical micelle concentration (CMC). Finally, the solution contains PEO/SDS complexes and free SDS micelles and ions. Although the behavior of SDS micellization in PEO solution was investigated by many authors, whether the aggregation number of SDS per micelle in polymer/SDS solutions is maintained or not, regardless of polymer concentration, is ambiguous as the phase behavior is generally studied by conductivity, surface tension, and viscosity.<sup>29, 31</sup> SANS is a powerful tool to investigate the micellization of SDS in polymer solutions since it is possible to distinguish scattering between polymer and micelle using H/D contrast-matching methods.<sup>14, 16</sup> From the SANS data, the size and shape of the micelles can be obtained using a modeling. Recently, SDS micellization in poly(propylene oxide) methacrylate (PPOMA) solutions was investigated using SANS.<sup>70</sup> They have found that as the PPOMA concentration increases, the SDS aggregation number per micelle decreases as more PPOMA participates in the micellization. When it comes forming to a structured hydrogel templated with micelles, the size and shape of the micelles in the polymer solution before

crosslinking is crucial since it is related to the size and shape of the pores generated after removing micelles in the corresponding hydrogel. In this work, we have studied the micellization of SDS as a function of PDMAEMA concentration using H/D contrast matching methods with SANS.

### 3.2 Experimental

For SANS measurements, D<sub>2</sub>O and deuterated SDS (d-SDS) were purchased from Cambridge Isotope Laboratories, Inc. and, hydrogenated SDS (h-SDS) was purchased from Aldrich. PDMAEMA of 60,000 g/mol with 1.12 PDI was synthesized using group transfer polymerization. A series of PDMAEMA solutions in D<sub>2</sub>O with desired SDS concentrations were prepared by mixing two stock solutions: PDMAEMA solution and SDS solution. The shape of d-SDS micelles formed in solution was observed at the H<sub>2</sub>O/D<sub>2</sub>O ratio where the PDMAEMA was contrast-matched (80% H<sub>2</sub>O / 20% D<sub>2</sub>O). Each solution was kept in a demountable titanium sample cell with a 1 mm or 2 mm path length for SANS measurement. SANS experiments were carried out at the Center for Neutron Research at the National Institute of Standards and Technology on the 30 m NIST-NG7 instrument.<sup>41</sup> The raw data were corrected for scattering from the empty cell, incoherent scattering, detector dark current, detector sensitivity, sample transmission, and thickness. Following these corrections the data were placed on an absolute scale using a direct beam measurement and circularly averaged to produce I(q) versus q plots where I(q) is the scattered intensity and q is the scattering vector ( $q=4\pi\sin\theta/\lambda$ ). The q range was 0.005–0.40 Å<sup>-1</sup> and the neutron wavelength was 6 Å with a wavelength spread  $\Delta\lambda/\lambda=0.11$ .

### 3.3 Theory

In general, the SANS intensity of charged spherical micelles can be described in terms of a form factor  $P(q)$  and a structure factor  $S(q)$ .<sup>14</sup>

$$I(q) = n_p P(q) S(q) \quad (3.1)$$

where  $n_p$  is the number density of charged spherical micelles. The form factor  $P(q)$  depends on the shape of the scattering particles. Because micelles are formed in water due to the hydrophobic effect,<sup>63</sup> the chemical composition of the hydrophobic core and the hydrated shell are quite different, resulting in different neutron scattering length densities of the core and the shell. A spherical micelle, as shown in Figure 3.1, can be considered a spherical core-shell system where  $P(q)$  is described by<sup>14, 75</sup>

$$P(q) = \left( V_1 (\rho_1 - \rho_2) f_0(qR_1) + V_3 (\rho_2 - \rho_0) f_0(qR_3) \right)^2 \quad (3.2)$$

with  $f_0(x) = 3(\sin x - x \cos x) / x^3$ .  $\rho_1$ ,  $\rho_2$  and  $\rho_0$  represent neutron scattering length densities of the core, the shell, and solvent, respectively. The volumes of the core  $V_1$  and of the whole micelle  $V_3$  are calculated from the radius of the core  $R_1$  and the external radius  $R_3$ .

In the Hayter and Penfold model<sup>68</sup>, which describes single-chain surfactants comprising an alkyl chain  $CH_3(CH_2)_n$ , a head group  $HG^\pm$  and a counterion  $CI^\mp$ , the dry core of radius  $R_1$  has its methyl group and a fraction  $\alpha$  of its methylene groups. The remaining methylenes, the hydrated headgroups and any non-ionized hydrated counter ions are distributed uniformly in the shell, while the methyl distribution in the

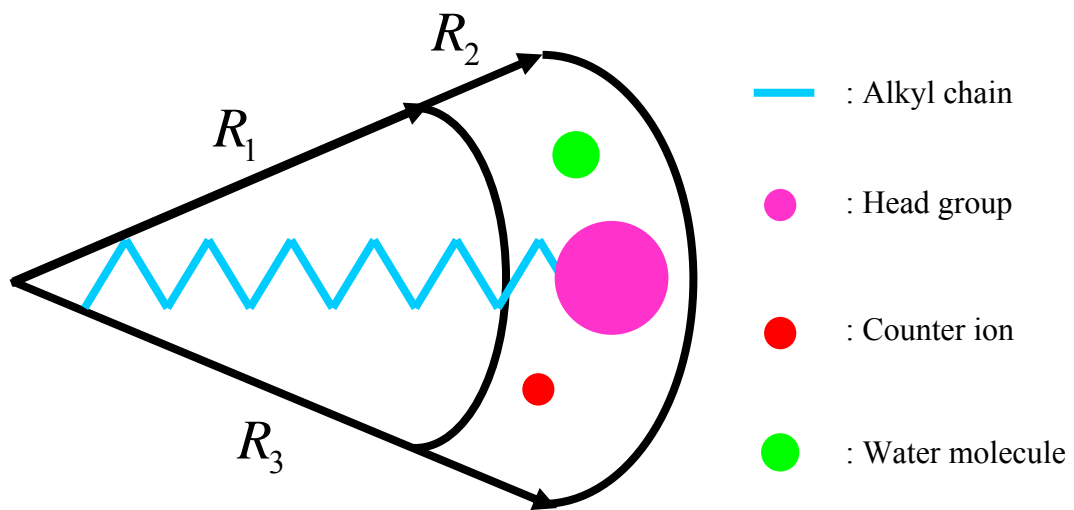


Figure 3.1. A schematic of a spherical core-shell micelle of mean radii  $R_1$  and  $R_3$

core is taken as random. In the model, the micelle geometry is calculated for a given aggregation number  $\nu$  and a given degree of ionization  $\delta$  as follows. First, the radius of the sphere, which contains all of the hydrocarbons, is calculated by the relationship:

$$R_h = \left[ 3\nu(V_{CH_3} + nV_{CH_2}) / 4\pi \right]^{1/3} \quad (3.3)$$

where  $n$  is the number of methylene groups in the surfactant, and  $V_{CH_3}$  and  $V_{CH_2}$  are the volumes of the methyl and methylene groups, respectively. If  $R_h \leq l_c$ , they set  $\alpha = 1$  and take  $R_1 = R_h$ . Otherwise, they set  $R_1 = l_c$  and calculate  $\alpha = (V_1 - \nu V_{CH_3}) / n\nu V_{CH_2}$  where  $V_1 = 4\pi R_1^3 / 3$ . Here,  $l_c$  is the length of the hydrocarbon chain and is taken as  $0.2765 + 0.1265 n$  (nm). From the total volume,

$$V_3 = \nu \left[ V_{CH_3} + nV_{CH_2} + V_{HG} + \omega_{HG}V_S + (1 - \delta)(V_{CI} + \omega_{CI}V_S) \right] \quad (3.4)$$

$R_3 = (3V_3 / 4\pi)^{1/3}$  is obtained, where  $V_S$  is the volume of a solvent molecule in the head group or counter ion hydration shell. The remaining required parameters are the volume of the head group  $V_{HG}$  and hydration number  $\omega_{HG}$  of the head group, together with the corresponding values  $V_{CI}$  and  $\omega_{CI}$  for the counter ion. Table 3.1 shows volumes of chemical groups ( $V$ ) and hydration numbers ( $\omega$ ) used in the data analysis.<sup>68</sup>

The structure factor  $S(q)$  represents a correlation between charged micelles and can be calculated from the interparticle potential that determines the equilibrium arrangement of charged micelles. The interaction between identical charged spherical

micelles of radius  $R_3$  can be described by a screened coulomb interaction potential  $U(r)$  as follows<sup>61-63</sup>:

$$U(r) = \frac{z_m^2}{4\pi\epsilon_0\epsilon(1+\kappa R_3)^2} \exp[-\kappa(r-2R_3)]/r \quad \text{for } r > 2R_3 \quad (3.5)$$

where  $r$  is a center-to-center distance.  $z_m$  is the charge on the micelle,  $\epsilon_0$  is the permittivity of free space,  $\epsilon$  is the dielectric constant of the solvent, and  $\kappa$  is the Debye-Hückel inverse screening length. The structure factor of charged spherical micelles is calculated for a given micellar charge and ionic screening using the mean spherical approximation (MSA) given by Hayter and Penfold when a volume fraction of scattering objects is sufficiently large. For smaller volume fractions, a rescaled MSA model was proposed which introduced a rescaled radius larger than the radius  $R_3$ .<sup>60</sup>

Table 3.1. Volumes of chemical groups ( $V$ ) and hydration numbers ( $\omega$ ) used in the data analysis. The values were adopted from the Hayter and Penfold model.<sup>68</sup>

Chemical group	$V$ (nm <sup>3</sup> )	$\omega$
$CH_3$	0.0543	
$CH_2$	0.0248	
$SO_4^-$	0.0606	5
$Na^+$	0.0136	6
$D_2O$	0.0302	
$H_2O$	0.0299	

## 3.4 Results

### 3.4.1 Concentrated PDMAEMA solutions with 100 mM h-SDS or d-SDS

Figure 3.2 shows the SANS intensity of 100 mM h-SDS in D<sub>2</sub>O as a function of PDMAEMA concentration. For comparison, the SANS intensity of 100 mM h-SDS in D<sub>2</sub>O (black squares) was also measured. In our ternary system, SANS intensity can be expressed in terms of three partial structure factors  $S_{ij}(q)$ , where the subscripts  $i$  and  $j$  refer to PDMAEMA (P) and SDS (S).<sup>15</sup>

$$I(q) \sim \left[ (\rho_P - \rho_0)^2 S_{PP}(q) + (\rho_S - \rho_0)^2 S_{SS}(q) + (\rho_P - \rho_0)(\rho_S - \rho_0) S_{PS}(q) \right] \quad (3.6)$$

Here,  $\rho_P$  and  $\rho_S$  are neutron scattering length densities of the polymer and surfactant, respectively. Since neutron scattering lengths of H and D atoms are different, the scattering contrast can be enhanced (or varied) through isotopic labeling. Table 3.2 shows neutron scattering length densities of PDMAEMA<sup>76</sup>, h-SDS<sup>54</sup>, d-SDS<sup>54</sup>, D<sub>2</sub>O and H<sub>2</sub>O. In Figure 3.2, the overall intensity increases as the PDMAEMA concentration increases. The measured SANS intensity shows a characteristic peak from the h-SDS micelles and the peak position has shifted to higher  $q$  with increasing PDMAEMA concentration (h-SDS concentration was fixed at 100 mM in all the solutions). In general, a shift of the position of the correlation peak to higher  $q$  represents a decrease of the inter-distance between particles in the solution. In our case, it can be understood that the number density of h-SDS micelles in the solution increases due to a decrease of the CAC or the aggregation number per micelle, as the polymer concentration increases.

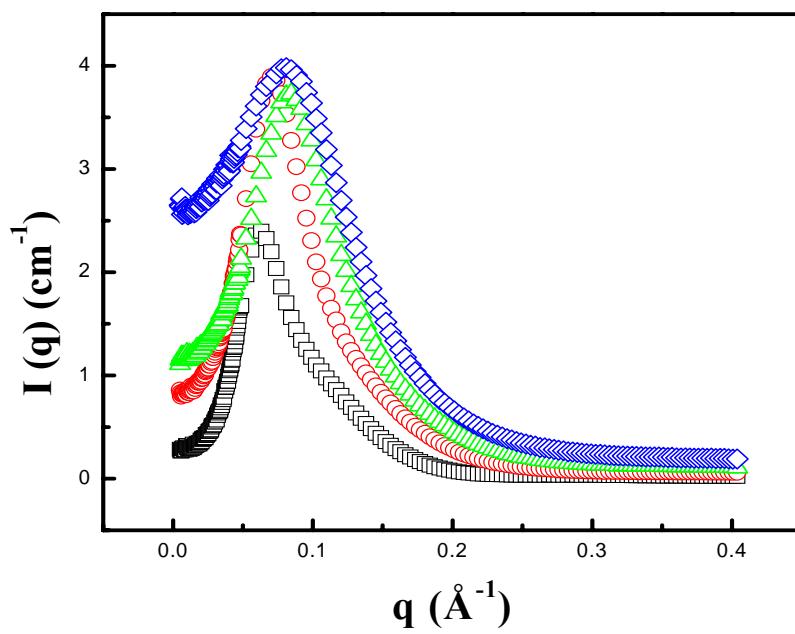


Figure 3.2. SANS of PDMAEMA solutions with 100 mM h-SDS in pure  $\text{D}_2\text{O}$ : no polymer (black squares), 50 mg/ml PDMAEMA (red circles), 100 mg/ml PDMAEMA (green triangles) and 200 mg/ml PDMAEMA (blue diamonds)

Table 3.2. Neutron scattering length densities of the molecules used in this work

Molecule	$\rho$ ( $\text{\AA}^{-2} \cdot 10^{-6}$ )
PDMAEMA <sup>76</sup>	0.8
h-SDS <sup>54</sup>	0.389
d-SDS <sup>54</sup>	6.736
D <sub>2</sub> O	6.34
H <sub>2</sub> O	-0.56
80%H <sub>2</sub> O/20%D <sub>2</sub> O	0.82

Both require favorable interactions between the h-SDS and the PDMAEMA.<sup>51-53</sup> Although binding of SDS to PDMAEMA and the structure of SDS micelles in a dilute PDMAEMA solution has been observed by many authors,<sup>39, 43</sup> (including our group), the origin of the change in SANS intensity in Figure 3.2 needs further clarification since the SANS intensity is composed of three components, as shown in equation (3.6). In order to understand the measured SANS intensity in Figure 3.2, h-SDS surfactants were replaced with d-SDS surfactants to vary the SANS intensity. Since the neutron scattering length density of d-SDS surfactant is very close to that of D<sub>2</sub>O, d-SDS micelles can be considered as contrast-matched to D<sub>2</sub>O.<sup>33, 34, 39, 55, 56</sup> Figure 3.3 shows SANS intensity of PDMAEMA solutions with 100 mM d-SDS in D<sub>2</sub>O. The measured SANS intensity increases with the PDMAEMA concentration and all curves show a peak. The peak position shifts to high  $q$  as the PDMAEMA concentration increases, similar to the behavior observed in Figure 3.2. Since SANS intensity from the PDMAEMA solutions without d-SDS in D<sub>2</sub>O shows a monotonically decreasing function with angle, the observed peak indicates that d-SDS micelles wrapped by PDMAEMA chains are formed in the concentrated PDMAEMA solutions. The shift of a peak position to high  $q$  region means there is a smaller distance between d-SDS micelles as PDMAEMA concentration increases. This requires a decrease in the aggregation number per micelle as the CAC in a polymer solution is usually insensitive to polymer concentration.<sup>29, 31, 33</sup> When it comes to contrast-matching PDMAEMA/d-SDS solutions, it is questionable whether d-SDS micelles remain invisible in D<sub>2</sub>O as the solvent. Although scattering from d-SDS micelles in pure D<sub>2</sub>O is negligible,<sup>70</sup> when d-SDS micelles are formed in a

polymer solution in D<sub>2</sub>O, where strong interactions exist between the polymer and d-SDS surfactant, like our system, the scattering from d-SDS micelles cannot be ignored as chemical composition of the shell of d-SDS micelles can change due to the incorporation of hydrogenated PDMAEMA segments to the micelle shell. This can induce a large change in the contrast factor of the micelle. It has been shown that when a neutral polymer such as PEO binds to SDS micelles, the polymer segments are incorporated into the shell using <sup>13</sup>C-NMR.<sup>32</sup> When similar binding occurs in PDMAEMA/d-SDS solutions, the contrast-matching conditions are shifted. From the shift in the scattering peak, it is clear that the micelles are decreasing in size as the PDMAEMA concentration increases, leading to a decrease in the aggregation number per micelle. This leads to a decrease in the volume of the d-SDS micelles. Correspondingly, the number of charged micelles in the solutions will increase due to the formation of smaller micelles, and this contributes to an increase of the SANS intensity. Although the decrease in the aggregation number has two opposing effects on the SANS intensity, overall effect is expected to decrease the SANS intensity since it is proportional to the volume squared, but is proportional to the number of PDMAEMA segments wrapping d-SDS micelles. In Figure 3.3, although the increase of free PDMAEMA segments with the increase in PDMAEMA concentration makes it difficult to determine an absolute contribution of PDMAEMA segments wrapping the micelles to the measured SANS intensity, it is pointed out at the SANS intensity around the peak position increases indicating a change in the micelle contrast factor.

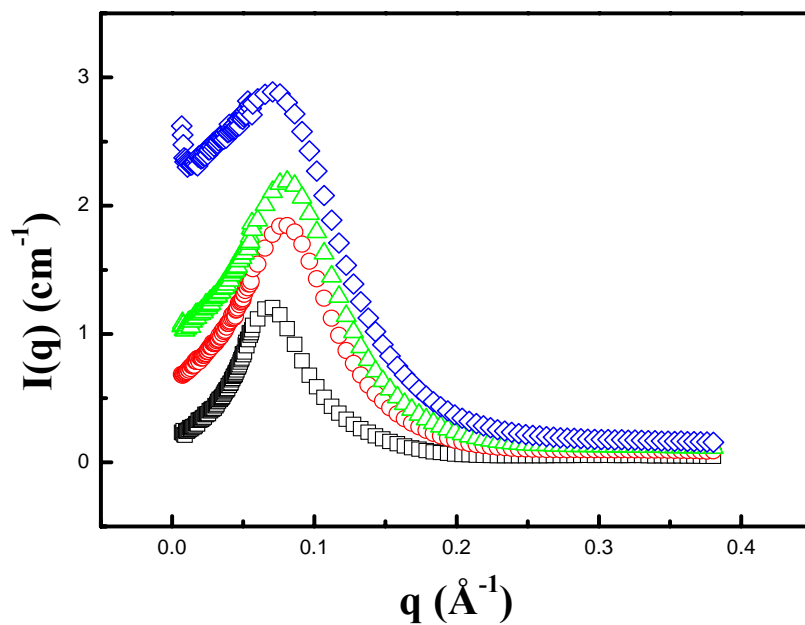


Figure 3.3. SANS of PDMAEMA solutions with 100 mM d-SDS in pure  $\text{D}_2\text{O}$ : 50 mg/ml PDMAEMA (black squares), 100 mg/ml PDMAEMA (red circles), 150 mg/ml PDMAEMA (green triangles), and 200 mg/ml PDMAEMA (blue diamonds).

### 3.4.2 A model fit of 100 mM d-SDS in PDMAEMA solutions

It is possible to obtain information about the structure of the micelles and to determine whether the contrast factor of the d-SDS micelles was affected by the interaction with the PDMAEMA segments by measuring the SANS intensity at the condition where PDMAEMA is contrast matched. This condition was achieved by using a mixture of 80% H<sub>2</sub>O and 20% D<sub>2</sub>O, and the results are shown in Figure 3.4. Since the neutron scattering length density of PDMAEMA does not change by adding d-SDS to the solution, the first and the last terms in equation (3.6) are cancelled out, and the SANS intensity is attributed to only the d-SDS micelles. When the measured SANS intensity of 100 mM d-SDS in PDMAEMA solution was compared to that of 100 mM d-SDS without the polymer, the peak position shifted to higher  $q$ , consistent with the previous results, and overall intensity decreased with increasing PDMAEMA concentration. Both facts explain a decrease in the aggregation number per micelle, leading to an increase of the number of d-SDS micelles. The driving force of the micelle formation is the elimination of the contact between the alkyl chains and water.<sup>63</sup> The larger a spherical micelle is, the more efficient it is since the volume-to-surface area ratio increases. Therefore, decreasing the micelle size always leads to increasing hydrocarbon-water contacts, which is unfavorable. A decrease of the micelle size is observed in a mixture of a neutral polymer and surfactants in water, caused by the reduction in the micellar core-water interfacial energy owing to the partial shielding provided by the polymer.<sup>51-53</sup> In this case where the polymer is interacting with the micelle shell, there is a chemical composition change, which affects the SANS intensity.

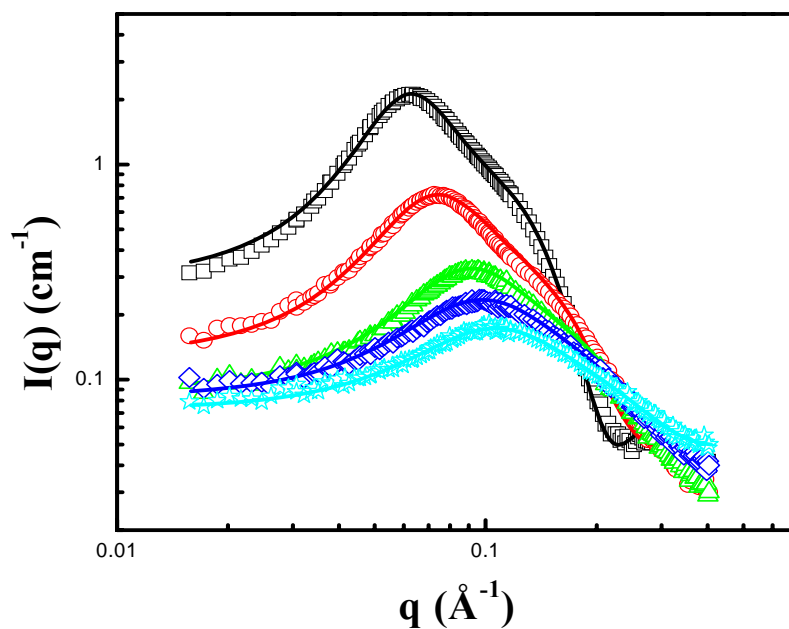


Figure 3.4. SANS of PDMAEMA solutions with 100 mM d-SDS in a mixture of 80% H<sub>2</sub>O and 20% D<sub>2</sub>O: no polymer (black squares), 50 mg/ml PDMAEMA (red circles), 100 mg/ml PDMAEMA (green triangles), 150 mg/ml PDMAEMA (blue diamonds), and 200 mg/ml PDMAEMA (sky blue stars) The solid lines represent fit results obtained using a spherical core-shell model with the rescaled MSA closure.

Model fitting to the SANS data enables us to gain insight into the size and shape of micelles and also understand the chemical composition change due to the incorporation of hydrogenated polymer segments into the micelle shell. The schematic representation in Figure 3.5 represents the structure of d-SDS micelle in PDMAEMA solutions.

It has been reported that for spherical polyelectrolyte systems, the location of the scattering peak moves to high  $q$  as the concentration increases, following the scaling law  $q^* \sim N_p^{-n}$ , with  $n = 1/3$ , where  $N_p$  is the number of particles in the solution. This corresponds to a simple volume expansion of the interparticle distance with decreasing particle number.<sup>46, 57-59</sup> Recently, a peak position shift to high  $q$  in SANS intensity of PPOMA/d-SDS solutions as the polymer concentration increased was observed<sup>70</sup>, similar to our findings. Due to the low molecular weight of the PPOMA (437 g/mol), it was proposed that d-SDS micelles associated with the PPOMA chain uniformly. The authors calculated the micelle aggregation number from the peak position, assuming different cubic lattices such as simple cubic (sc), body-centered cubic (bcc), and face-centered cubic (fcc), and showed that for the aggregation number, for the sc lattice lead to a better agreement with fluorescence data<sup>71</sup>, the bcc and the fcc lattices gave overestimated values of the aggregation number. The above approach was adopted for our SANS analysis as it is expected that the micelles are distributed evenly in the solution since PDMAEMA solutions are relatively concentrated. To quantitatively understand d-SDS micellization in PDMAEMA solutions, the SANS data were fit to a spherical core-shell model with the rescaled

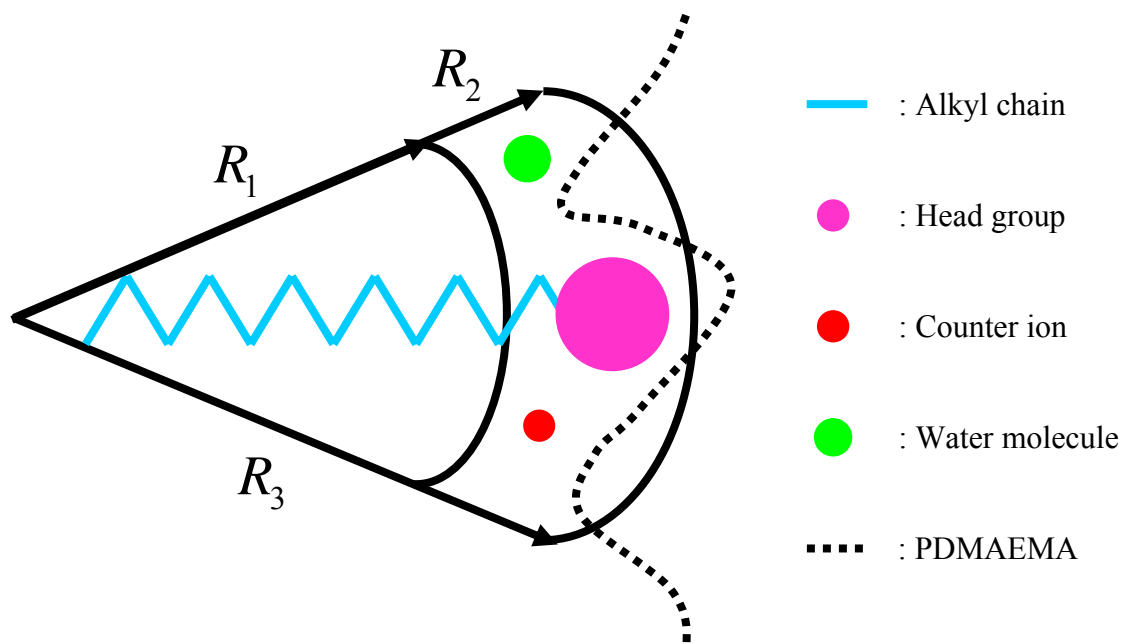


Figure 3.5. A schematic of the mixed micelle of mean radii  $R_1$  and  $R_3$  in PDMAEMA solutions

MSA closure.<sup>60</sup> The fit results are shown in Figure 3.4 as solid lines. The micellar concentration  $C_{mic}$  (mol/l) is proportional to  $(q^*)^3$ :

$$C_{mic} = a \times \frac{10^{27}}{\left(\frac{2\pi}{q^*}\right)^3 \times N_A} \quad (3.7)$$

where  $N_A$  is Avogadro's number and  $a$  is a numerical factor which depends on the average position between micelles and  $a = 1$  for a sc lattice.<sup>70</sup> The aggregation number  $\nu$  of d-SDS can be evaluated as

$$\nu = \frac{(C_{d-SDS} - CAC)}{C_{mic}} \quad (3.8)$$

where  $C_{d-SDS}$  is the added d-SDS concentration. The core radius  $R_1$  is composed of a methyl group and of a fraction  $\alpha$  of 11 methylene groups, and  $\alpha$  can be calculated from the following equation.

$$\alpha = (V_1 - \nu V_{CD_3}) / 11\nu V_{CD_2} \quad (3.9)$$

where  $V_{CD_3}$  and  $V_{CD_2}$  are the volumes of methyl and methylene groups, respectively. The shell is composed of the remaining fraction of the methylene groups, sulfate groups, sodium ions, water molecules solvating the sulfate groups and sodium ions, and PDMAEMA segments. From the measured  $q^*$ , the aggregation number  $\nu$  of d-SDS per micelle in each solution was calculated using equation (3.7) and (3.8). Based on the aggregation number  $\nu$ , the radius of the sphere, which would contain all of the hydrocarbons, was calculated by  $R_h = \left[3\nu(V_{CD_3} + nV_{CD_2}) / 4\pi\right]^{1/3}$ . According to the

Hayter and Penfold model<sup>68</sup>, when  $R_h \leq l_c$ , all hydrocarbons are contained in the core. Otherwise,  $R_1 = l_c$  and  $\alpha$  is calculated from equation (3.9). From the aggregation number  $\nu$ , it is also possible to calculate neutron scattering length density of the core since the scattering length density of the core  $\rho_1$  is represented by  $\rho_1 = \nu \sum b_i / V_1$  where  $\sum b_i$  is the sum of  $b_{CD_3}$  and  $11\alpha b_{CD_2}$  from the d-SDS surfactant in the core. Table 3.3 summarizes the values, which are adopted from Cabane et al.<sup>54</sup> and used to calculate  $R_1$ ,  $\alpha$ , and  $\rho_1$ . In the fit process, the scattering length density of solvent was fixed at  $8.2 \times 10^{-7} \text{ \AA}^{-2}$ . However, the scattering length density of the shell and the shell thickness were left as floating values to account for the participation of PDMAEMA segments in the micelle shell. The PDMAEMA chains are potentially incorporated into the shell to prevent water from penetrating into the core. To calculate a structure factor, 2.5 mM CAC was used.<sup>43</sup> Table 3.4 summaries the values of the optimized fit parameters together with  $\nu$  and  $\alpha$  calculated using equation (3.7), (3.8) and (3.9).

Based on  $\nu$ , which decreases from 59 to 12 as the PDMAEMA concentration increases,  $R_h$  was calculated to yield  $R_1$  and  $\alpha$  according to the Hayter and Penfold model<sup>68</sup>.  $R_1$  decreased from 16.7  $\text{\AA}$  to 10  $\text{\AA}$ , and  $\alpha$  increased from 0.93 to 1, indicating that in the PDMAEMA solutions, all hydrocarbon tails in the surfactant are found in the core of the micelle. Since the optimized  $R_3$  is lower in the PDMAEMA solutions than in water, the surface area per d-SDS surfactant ( $SA = 4\pi R_3^2 / \nu$ ) in the

Table 3.3. Scattering lengths, volumes and neutron scattering length densities of chemical groups adopted from Cabane et al.<sup>54</sup>

Chemical group	$b$	$V$	$\rho$
$CD_2$	1.999	27	7.41
$CD_3$	2.666	54.3	4.91
$SO_4Na$	2.965	67.8	54.37
$C_{12}D_{25}$	24.655	353.7	6.97
$H_2O$	-0.168	30	-0.56
$D_2O$	1.92	30	6.39

$b$  : Neutron scattering length per group in  $\text{cm} \cdot 10^{12}$

$V$  : Volume per group in  $\text{\AA}^3$  at 24 °C

$\rho$  : Neutron scattering length density in  $\text{\AA}^{-2} \cdot 10^{-6}$

micelle increases from 94 nm<sup>2</sup> to 204 nm<sup>2</sup> as the PDMAEMA concentration increases. The increase of surface area accompanies the increase of the micellar core-water interfacial energy, which is unfavorable for the formation of micelles, so the partial shielding provided by PDMAEMA segments is required to maintain the micelle structure. The volume of PDMAEMA segments solvated with water  $V_p$  in the shell was estimated from the following relationship:

$$V_p = (V_3 - V_1) - v \left[ (1 - \alpha) V_{CD_2} + V_{SO_4^-} + (1 - \sigma) V_{Na^+} + \left( \omega_{SO_4^-} + (1 - \sigma) \omega_{Na^+} \right) V_s \right] \quad (3.10)$$

where  $V_{SO_4^-}$  and  $V_{Na^+}$ , are the volume of  $SO_4^-$  and  $Na^+$ , respectively. Here,  $\omega_{SO_4^-}$  and  $\omega_{Na^+}$  are hydration numbers of  $SO_4^-$  and  $Na^+$ . The fraction ( $F = V_p / (V_3 - V_1)$ ) in the shell was calculated and is shown in Table 3.4. It is notable that the fraction of PDMAEMA in the shell obtained from the fit for the d-SDS solution without PDMAEMA is -0.0036, confirming the validity of the adopted values to calculate  $V_p$ . In PDMAEMA solutions with 100 mM d-SDS, the fraction in the shell was positive and increased from 0.18 to 0.5 with PDMAEMA concentration. In the mixed micelle in PPOMA/SDS system, a similar behavior with a decrease of SDS volume fraction from 1 to 0.5 was observed as the PPOMA concentration increased.<sup>70</sup> The incorporation of hydrogenated PDMAEMA segments into the shell was also reflected in the decrease of the scattering length density of the shell as PDMAEMA concentration increased, as shown in Figure 3.6. The form factors of the mixed micelles are calculated using the optimized values and plotted in Figure 3.7, which shows reduced SANS intensity at low  $q$  region due to the smaller aggregation number

Table 3.4. Optimized parameters from model fits

PDMAEMA concentration	$\nu$	$\alpha$	$R_1$	$R_3$	$\rho_1$	$\rho_2$	$z_m$	$F$	$SA$
0 mg/ml	59	0.927	16.7	21	6.99	4.49	29	-0.0036	94
50 mg/ml	35	1	14.3	18.4	7.01	1.64	16	0.18	120
100 mg/ml	18	1	11.6	15	7.01	1.19	11	0.3	153.7
150 mg/ml	15	1	10.8	14.48	7.01	0.97	8.2	0.39	175
200 mg/ml	12	1	9.8	13.5	7.01	0.9	7.3	0.5	204

$\nu$  : Aggregation number of d-SDS per micelle

$\alpha$  : Fraction of methylene groups in the core

$R_1$  : Core radius in Å

$R_3$  : External radius in Å

$\rho_1$  : Neutron scattering length density of the core in Å<sup>-2</sup>\*10<sup>-6</sup>

$\rho_2$  : Neutron scattering length density of the shell in Å<sup>-2</sup>\*10<sup>-6</sup>

$z_m$  : Surface charge per micelle

$F$  : Volume fraction of PDMAEMA segments solvated with water in the shell

$SA$  : Surface area per d-SDS surfactant in a micelle

of d-SDS surfactants per micelle and the lower contrast due to the PDMAEMA segments in the micelle shell as the PDMAEMA concentration increases. This explains the decrease in overall SANS intensity as the PDMAEMA concentration increases. Also, it is rationalized that the increase of SANS intensity at the peak position in Figure 3.3 is attributed to the enhanced contrast of d-SDS micelles in D<sub>2</sub>O due to the incorporation of hydrogenated PDMAEMA segments in spite of the decreased volume of the micelles.

Another characteristic of the measured SANS intensity, shown in Figure 3.4, is that the peak gets broader as the PDMAEMA concentration increases. In the scattering from charged micelles, the peak position and broadness is governed mainly by the structure factor although the overall scattering intensity is represented by both product of the form factor and the structure factor. From the values obtained from the fit results to the SANS data, the structure factors of the micelles were calculated and plotted in Figure 3.8. In the structure factors, all three features in SANS intensity in Figure 3.4 are reflected: a peak position shift to higher  $q$ , a reduced peak maximum, and a broader peak with increasing PDMAEMA concentration. The shift of the peak position agrees with the decrease in the aggregation number as the PDMAEMA concentration increases as it indicates more mixed micelles are formed at a fixed d-SDS concentration. Although the distance between charged micelles is smaller in more concentrated PDMAEMA solutions, it is interesting that the peak also gets broader and the height is reduced. This indicates that the liquid-like order of the micelles worse.

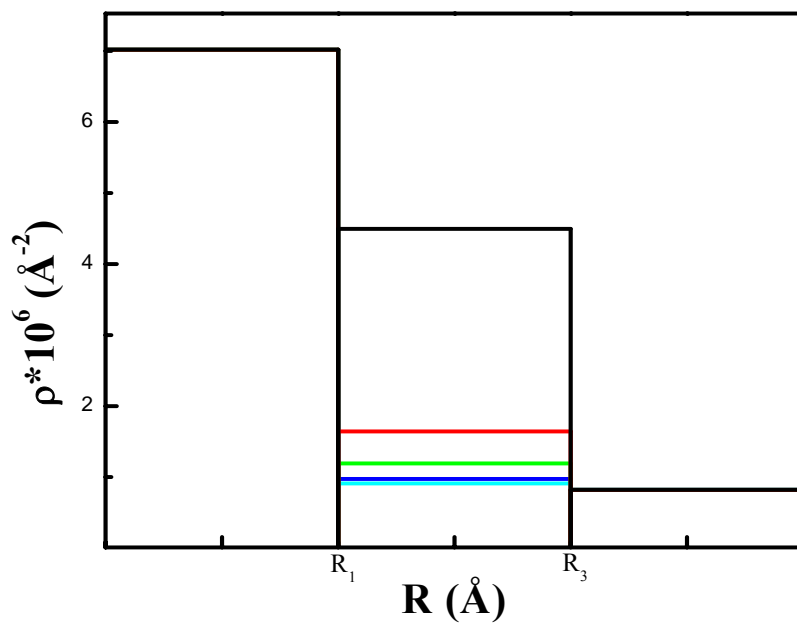


Figure 3.6. The scattering length densities of core and shell obtained from the model fit. (black line : no PDMAEMA, red line : 50 mg/ml PDMAEMA, green line : 100 mg/ml PDMAEMA, blue line: 150 mg/ml PDMAEMA, sky blue line : 200 mg/ml PDMAEMA)  $R_1$  and  $R_3$  represent the core radius and the external radius, respectively.

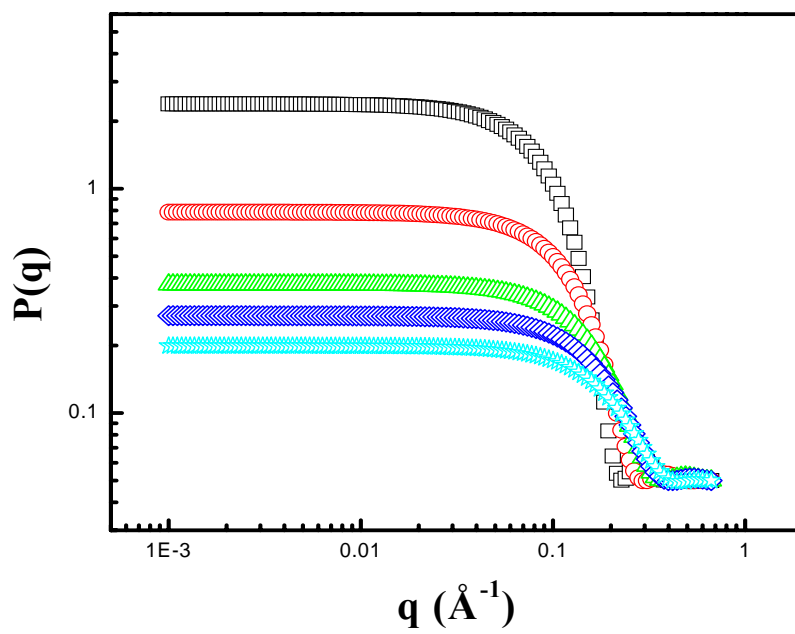


Figure 3.7. The form factors of d-SDS micelles in PDMAEMA solutions at the condition that PDMAEMA was contrast matched to a mixture of 80% H<sub>2</sub>O and 20% D<sub>2</sub>O: no polymer (black squares), 50 mg/ml PDMAEMA (red circles), 100 mg/ml PDMAEMA (green triangles), 150 mg/ml PDMAEMA (blue diamonds), and 200 mg/ml PDMAEMA (sky blue stars)

The charged spherical micelles of radius  $R_3$  are interacting with each other through a screened coulomb interaction potential given by equation (3.5). Since the potential increases exponentially as the spacing decreases, it is apparent that a change in the potential is required for the formation of smaller micelles favorable. micelles worse. The charged spherical micelles of radius  $R_3$  are interacting with each other through a screened coulomb interaction potential given by equation (3.5). This is consistent with the reduction in the surface charge of the micelles from 29 to 7.3, as the PDMAEMA concentration increases. Also, it is responsible for a reduced peak maximum and a broader peak. The change of the interaction potential can be roughly estimated as follows. Using equation (3.5), a relationship for the repulsive interaction potentials between charged micelles at lower PDMAEMA concentrations (a) and charged micelles at higher PDMAEMA concentrations (b) was obtained with the assumption that  $U(r)$  is affected mainly by  $R_3$  and  $z_m$  as no salt is present in the solutions.

$$\log \frac{U(r)_a}{U(r)_b} = \log \frac{\frac{z_{m,a}^2}{4\pi\epsilon_0\epsilon(1+\kappa R_{3,a})^2} r}{\frac{z_{m,b}^2}{4\pi\epsilon_0\epsilon(1+\kappa R_{3,b})^2} r} - \kappa(r-2R_{3,a}) + \kappa(r-2R_{3,b}) \quad (3.11)$$

$$= \log \frac{z_{m,a}^2 (1+\kappa R_{3,b})^2}{z_{m,b}^2 (1+\kappa R_{3,a})^2} + 2\kappa(R_{3,b} - R_{3,a})$$

Since both terms are positive from the fit results,  $U(r)_a$  is always higher than  $U(r)_b$  at a distance  $r$ . This indicates that as the PDMAEMA concentration increases, the repulsion between the micelles decreases which enables more micelles to form with a corresponding drop in the liquid-like order.

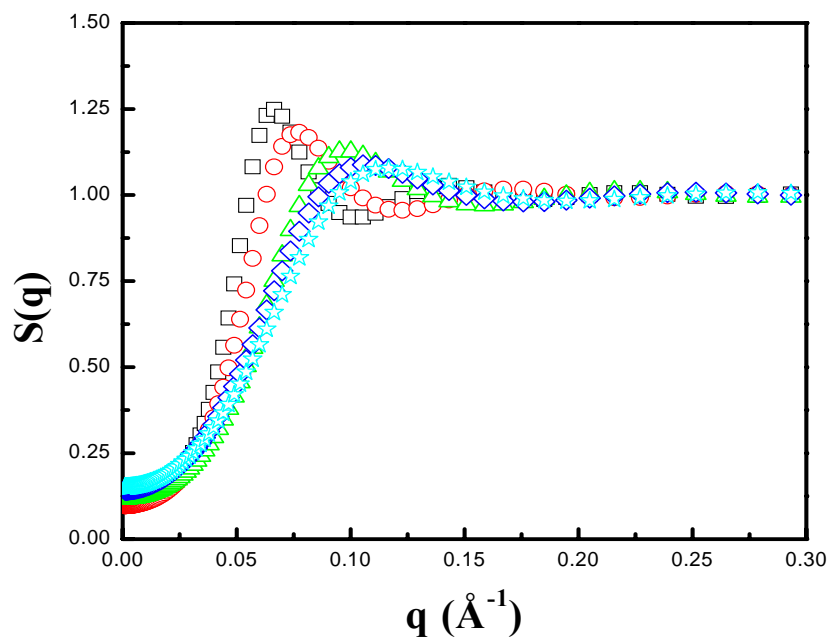


Figure 3.8. The structure factors of d-SDS micelles in PDMAEMA solutions. PDMAEMA contrast match point (80% $\text{H}_2\text{O}/20\%\text{D}_2\text{O}$ ): no polymer (black squares), 50 mg/ml PDMAEMA (red circles), 100 mg/ml PDMAEMA (green triangles), 150 mg/ml PDMAEMA (blue diamonds), and 200 mg/ml PDMAEMA (sky blue stars)

### 3.5 Conclusions

SDS micellization was studied as a function of PDMAEMA concentration using H/D contrast matching methods with SANS. Both h-SDS and d-SDS interacts with the polymer in water, leading to PDMAEMA/SDS complexes, as shown by the shift of the scattering peak position to higher  $q$  as the PDMAEMA concentration increases. A structural analysis of the d-SDS micelle/PDMAEMA mixture was performed at the condition where the PDMAEMA was contrast-matched with a mixture of 80% H<sub>2</sub>O and 20% D<sub>2</sub>O. From the model fit, it was found that the size of d-SDS micelle decreased with increasing PDMAEMA concentration, while maintaining its spherical shape. The result explains the observed peak position shift due to a reduction in the aggregation number of d-SDS per micelle with increasing PDMAEMA concentration. The reduction in size would generally be energetically unfavorable as it would cause an increase in the hydrocarbon-water interfacial area. However, the participation of PDMAEMA segments in the micelle shell, as evidenced by the decrease in the neutron scattering length density of the shell, allows for the reduction of the micelle size since the PDMAEMA segments provide a partial shielding of the hydrocarbon tails from contacting water. It is pointed out that the incorporation of PDMAEMA segments in the shell also changed the contrast factor of the d-SDS micelle, shifting the system away from the contrast match point. The reduction in the aggregation number of d-SDS surfactant molecule per micelle led to a smaller average distance between micelles as the PDMAEMA concentration increased. Although the smaller distance would be expected to be unfavorable due to the repulsive potential, from the form factors and the structure factors obtained from fitting the SANS data, it was

found that the formation of smaller micelles with lower surface charge reduces the repulsive interaction potential between the micelles significantly.

## **Chapter 4: Construction of structured hydrogels with anionic micelles**

In this chapter, we created poly((2-dimethylamino)ethyl methacrylate) (PDMAEMA) hydrogels containing sodium dodecylsulfate (SDS) micelles using a crosslinker, 1,2-bis(2-iodoethoxy)ethane (BIEE). The size and shape of SDS micelles before and after crosslinking was studied using small angle neutron scattering (SANS) with H/D contrast matching method as a function of a crosslinking ratio.

### **4.1 Introduction**

Molecularly imprinted polymer (MIP)<sup>77-79</sup> is created by crosslinking polymers or monomers in the presence of template molecules, usually in a solvent such as water. Initially, functional groups on the polymer or the monomer are bound either covalently or noncovalently to the template molecule, and crosslinking results in a highly crosslinked hydrogel. The MIPs containing templates are immersed in a large amount of fresh solvent and the difference in the osmotic pressure between the hydrogel and surrounding solvent drives the templates out of the MIP, leaving pores in the polymer network containing the functional groups in a geometric arrangement related to the original template molecule. It is argued that these pores are complementary in size and shape to the template molecules and the functional groups of the polymer are positioned to preferentially rebind to the template molecule, so that this material has potential for applications in separation, drug delivery, biosensors,

etc. There is also interest in creating nanoporous hydrogels using micelles as templates which could be used as separation materials,<sup>10-13</sup> similar to MIPs although micelles are at a larger size scale than single molecules. In order to understand the proposed templating mechanism in MIPs, it is necessary to compare the resultant pores to the original templates with respect to size and shape. Moreover, when micelles are used as templates, the size and shape before and after crosslinking needs to be characterized as micelle structure depends on the solution thermodynamics.<sup>63</sup> In the previous chapters, we demonstrated that SDS surfactants form mixed micelles associated with PDMAEMA chains in a dilute PDMAEMA solution and concentrated PDMAEMA solutions. As PDMAEMA concentration increased from 0 to 200 mg/ml, the external radius of the micelle decreased from 21 Å to 13.5 Å, while spherical shape of the micelle was maintained. The PDMAEMA/SDS complexes in water give a convenient way to construct hydrogels containing micelles, which can be used as separation materials, since it is possible to crosslink PDMAEMA in water through the Menshutkin reaction between a dihalide and two tertiary amines.<sup>37, 38</sup> SANS has been widely used to investigate structures ranging from sub-nanometer to sub-micrometer.<sup>14-16</sup> Because the scattering lengths of H and D atoms are very different, the scattering contrast can be enhanced (and varied) through isotopic labeling. It is possible to investigate the structure of micelles in polymer solutions and hydrogels using H/D contrast-matching methods with SANS by contrast matching the polymer to the solvent. In this work, SANS of PDMAEMA/deuterated SDS (d-SDS) solutions and the corresponding hydrogels in water was measured to investigate the effect of crosslinking on the structure of the micelles.

## 4.2 Experimental

For the SANS measurements, D<sub>2</sub>O and d-SDS were purchased from Cambridge Isotope Laboratories, Inc. 60,000 g/mol PDMAEMA with 1.12 PDI was synthesized using group transfer polymerization. A series of PDMAEMA solutions in water with desired SDS concentrations were prepared by mixing two stock solutions: PDMAEMA solution and d-SDS solution. To create hydrogels with micelles, a crosslinker, BIEE, was added to PDMAEMA/d-SDS solutions and was completely mixed. As shown in Figure 4.1, crosslinking occurs between PDMAEMA and BIEE where two quaternized amines on the PDMAEMA are connected to each other through the BIEE (2-ethoxy) ethane. The amount of BIEE was used to control the positive charge density of the resulting hydrogels. A half of each mixture was injected using a syringe into a demountable titanium cell and was kept for 2 days until hydrogels are formed. Scattering intensity of PDMAEMA/d-SDS solutions and the corresponding hydrogels was varied by changing a volume ratio of H<sub>2</sub>O and D<sub>2</sub>O. Each solution or hydrogel was kept in a demountable titanium cell (1 mm or 2 mm path length) for the SANS measurements. Complete crosslinking was determined by the inversion of the rest of each mixture. SANS experiments were carried out at the Center for Neutron Research at the National Institute of Standards and Technology on the 30 m NIST-NG7 instrument.<sup>41</sup> The raw data were corrected for scattering from the empty cell, incoherent scattering, detector dark current, detector sensitivity, sample transmission, and thickness. Following these corrections the data were placed on an absolute scale using a direct beam measurement and then circularly averaged to

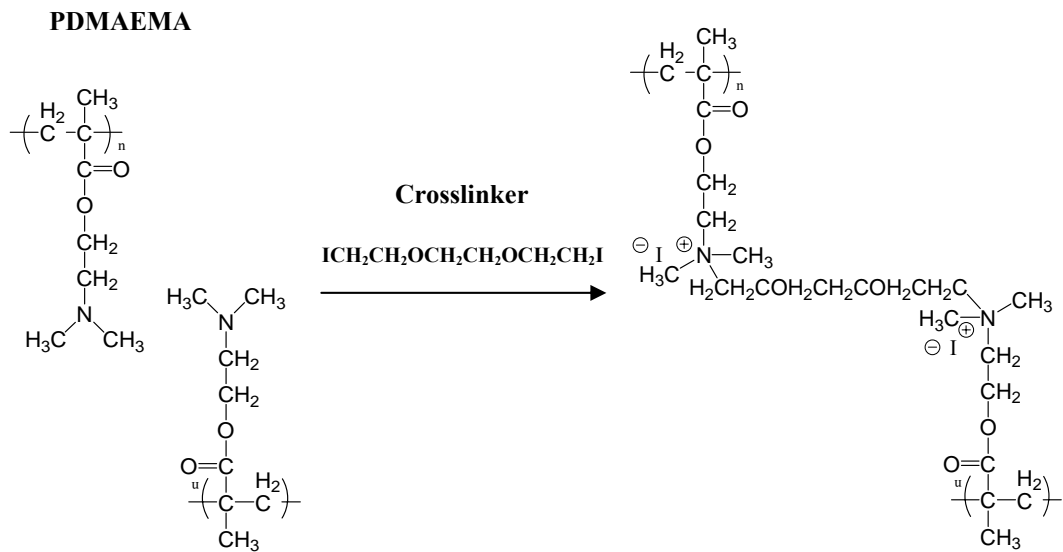


Figure 4.1. A scheme of the crosslinking reaction between PDMAEMA and BIEE

produce  $I(q)$  versus  $q$  plots where  $I(q)$  is the scattered intensity and  $q$  is the scattering vector ( $q=4\pi\sin\theta/\lambda$ ). The  $q$  range was 0.005–0.40  $\text{\AA}^{-1}$  and the neutron wavelength was 6  $\text{\AA}$  with a wavelength spread  $\Delta\lambda/\lambda=0.11$ .

### 4.3 Results

The black squares in Figure 4.2 represent SANS intensity of a 200 mg/ml PDMAEMA solution in  $D_2O$ . The measured scattering is a monotonically decreasing function with angle, which is a characteristic of concentrated polymer solutions. It was fit to a modified Lorentzian function:<sup>80, 81</sup>

$$I(q) = \frac{A}{1+(qL)^m} + B \quad (4.1)$$

In this function,  $A$  is the scattering scale,  $L$  is a correlation length,  $m$  is the Porod exponent, and  $B$  is a background. The solid line shows the fit result where  $C$  is 36.5  $\text{cm}^{-1}$ ,  $L$  is 42.6  $\text{\AA}$ , and  $m$  is 1.92. Since the Porod exponent  $m$  is related to the Flory excluded volume exponent  $\nu$  as  $m=1/\nu$ ,<sup>80</sup> it is apparent that  $D_2O$  is approximately a theta solvent at 25 °C. Since the scattering length density of d-SDS surfactant is close to  $D_2O$ , scattering of d-SDS micelles in  $D_2O$  is negligible.<sup>33, 34, 39, 55, 56, 70</sup> However, when hydrogenated PDMAEMA segments participate in d-SDS micellization, it enhances the scattering from the micelles. This fact gives a convenient way to confirm the interactions between PDMAEMA and d-SDS in solutions and hydrogels. SANS intensity of a 200 mg/ml PDMAEMA solution with 100 mM d-SDS in  $D_2O$  decreases in all measured  $q$  ranges compared to SANS of the corresponding solution

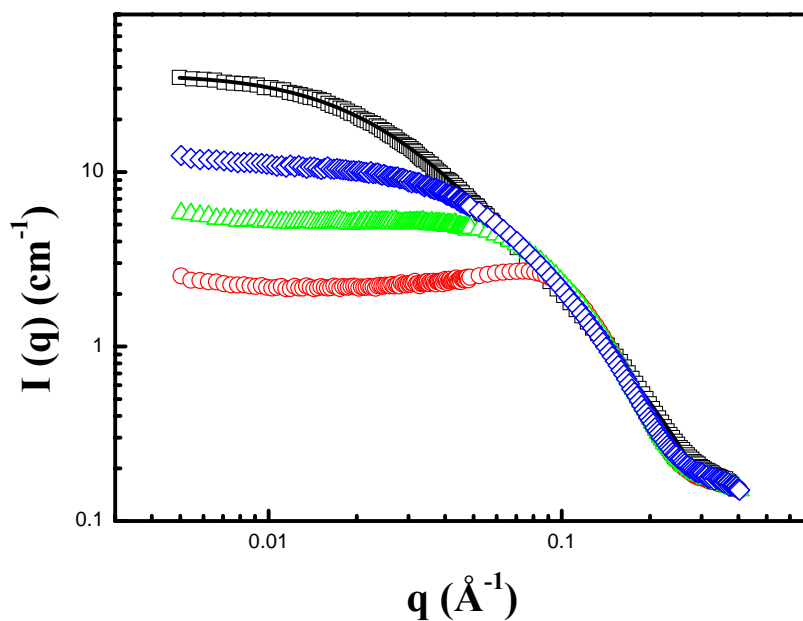


Figure 4.2. SANS intensity of a 200 mg/ml PDMAEMA solution with 100 mM d-SDS in D<sub>2</sub>O (red circles) and its corresponding hydrogels. (Crosslinking ratio: 0.02 (green triangles), and 0.04 (blue diamonds)) For comparison, SANS of 200 mg/ml PDMAEMA solution in D<sub>2</sub>O is shown (black squares), and it was fit to a modified Lorentzian function. (black line)

without d-SDS, but the decrease of SANS intensity in low  $q$  region is higher, resulting in a peak in SANS intensity. Since the observed peak is a characteristic of ionic micelles, it indicates that d-SDS micelles incorporate PDMAEMA segments. PDMAEMA hydrogels with 100 mM d-SDS were created by adding BIEE to a 200 mg/ml PDMAEMA solution in  $D_2O$ . Here, a crosslinking ratio is defined as the moles of BIEE over the moles of PDMAEMA monomer. At a crosslinking ratio of 0.02, the peak shifts to a lower  $q$  and, it disappears at a crosslinking ratio of 0.04. The disappearance of the charged micelle characteristic peak might be interpreted as the micelles being destroyed in the crosslinked hydrogel. However, it should be emphasized that in our case, crosslinking generates quaternized PDMAEMAs which can interact more strongly with d-SDS micelles through electrostatic attractive interactions. The observed phenomena can be explained by screening of the surface charges on the micelle induced by the electrolyte. Generally, SDS micelles repel each other in water due to their negative charge, and the repulsion causes SDS micelles to maintain a long range order in water.<sup>29, 31, 50, 63</sup> The order is reflected in the SANS data as a peak, suppressing the SANS intensity in the low  $q$  region due to the structure factor. When electrolytes are added to a SDS solution, two behaviors are generally observed.<sup>50, 63, 66, 67</sup> First, the electrostatic repulsion between the charged SDS head-groups is screened due to the added electrolyte, leading to a loss of the peak in the SANS data. Then, with further addition of electrolyte leads to a transition from spherical to cylindrical micelles as the micelle shape is dependent on the critical packing parameter,<sup>34, 50, 63</sup> which is the ratio of the effective head group area of the surfactant to the area of its tail. It is notable that in Figure 4.2, the increase of

scattering intensity at low  $q$  is observed as the crosslinking ratio increased. When quaternized PDMAEMA segments participate in d-SDS micellization, the hydrogenated PDMAEMA segments alter the scattering contrast of the micelles as well as alter the electrostatic repulsions between the charged headgroups.

The size and shape of the mixed micelles in solution and in the corresponding hydrogels with different crosslinking ratios was investigated by SANS at the condition where the PDMAEMA was contrast-matched to solvent (80% H<sub>2</sub>O and 20% D<sub>2</sub>O).<sup>76</sup> As shown in Figure 4.3, the SANS intensity for a 200 mg/ml PDMAEMA solution and its hydrogels with 100 mM d-SDS in contrast matched H<sub>2</sub>O/D<sub>2</sub>O increases in the low  $q$  region as the crosslinking ratio increases. As a control experiment, we confirmed that the SANS intensity of a 200 mg/ml PDMAEMA hydrogel in contrast matched H<sub>2</sub>O/D<sub>2</sub>O without d-SDS is flat in the measured  $q$  region. This means the crosslinking of PDMAEMA with BIEE did not induce the phase separation of the hydrogel and the contrast factor of the PDMAEMA hydrogel is not significantly different from the PDMAEMA solution. When the crosslinking ratio is 0.02, the peak position has shifted to slightly lower  $q$  compared to the corresponding solution, indicating that the form factor and the structure factor have changed. This trend continued, leading to a disappearance of the peak at 0.04 crosslinking ratio. Both results agree well with the change of SANS intensity shown in Figure 4.2. Since the change of micellization in the hydrogels induced by crosslinking was reflected in scattering, regardless of whether either PDMAEMA or

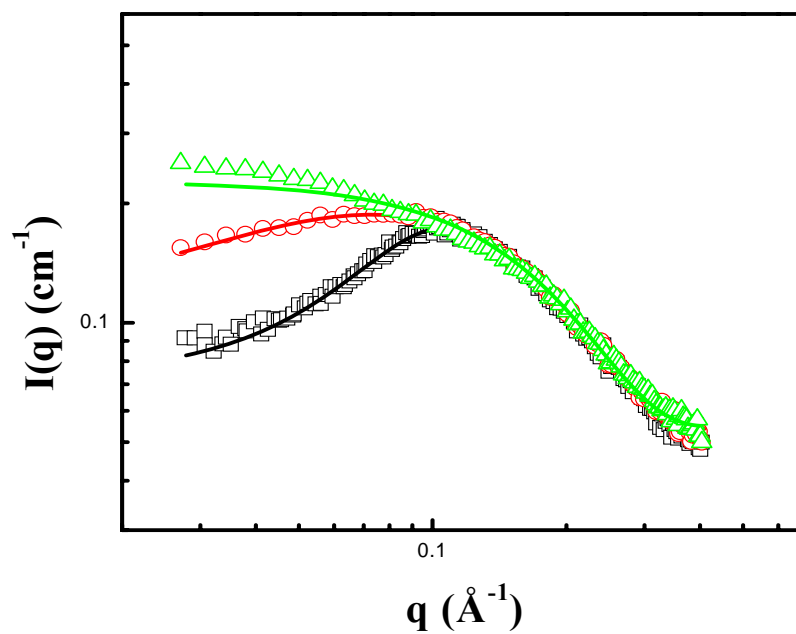


Figure 4.3. SANS intensity of a 200 mg/ml PDMAEMA solution with 100 mM d-SDS (black squares) and its corresponding hydrogels in a mixture of 80% H<sub>2</sub>O and 20% D<sub>2</sub>O (Crosslinking ratio: 0.02 (red circles), and 0.04 (green triangles)). The measured SANS intensity was fit to a core-shell model with or without the rescaled MSA closure and the results are shown as lines.

d-SDS was contrast-matched to the solvent, this indicates that the formation of mixed micelles is assisted by the PDMAEMA segments in the corresponding hydrogels, and the polymer conformation is governed by the micelles. The measured SANS intensity in Figure 4.3 was fit to a spherical core-shell model with and without the rescaled MSA closure<sup>14, 60-62, 75</sup> in order to determine the size and shape of the mixed micelles. In the fit process, the core radius of the mixed micelle was constrained to be less than 16.7 Å,<sup>68</sup> which is the length of a fully extended alkyl chain of d-SDS, and the scattering length densities of the core and solvent were fixed at  $7.01 \times 10^{-6} \text{ \AA}^{-2}$  and  $8.2 \times 10^{-7} \text{ \AA}^{-2}$ , respectively. The neutron scattering length density of the core ( $\rho_{core}$ ) was calculated from the relationship:  $\rho_{core} = \sum b_i / V$  where  $\sum b_i$  is the sum of  $b_{CD_3}$  and  $11b_{CD_2}$  of a d-SDS surfactant and  $V$  is the volume of the alkyl chain, composed of a methyl group and 11 methylene groups. The scattering length and the volume per chemical group were adopted from Cabane et al.<sup>54</sup> However, the scattering length density of the shell left as a floating value to allow for the participation of polymer segments. The results are shown as lines in Figure 4.3. As the crosslinking ratio increases, the core radius,  $R_1$ , increased from 9.8 to 10.8 and 12 Å. According to the Hayter and Penfold model,<sup>68</sup> when  $R_1$  is less than a fully extended hydrocarbon length for the surfactant, all hydrocarbons are contained in the core. Based on the core radius, the aggregation number of d-SDS surfactants per micelle,  $\nu$ , can be calculated from the relationship:

$$\nu = \left( \frac{4\pi}{3} R_1^3 \right) / (V_{CD_3} + 11V_{CD_2}) \quad (4.2)$$

where  $V_{CD_3}$  and  $V_{CD_2}$  are the volume of the methyl and methylene groups,  $54.3 \text{ \AA}^3$  and  $27 \text{ \AA}^3$ ,<sup>54</sup> respectively. The aggregation number of d-SDS surfactants per micelle, calculated using the equation (4.2), increased from 12, 15 to 21 as the crosslinking ratio increased from 0, 0.02 to 0.04. All the values are lower than the aggregation number of SDS ( $\sim 70$ <sup>34</sup>) in water at 25 °C. This condition is satisfied when the polymers, added to the SDS solution, provide a partial shielding in order to lower the interfacial area between water and hydrophobic hydrocarbons. When the polymer is positively charged, the screening of the electrostatic repulsions between charged head-groups in a micelle occurs in addition. Since the screening reduces the distance between charged head-groups of the surfactants in the micelles, more water can contact hydrophobic hydrocarbons as the screening increases. From the fit results, it can be seen that the unfavorable interactions were decreased with increasing aggregation number of micelles.

Another aspect of the charge screening induced by quaternized PDMAEMA segments is observed in the structure factor of the SANS intensity. Since the repulsive interactions between ionic micelles are long-range, they form a liquid-like ordered structure. When the surface charges on ionic micelles are screened, the correlation between them is randomized as hard sphere interactions become short-range. This behavior is reflected in the measured SANS intensity in Figure 4.3. The surface charge per micelle of 7.3 in 200 mg/ml PDMAEMA solution decreased to 2 in the corresponding hydrogel at a crosslinking ration of 0.02. The fact that the SANS intensity of the hydrogel at 0.04 crosslinking ratio was fit to a spherical core-shell

model means that all of the surface charge on the micelle was effectively screened. With an assumption that all the BIEE was reacted at 0.02 and 0.04 crosslinking ratio, a molar concentration of quaternized PDMAEMA monomer in the hydrogels is 50.9 mM and 101.8 mM, respectively, since the BIEE can generate two quaternized amines. As the d-SDS molar concentration in the hydrogels is fixed at 100 mM, the molar ratio of quaternized PDMAEMA monomer to d-SDS corresponds to approximately 0.5 and 1, respectively. When we consider that the degree of ionization of SDS micelles in water is less than 30%,<sup>68</sup> the degree of quaternization of PDMAEMA seems to be sufficient to fully screen the electrostatic repulsions between micelles.

#### **4.4 Conclusions**

The micellization of d-SDS surfactants in a concentrated PDMAEMA solution and the corresponding hydrogels were investigated using SANS at the condition where either the d-SDS surfactant or the PDMAEMA was contrast-matched to solvent. When 100 mM d-SDS was added to a 200 mg/ml PDMAEMA solution, it was found that mixed micelles containing PDMAEMA segments are formed along the polymer chains. Since incorporation of PDMAEMA segments into the shell of the d-SDS micelles provides partial shielding which reduces the unfavorable contact between hydrocarbons and water and results in smaller micelles being formed, compared to in pure water. Using the PDMAEMA/d-SDS complexes in solution, structured hydrogels with micelles were created by crosslinking the polymers with BIEE. Since each BIEE molecule generated two quaternized amines, the quaternized amines

influenced d-SDS micellization similar to the effect of an electrolyte. From the model fits, it was found that the aggregation number of d-SDS surfactants per micelle increased to compensate for increased water contact due to the charge screening. The effect of the charge screening on the d-SDS micellization was confirmed from the reduced surface charges per micelle as the crosslinking ratio increased, disrupting the liquid-like order and eventually leading to a randomized distribution of the mixed micelles in hydrogel.

## **Chapter 5: The effect of the degree of quaternization of poly((2-dimethylamino)ethyl methacrylate) on deuterated sodium dodecylsulfate micellization**

In order to control the size and shape of sodium dodecylsulfate (SDS) micelles in poly((2-dimethylamino)ethyl methacrylate) (PDMAEMA) hydrogels, PDMAEMA was quaternized to have various degrees of charge density using methyl iodide. In this chapter, we will address the modification of PDMAEMA and its characterization. And, SDS micellization in quaternized PDMAEMA solutions and hydrogels was investigated using small angle neutron scattering (SANS).

### **5.1 Introduction**

Interactions between polymers and surfactants in water have been widely investigated because of potential applications such as detergents,<sup>25</sup> rheology modifiers,<sup>26</sup> and gelation agents.<sup>27, 28</sup> Recently, there has been interest in creating nanoporous hydrogels using micelles as templates which could be used as separation materials,<sup>10-13</sup> similar to MIPs.<sup>77-79</sup> Several methods have been introduced in the literature to create hydrogels with micelles. For example, monomers in solution with surfactants can be crosslinked,<sup>10-13</sup> or polyelectrolyte hydrogels can be immersed into surfactant solutions in order to take up surfactants. In both cases, since the micelle containing hydrogels were analyzed using small angle x-ray scattering, it was only

possible to determine the existence of micelles (or hierarchical micelle/polymer structures) formed in the hydrogels. It is important to investigate the size and shape of micelles in hydrogels as the structure will be directly related to the size and shape of pores that are generated after the removal of the micelles. SANS has been widely used to investigate similar structures ranging from sub-nanometer to sub-micrometer.<sup>14-16</sup> And, because the scattering lengths of H and D atoms are quite different, the scattering contrast can be enhanced (and varied) through isotopic labeling. Therefore, it is possible to investigate the structure of micelles in polymer solutions and hydrogels using H/D contrast matching methods with SANS. In the previous chapters, we demonstrated that deuterated SDS (d-SDS) surfactants form spherical micelles associated with PDMAEMA chains in water and the PDMAEMA/SDS complexes can be used to construct hydrogels with spherical micelles, since it is possible to crosslink PDMAEMA through the Menshutkin reactions between a dihalide and two tertiary amines.<sup>37, 38</sup> In this study, we attempted to induce the transformation of spherical micelles to cylindrical micelles using positively charged polyelectrolytes. For this aim, PDMAEMA was quaternized to various degrees by reacting with methyl iodide.<sup>82</sup> SANS of (quaternized) PDMAEMA/ d-SDS solutions and the corresponding hydrogels in water was measured to investigate the effect of the degree of quaternization on d-SDS micellization.

## 5.2 Experimental

All reagents were purchased from Aldrich, unless otherwise stated. D<sub>2</sub>O and d-SDS were purchased from Cambridge Isotope Laboratories, Inc. 60,000 g/mol PDMAEMA with 1.12 PDI was synthesized using group transfer polymerization. To quaternize the PDMAEMA, the polymer was dissolved in tetrahydrofuran (THF) and different amounts of methyl iodide was added dropwise and by regulating the ratio of moles of added methyl iodide to moles of PDMAEMA monomer. During the quaternization, transparent PDMAEMA solutions turned turbid yellow. After complete reaction, all the polymers precipitated as THF is a non-solvent for the quaternized polymers. The resulting polymers were filtered and washed in hexane several times. The polymers were dried in a vacuum oven for 1 day at 45 °C. The degree of quaternization was determined using a Bruker 400 MHz <sup>1</sup>H-NMR with D<sub>2</sub>O as the solvent. The effect of the degree of quaternization on the d-SDS micellization in PDMAEMA solutions and the corresponding hydrogels was measured using SANS. SANS experiments were carried out at the Center for Neutron Research at the National Institute of Standards and Technology on the 30 m NIST-NG3 and NG7 instruments.<sup>41</sup> The raw data were corrected for scattering from the empty cell, incoherent scattering, detector dark current, detector sensitivity, sample transmission, and thickness. Following these corrections the data were placed on an absolute scale using the direct beam measurement and circularly averaged to produce I(q) versus q plots where I(q) is the scattered intensity and q is the scattering vector ( $q=4\pi\sin\theta/\lambda$ ). The q range was 0.005–0.40 Å<sup>-1</sup> and the neutron wavelength was 6 Å with a wavelength spread  $\Delta\lambda/\lambda = 0.11$  or 0.15. A demountable titanium cell with a 1 mm or 2

mm path length was used for SANS measurement. A series of (quaternized) PDMAEMA solutions in water with desired d-SDS concentrations were prepared by mixing two stock solutions: (quaternized) PDMAEMA solution and d-SDS solution. To create hydrogels with micelles, 1,2-bis(2-iodoethoxy)ethane (BIEE) crosslinker was added to the solutions. Half of each mixture was injected using a syringe into a demountable titanium cell which kept until hydrogel formed. Complete crosslinking was determined by the inversion of the remaining mixture.

## **5.3 Results**

### **5.3.1 Quaternization of PDMAEMA and characterization**

In the previous chapter, we demonstrated that structured hydrogels templated using mixed micelles can be created by crosslinking PDMAEMAs with BIEE in the presence of d-SDS surfactants. Additionally, it was found that the aggregation number of d-SDS per micelle in PDMAEMA hydrogels increased as the degree of quaternization of the PDMAEMA increased due to charge screening, although the spherical form of the micelles was maintained. In literature, the growth of spherical SDS micelles into cylindrical micelles has been observed by adding electrolytes,<sup>50, 63, 66, 67</sup> or polyelectrolytes<sup>69-72</sup>. When the growth occurs in polyelectrolyte hydrogels, it can provide a method to control the size and shape of pores in the hydrogels, generated after the removal of the micelles. In creating such hydrogels, the control of the size and shape of SDS micelles in polyelectrolyte solutions is a prerequisite. In contrast to simple electrolytes, when polyelectrolytes are added to SDS micelle

solutions, the charge ratio of polyelectrolyte to SDS surfactants plays an important role in determining phase behavior of polyelectrolyte/SDS complexes in water. For example, when either SDS or the polyelectrolyte is in sufficient excess, the solutions are clear and isotropic. On the other hand, as the charge ratio of polyelectrolyte to SDS approaches 1, phase separation into a precipitate and a clear liquid solution occurs. Prior to precipitation, as the charge ratio is varied, the solutions are turbid due to the existence of large polyelectrolyte/SDS complexes. In the current study, since we have interest in controlling the size and shape of d-SDS micelles, we will vary the positive charge density of the PDMAEMA. PDMAEMA is positively charged at acidic pH, but using pH may also alter the SDS micellization behavior<sup>50</sup>. To avoid this, PDMAEMA was quaternized using methyl iodide in THF at room temperature. To regulate the degree of quaternization, the total amount of methyl iodide added was varied. After methyl iodide was added, the PDMAEMA solutions turned turbid yellow as THF is a non-solvent for quaternized PDMAEMAs. The solutions were stirred overnight to ensure the completion of chemical reaction, and then the polymers were filtered and dried in vacuum for one day at 45 °C. The resulting polymers were dissolved in D<sub>2</sub>O and <sup>1</sup>H-NMR was used to determine the polymer structure. The chemical structure of PDMAEMA before and after quaternization and their <sup>1</sup>H-NMR results are shown in Figure 5.1. The chemical shifts of peaks of side chain protons to higher ppm due to the quaternization can be observed, and are assigned in Figure 5.1. On the other hand, the peaks from the main-chain methylene protons and side methyl group protons are not affected as these protons are far from the reaction site.

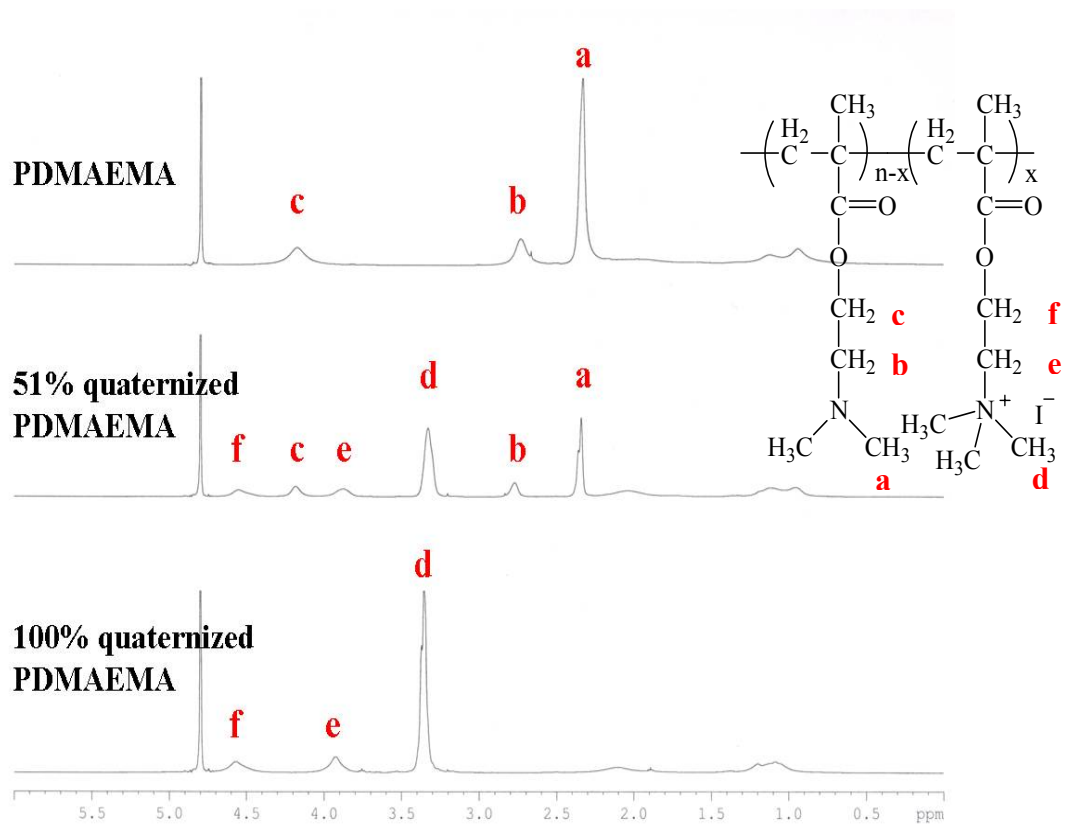


Figure 5.1. <sup>1</sup>H-NMR of (quaternized) PDMAEMAs in D<sub>2</sub>O

Table 5.1. Degree of quaternization (DQ) obtained from  $^1\text{H-NMR}$  results

<b>Polymer</b>	<b>Expected DQ (%)</b>	<b>(n-x)/n</b>	<b>x/n</b>	<b>Calculated DQ (%)</b>
<b>PDMAEMA</b>	<b>0</b>	<b>1</b>	<b>0</b>	<b>0</b>
<b>24% quaternized PDMAEMA</b>	<b>25</b>	<b>0.76</b>	<b>0.24</b>	<b>24</b>
<b>51% quaternized PDMAEMA</b>	<b>50</b>	<b>0.49</b>	<b>0.51</b>	<b>51</b>
<b>74% quaternized PDMAEMA</b>	<b>75</b>	<b>0.26</b>	<b>0.74</b>	<b>74</b>
<b>100% quaternized PDMAEMA</b>	<b>100</b>	<b>0</b>	<b>1</b>	<b>100</b>

The degree of quaternization was calculated by comparing the peak area of tertiary amines to the peak area of quaternized amines, and the results are summarized in Table 5.1.

### **5.3.2 SANS of quaternized PDMAEMA solutions/hydrogels with 100 mM d-SDS**

Since a 200 mg/ml PDMAEMA solution, corresponding to 1.27 M concentration of monomers, mixed with 100 mM d-SDS, was successfully crosslinked using BIEE, each polyelectrolyte solution was prepared with the same monomer molar amount, resulting in an increase in the polymer concentration as the quaternized PDMAEMA contains (heavy) iodine ions. In all the polymer solutions, the d-SDS concentration was fixed at 100 mM. This resulted in transparent homogeneous polymer/d-SDS solutions since the ratio of quaternized PDMAEMA monomer charge to d-SDS is well above 1. This means that the d-SDS micelles are well-dispersed in the concentrated polymer solution before crosslinking. Before addressing the d-SDS micelle structures in the quaternized PDMAEMA solution, it is useful to compare the effect of d-SDS on chain conformation for PDMAEMA and quaternized PDMAEMA as it can give direct evidence for interactions between the d-SDS and the polymer. Figure 5.2 shows SANS intensity of (quaternized) PDMAEMA solutions with or without 100 mM d-SDS in D<sub>2</sub>O. The SANS intensity of the 200 mg/ml PDMAEMA solution is a monotonically decreasing function with angle, which is a characteristic of concentrated neutral polymer solutions. The data was fit to a modified Lorentzian function as follows:<sup>80, 81</sup>

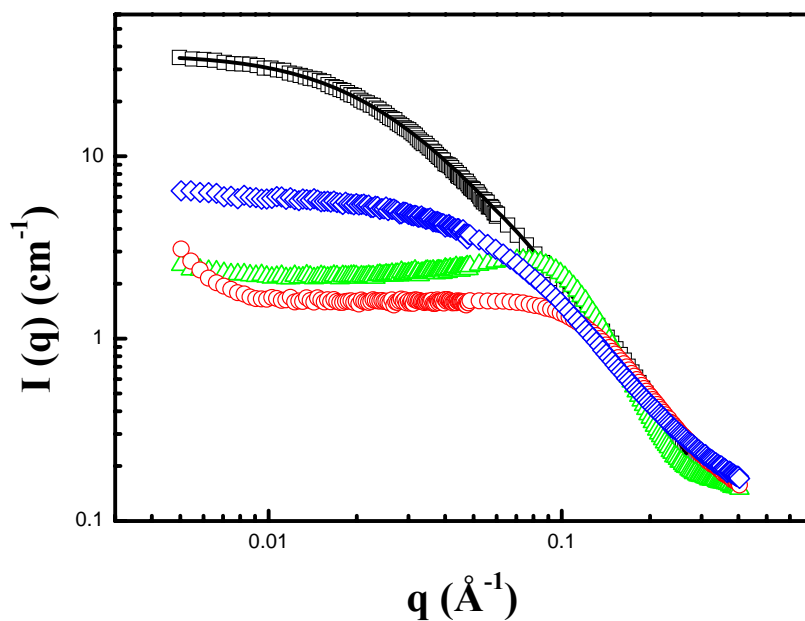


Figure 5.2. SANS intensity of a 200 mg/ml PDMAEMA solution (black squares) and a 290 mg/ml 51% quaternized PDMAEMA solution (red circles) in D2O. SANS intensity of a 200 mg/ml PDMAEMA solution was fit to a modified Lorentzian function. (black line). The changes of SANS intensity of the polymer solutions induced by adding 100 mM d-SDS with are also measured: 200 mg/ml PDMAEMA solution with 100 mM d-SDS (green triangles) and 290 mg/ml quaternized PDMAEMA solution with 100 mM d-SDS (blue diamonds)

$$I(q) = \frac{A}{1 + (qL)^m} + B \quad (5.1)$$

In this function,  $A$  is the scattering scale,  $L$  is a correlation length,  $m$  is the Porod exponent, and  $B$  is a background. The solid line shows the fit result where  $C$  is  $36.5 \text{ cm}^{-1}$ ,  $L$  is  $42.6 \text{ \AA}$ , and  $m$  is  $1.92$ . Since the Porod exponent  $m$  is related to the Flory excluded volume exponent  $\nu$  as  $m = 1/\nu$ ,<sup>80</sup> it is apparent that  $\text{D}_2\text{O}$  is approximately a theta solvent at  $25 \text{ }^\circ\text{C}$ . The SANS intensity of the  $290 \text{ mg/ml}$   $51\%$  quaternized PDMAEMA solution shows an upturn in the low  $q$  region and a peak at about  $q \sim 0.08 \text{ \AA}^{-1}$ , which are characteristic of polyelectrolyte solutions. When  $100 \text{ mM}$  d-SDS is added to the polymer solution, the SANS intensity changed significantly, indicating that the polymer conformation is altered by the added surfactant. For example, a peak observed in SANS intensity of  $200 \text{ mg/ml}$  PDMAEMA mixed with  $100 \text{ mM}$  d-SDS indicates that charged d-SDS micelles containing PDMAEMA segments are preferably formed. However, in the  $51\%$  quaternized PDMAEMA solution, the presence of  $100 \text{ mM}$  d-SDS surfactants caused an increase in SANS intensity as well as the disappearance of the upturn at low  $q$  region. Since the upturn represents large clusters in the polyelectrolyte solution, its disappearance indicates that the added d-SDS surfactants have disrupted the electrolyte behavior of the quaternized PDMAEMA. The anionic d-SDS surfactants will bind to the positively charged PDMAEMA monomers via electrostatic attractions in the solution. At the same time, it is expected that the d-SDS surfactants should form micelles to shield the d-SDS hydrocarbon tails from water. In the micellization of d-SDS surfactants, the oppositely charged PDMAEMA monomers interacting with d-SDS surfactants via electrostatic attractions should be involved.

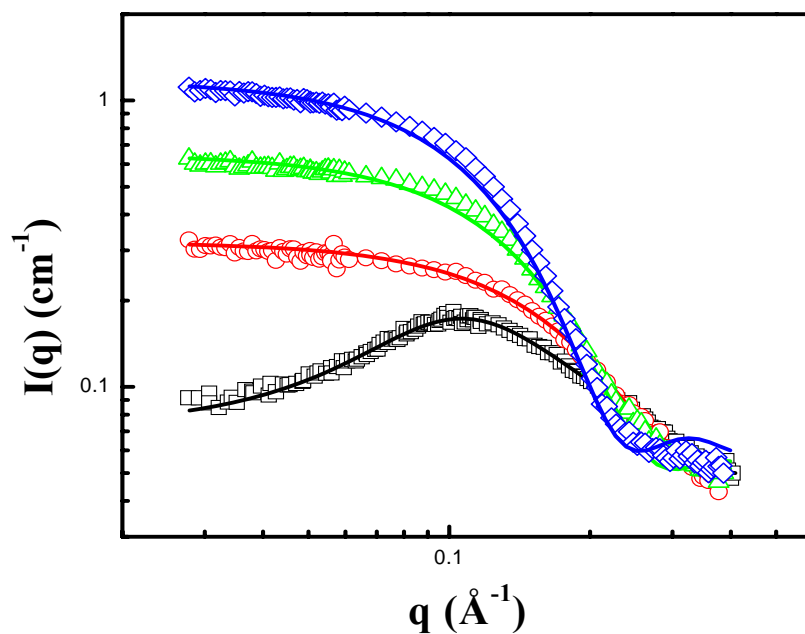


Figure 5.3. SANS intensity of (quaternized) PDMAEMA solutions with 100 mM d-SDS in a mixture of 80% H<sub>2</sub>O and 20% D<sub>2</sub>O: 200 mg/ml PDMAEMA (black squares), 245 mg/ml 24% quaternized PDMAEMA (red circles), 290 mg/ml 51% quaternized PDMAEMA (green triangles) and 335 mg/ml 74% quaternized PDMAEMA solution (blue diamonds) The solid lines represent the fit results.

The presence of d-SDS affects the conformation of the 51% quaternized PDMAEMA chains in the solution, not to form clusters although the ratio of the molar of d-SDS surfactant to the molar of the quaternized PDMAEMA monomer is  $\sim 0.2$ , while the disappearance of an upturn in SANS intensity is observed at excess electrolytes in polyelectrolyte/electrolyte solutions. The structure of micelles was investigated at the condition where the polymer was contrast-matched to a mixture of 80% H<sub>2</sub>O and 20% D<sub>2</sub>O,<sup>76</sup> as shown in Figure 5.3. A peak characteristic of charged micelles is observed only in the PDMAEMA solution, and not in the quaternized PDMAEMA solution. It is observed that the SANS intensity in the low  $q$  region increases as the degree of quaternization of PDMAEMA increases, indicating a growth of mixed micelles in the solution. Several different shapes are possible for the micelles, including spheres, ellipsoids, cylinders, and bilayers. In general, the shape of the micelle can be rationalized based on the net geometry of the amphiphilic molecules using a term called the critical packing parameter (CPP),<sup>34, 50, 63</sup> which is defined as:

$$CPP = \frac{a_{tail}}{a_{hg}} \quad (5.2)$$

where  $a_{hg}$  is the effective area of hydrophilic headgroup and  $a_{tail}$  is the average area of the hydrophobic tail. The larger the headgroup area compared to the tail area, the more curved the aggregates. At a CPP less than 1/3, corresponding to a cone shape, leads to spherical micelles while a CPP between 1/3 and 1/2 corresponds to cylindrical micelles. Finally, a CPP between 1/2 and 1 assemble into bilayer structures in water. It is notable that one can change  $a_{hg}$  by decreasing or increasing the electrolyte concentration in the case of ionic surfactants. In our case, as the molar

concentration of quaternized PDMAEMA monomers at fixed d-SDS molar concentration increases, the CPP of the d-SDS surfactant will decrease, resulting in a change in the favored micelle structure. It has also been observed that a long range interaction between charged d-SDS micelles disappears due to charge screening between the anionic d-SDS and the positively charged PDMAEMA. The size and shape of the micelles was obtained by modeling the SANS data. Depending on whether the polymer was quaternized or not, different models were used. For example, in the case of PDMAEMA/d-SDS solution, a spherical core-shell model with a rescaled mean spherical approximation closure<sup>14, 60-62, 75</sup> was adapted as PDMAEMA is almost neutral at its natural pH. However, in case of quaternized PDMAEMA/d-SDS solutions, a cylindrical core-shell model<sup>83</sup> was used to account for the charge screening effect. For spherical micelles, the core radius of the mixed micelle was constrained to be less than 16.7 Å,<sup>68</sup> which is the length of a fully extended alkyl chain of d-SDS, and the scattering length density of the solvent,  $8.2 \times 10^{-7} \text{ \AA}^{-2}$  was used. The neutron scattering length density of the core ( $\rho_{core}$ ) was calculated from the relationship:  $\rho_{core} = \frac{\sum b_i}{V}$  where  $\sum b_i$  is the sum of  $b_{CD_2}$  and  $11b_{CD_2}$  of a d-SDS surfactant in the core and  $V$  is the volume of the alkyl chain, composed of a methyl group and 11 methylene groups, as found in a d-SDS surfactant. The scattering length and the volume per chemical group were adopted from Cabane et al.<sup>54</sup> However, the scattering length density of the shell was left as a floating value to account for the participation of PDMAEMA segments in the shell. The values obtained are used in the fit of the cylindrical core-shell model, by allowing the core radius and the cylinder length to float during the fit process in order

Table 5.2. Optimized parameters from model fits

Polymer Concentration	$R_1$ (Å)	$L$ (Å)
200 mg/ml PDMAEMA	9.8	-
245 mg/ml 24 % quaternized PDMAEMA	10.5±0.36	19.85±1.41
290 mg/ml 51 % quaternized PDMAEMA	13.34±1.44	23.45±4.99
335 mg/ml 74 % quaternized PDMAEMA	15.85±1.07	27.96±3.75

$R_1$  : Core radius in Å

$L$  : Core length in Å

to describe the growth of the micelles. The results are shown as lines in Figure 5.3 and the optimized values are given in Table 5.2. The fit results indicate that the charge screening provided by quaternizing the PDMAEMA leads to a transition of spherical to cylindrical micelles in both directions: radius and length. It was shown before that PDMAEMA hydrogels with spherical d-SDS micelles can be created through chemical crosslinking of PDMAEMA monomers using BIEE. The same method was adapted to create quaternized PDMAEMA hydrogels with cylindrical micelles. To control the crosslinking ratio, the desired amount of BIEE was added to 290 mg/ml 51% quaternized PDMAEMA solution with 100 mM d-SDS. Here, the crosslinking ratio is defined as the moles of BIEE over the total moles of PDMAEMA monomer. The structure of d-SDS micelles in the hydrogels was observed using SANS at the condition where the polymer was contrast-matched and the results are shown in Figure 5.4. The results confirm that the micelles are stable after the crosslinking reaction. From a cylindrical core-shell model fit, it was found that although the shape of the micelles in the solution was maintained after crosslinking, the core radius and the length of mixed micelles increased to  $14.8 \pm 0.6 \text{ \AA}$  and  $26.6 \pm 2.2 \text{ \AA}$ , respectively. Since the chemical reaction between two uncharged monomers of the 51% quaternized PDMAEMA and BIEE generates two quaternized monomers, at the crosslinking ratio (0.04), the degree of quaternization increases from 51% to 59%, leading to the growth of the mixed micelles.

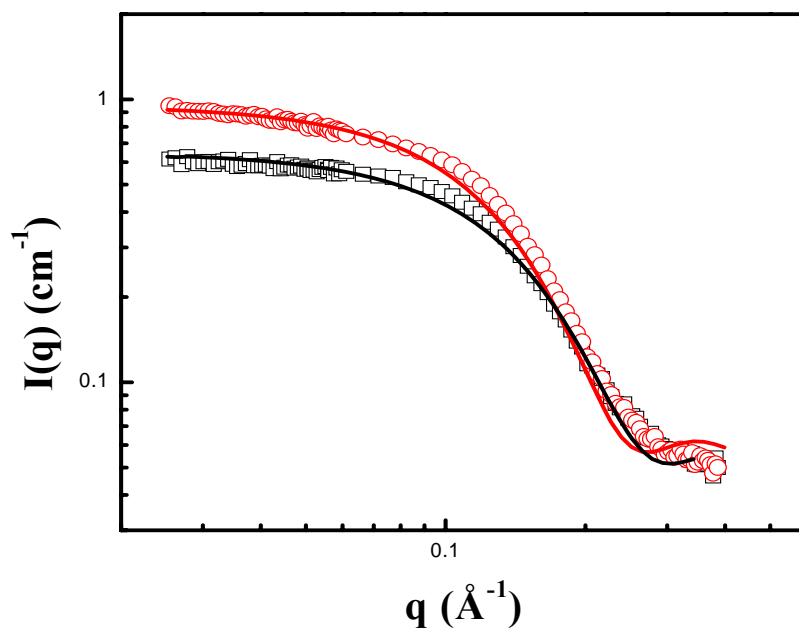


Figure 5.4. SANS intensity of a 290 mg/ml 51% quaternized PDMAEMA solution with 100 mM d-SDS (black squares) and its corresponding hydrogel with 0.04 crosslinking ratio (red circles) in a mixture of 80% H<sub>2</sub>O and 20% D<sub>2</sub>O. The solid lines represent the fit results.

## 5.4 Conclusions

PDMAEMA of 60,000 g/mol with 1.12 PDI was synthesized using GTP and quaternized using methyl iodide in THF. The degree of quaternization of the resulting polymers was easily controlled, as determined using  $^1\text{H-NMR}$ . Using (quaternized) PDMAEMAs with different degrees of quaternization, it was attempted to control the micellization of d-SDS surfactants in the (quaternized) PDMAEMA solutions, and the structure was investigated using H/D contrast-matching methods with SANS. When 100 mM d-SDS was added to a 200 mg/ml PDMAEMA solution in  $\text{D}_2\text{O}$ , a peak characteristic of ionic micelles was observed. Since d-SDS is contrast-matched to  $\text{D}_2\text{O}$ , the result indicates that the liquid-like order of the d-SDS micelles is transferred to PDMAEMA chains by forming necklace-like structures, similar to what has been observed in PEO/SDS complexes. However, in a 290 mg/ml 51% quaternized PDMAEMA solution, the added d-SDS surfactants disrupted the cluster formation via electrostatic attractive interactions between the quaternized PDMAEMA monomers and the d-SDS surfactants, as evidenced by the disappearance of the large upturn in the scattering in the low  $q$  region. The effect of the charge screening was also observed in d-SDS micellization process as the positively charged PDMAEMA monomers reduced the effective area of anionic headgroup. Therefore, the characteristic micelle peak was not observed in SANS of the 51% quaternized PDMAEMA/d-SDS solution.

The structure of the micelles in (quaternized) PDMAEMA/d-SDS solutions was investigated at the condition where polymer was contrast-matched with a mixture of

80% H<sub>2</sub>O and 20% D<sub>2</sub>O. The characteristic peak of the ionic micelles is observed only in the PDMAEMA/d-SDS solution and the SANS intensity of the quaternized PDMAEMA/d-SDS solutions increases at low  $q$  as the degree of quaternization of the polymer increases, indicating a growth of mixed micelles due to charge screening. From the model fits, it was found that spherical micelles in the PDMAEMA/d-SDS solution grew in radius and length and transformed to cylindrical micelles. A quaternized PDMAEMA hydrogel with cylindrical micelles was created by adding BIEE to a 290 mg/ml 51% quaternized PDMAEMA solution with 100 mM d-SDS. Since the crosslinking reaction generates quaternized monomers, the increased degree of quaternization in the hydrogel caused a change in the size of the micelles while the cylindrical shape was maintained.

## **Chapter 6: A simple method for creating oriented nanopores in block-copolymer thin films**

A difficulty in directly observing the change of pores during swelling and deswelling of molecularly imprinted polymers (MIP) comes from the fact that pores exist inside MIPs. In order to overcome the restriction, it is required to make pores observable at the surface of MIPs. In order to create nanoporous films, we used the self-assembly of polystyrene-*b*-poly(4-vinyl pyridine) (PS-*b*-P4VP)/poly(4-vinyl pyridine) (P4VP) blend films. Using preference of the solvent (THF) for polystyrene (PS) compared to P4VP and by varying the total P4VP weight fraction, we could control the size of phase-separated P4VP domains in the films. The extraction of P4VP homopolymer from the films in ethanol enabled us to generate nanopores at multiple length scales.

### **6.1 Introduction**

Block copolymers are well-known to self-assemble into nano- and mesoscale structures and the use of block copolymers for nanostructured patterns has attracted increasing attention due to their potential use as templates and scaffolds for the fabrication of functional nanostructures.<sup>22, 84-86</sup> In order to realize the potential of these materials, it is required that orientation of the nanostructured patterns is controlled in a designated manner. Numerous methods have been developed to control orientation of nanostructures which include the manipulation of the interfacial

interactions,<sup>87</sup> use of electric fields,<sup>88</sup> and controlling the rate of solvent evaporation<sup>89</sup>. In addition, it has been shown that nanopores within cylindrical block copolymer domains oriented normal to the substrate can be generated by several novel methods.<sup>90, 91</sup> These methods use a homopolymer/block copolymer solution where a homopolymer has the identical chemical structure to or prefers one of the blocks in the block copolymer and nanoporous structures are generated by dissolving the homopolymer in a selective good solvent for the homopolymer. To control orientation of the cylinders in polystyrene-*b*-poly(methyl methacrylate) block copolymer (PS-*b*-PMMA) and PMMA homopolymer or poly(ethylene oxide) (PEO), a tailored surface to balance interactions between the segments of the copolymer and the interfaces as well as extended annealing of the films was required to induce a well-ordered self-assembled structure.<sup>90</sup> This drawback was overcome with polystyrene-*b*-poly(ethylene oxide) block copolymer (PS-*b*-PEO)/PEO or PS-*b*-PEO/PMMA where self-assembly occurs at the air surface and ordering then propagates through the film.<sup>91</sup> In this research, we adopted a similar strategy to generate nanopores oriented normal to the substrate in thin block copolymer films using polystyrene-*b*-poly(4vinylpyridine) block copolymer (PS-*b*-P4VP) and P4VP homopolymer tetrahydrofuran (THF) solutions, where THF has a preferential affinity for PS. Although it might be possible to regulate the size or order of nanodomains in as-spun PS-*b*-P4VP/P4VP through solvent annealing, in this communication we will focus on explaining the phase-separation behaviors of PS-*b*-P4VP/P4VP during spincoating since P4VP homopolymers are solubilized in the P4VP blocks without a macro-phase separation within our experimental conditions. It enabled us to control the pore size in

multiple length scale after the extraction of P4VP homopolymer using ethanol from the film, meaning a simple way to control refractive index of the nanoporous films.

## 6.2 Experimental

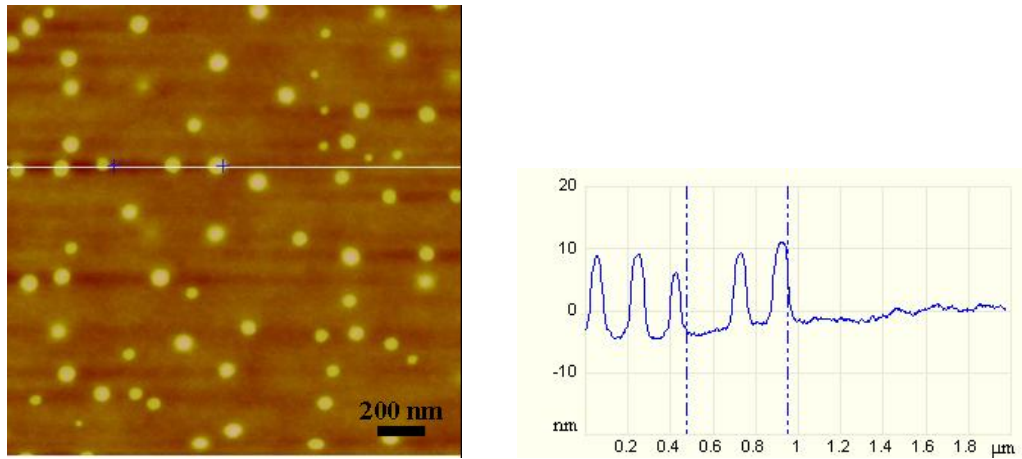
PS-b-P4VP (number average molecular weight  $M_n^{PS} = 310 \text{ kgmol}^{-1}$ ,  $M_n^{P4VP} = 10 \text{ kgmol}^{-1}$ , polydispersity index = 1.09), PS homopolymer ( $M_n = 300 \text{ kgmol}^{-1}$ , polydispersity index = 1.2) and P4VP homopolymer ( $M_n = 5.1 \text{ kgmol}^{-1}$ , polydispersity index = 1.06) were purchased from Polymer Source, Inc., and used without further purification. PS/P4VP and PS-b-P4VP/P4VP were dissolved in THF from Aldrich at 80 °C for 12 hours and cooled to room temperature. In the resulting solutions, the concentration of PS or PS-b-P4VP was fixed at 0.5 wt%, but the concentration of P4VP homopolymer was changed and, depending on the amount of P4VP homopolymer added, the P4VP weight fraction varied from 0.03 to 0.45. Here, P4VP weight fraction is defined by a ratio of the total P4VP weight to the total polymer weight in the solutions. The polymer solutions were prefiltered through Millipore 0.45  $\mu\text{m}$  poly(tetrafluoroethylene) filters. PS/P4VP and PS-b-P4VP/P4VP blend films were prepared by spin-coating at 3000 rpm for 60 s on silicon substrates or mica. Thin film surface morphology was characterized using a Dimension 3000 atomic force microscope (AFM) from Digital Instruments, Inc. Silicon tips on a cantilever with spring constants ranging between 20.0 and 80.0 Nm (as specified by the manufacturer) were used. To measure thin film thickness, the polymer films deposited on silicon substrates were scratched with a scalpel, and AFM images were

taken at the borders of the scratches. The surface morphology of as-spun PS/P4VP or PS-*b*-P4VP/P4VP blend films on silicon substrates was examined using AFM in tapping mode. Transmission electron microscopy (TEM) was performed using a JEOL JEM-2100F field emission TEM at 200kV coupled with a Gatan CCD camera. TEM samples were spun on mica with the same conditions described before, floated on deionized water, captured on a TEM grid, and stained with iodine. To prepare nanoporous films, as-spun PS-*b*-P4VP/P4VP blend films were soaked in ethanol, which is a selective solvent only for P4VP, for 3 hours and dried in air. In order to confirm whether nanopores penetrate through the entire film, the cross-sectional image of a PS-*b*-P4VP/P4VP blend film with 0.45 of P4VP weight fraction was observed using scanning electron microscope (SEM). A layer of gold was coated on the surface of a polymer film and then the film was cleaved in liquid nitrogen to preserve the morphology. SEM observation was conducted with a Hitachi SU-70 Schottky field emission gun scanning electron microscope working at 3kV accelerating voltage and working distance around 5mm.

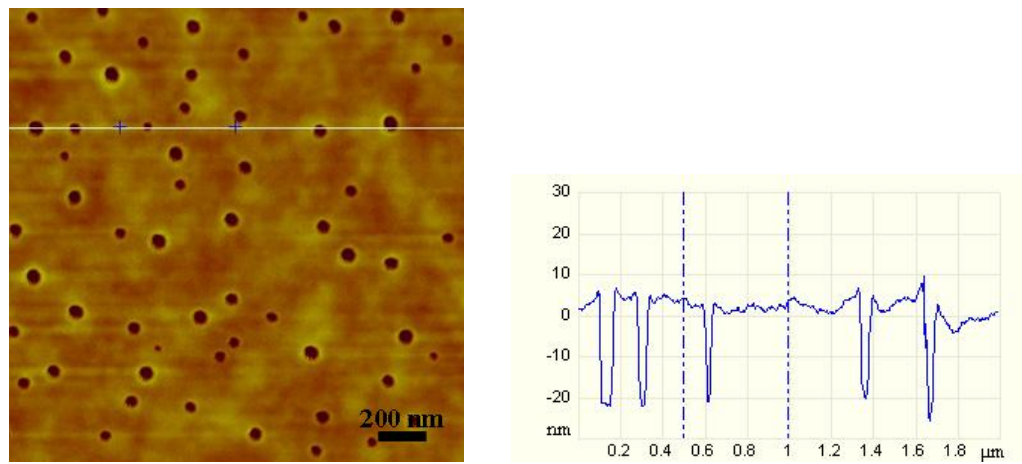
### 6.3 Results

It has been reported in the review paper by H. Colfen that P4VP is difficult to polymerize anionically due to insolubility in THF above a critical molecular weight.<sup>92</sup> For PS-*b*-P4VP block copolymers with P4VP weight fraction above 0.16, spherical PS-*b*-P4VP micelles in THF were observed using static and dynamic light scattering.<sup>93</sup> Recently, in the work by Ali and Park, PS-*b*-P4VP block copolymers (12k-*b*-11.8k and 3.3k-*b*-18.7k) in a toluene/THF mixture, which have a smaller  $M_n^{PS}$

and a similar  $M_n^{P4VP}$  compared to our PS-b-P4VP block copolymer, were studied using small angle x-ray scattering to investigate the effects of solvent selectivity and block copolymer composition on the micellar structure.<sup>94</sup> Ali and Park found that PS-b-P4VP formed micelles only in the mixture of toluene/THF because toluene is a selective solvent for PS and THF is non-selective due to the small  $M_n^{P4VP}$ . Our PS/P4VP and PS-b-P4VP/P4VP polymer solutions in THF were optically transparent indicating that no large aggregates are formed due to the low P4VP weight fraction (~0.03) and the small  $M_n^{P4VP}$ . Also, the 5.1 kg/mol P4VP homopolymer used here completely dissolved in THF even at room temperature as the  $M_n$  is relatively small. Figure 6.1 (a) is an AFM height image of an as-spun PS/P4VP blend film on a silicon substrate, from a 0.5 wt% PS solution in THF with 0.35 of P4VP weight fraction in  $2 \mu\text{m} \times 2 \mu\text{m}$  scale. The AFM images show that nodules with on average 10 nm height protrude above a continuous matrix. Similar morphologies have been observed in various homopolymer blend films by other researchers.<sup>95-99</sup> The morphology is formed due to the rapid quench by solvent evaporation. Initially, PS and P4VP are dissolved in THF. During spincoating, THF evaporates and phase-separation of PS and P4VP occurs. Since THF prefers PS to P4VP, P4VP-rich phases are more quickly depleted of the solvent and solidified earlier. Subsequent evaporation of the remaining solvent leads to a collapse of the PS-rich phases, leading to elevated P4VP nodules. It was confirmed that the morphology can be used to generate nanopores, which resemble the nodules in size and shape, by selectively dissolving P4VP homopolymer in ethanol, as shown in Figure 6.1 (b).



(a)



(b)

Figure 6.1. AFM height images of (a) an as-spun PS/P4VP blend film with 0.35 of P4VP weight fraction and (b) the PS/P4VP blend film after immersed in ethanol for 3 hours

The idea was extended to PS-*b*-P4VP/P4VP blend films. And, in an attempt to control the pore size, the amount of P4VP homopolymer in each solution was varied. As the concentration of P4VP homopolymer in the polymer solutions increases, the film thickness of the as-spun films increased from 25 nm to 45 nm. Figure 6.2 (a), (b), and (c) show AFM height images of as-spun PS-*b*-P4VP/P4VP blend films as a function of P4VP weight fraction. Although the PS-*b*-P4VP film without P4VP homopolymer in Figure 6.2 (a) has a weight fraction of about 0.03 of P4VP, the film showed a self-assembled structure with nodules in the PS matrix due to the strong repulsive interaction between the PS and the P4VP blocks. The reported Flory-Huggins interaction parameter,  $\chi$ , of PS-*b*-P4VP is approximately an order of magnitude greater than the largest values of reported  $\chi$  in other nonionic systems,<sup>100</sup> which is corroborated by block copolymer order-disorder transition temperatures well beyond 300 °C.<sup>101</sup> P4VP weight fraction in PS-*b*-P4VP/P4VP films was increased up to 0.45 by adding P4VP homopolymer to PS-*b*-P4VP solutions in THF. As the P4VP weight fraction in the polymer solutions increases, larger nodules are observed in the as-spun films, as shown in Figure 6.2 (b) and (c). In contrast to the PS/P4VP blend film (Figure 6.1), the nodules are more evenly and closely distributed throughout the films. A continuous structure, which has observed by Li et al. when the weight fraction of P4VP in a PS/P4VP blend film is about 0.5,<sup>97</sup> was not observed in these PS-*b*-P4VP/P4VP blend films. TEM was used to identify the P4VP domains in a PS-*b*-P4VP/P4VP film with 0.45 of P4VP weight fraction after iodine staining. Since iodine selectively stains the P4VP polymer, the P4VP domains appear darker in the TEM image, as shown in Figure 6.2 (d). As expected, the size and shape of nodules in

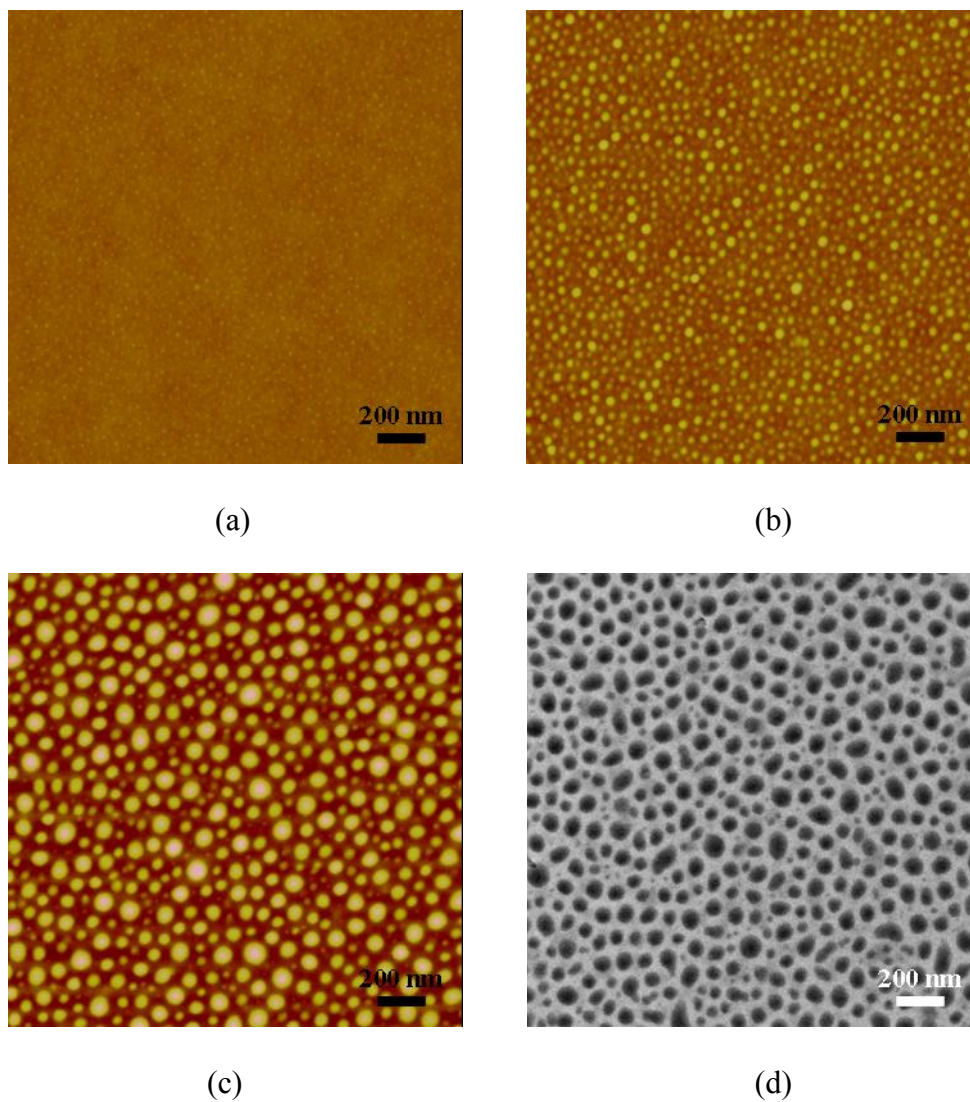
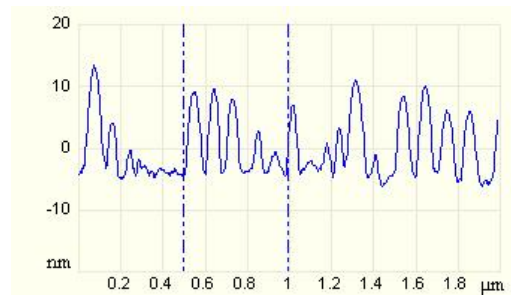
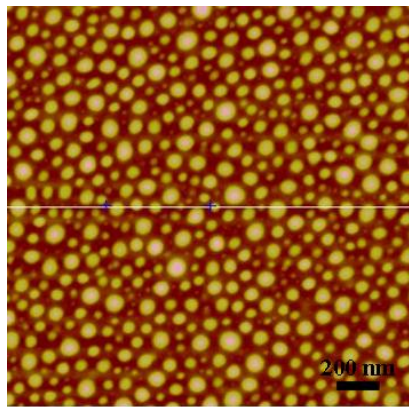


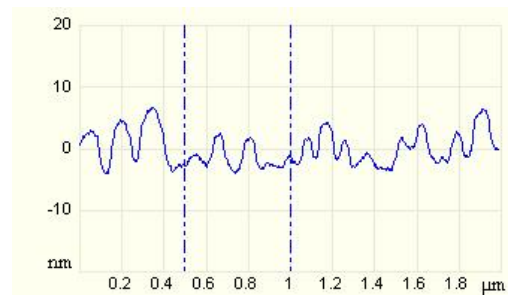
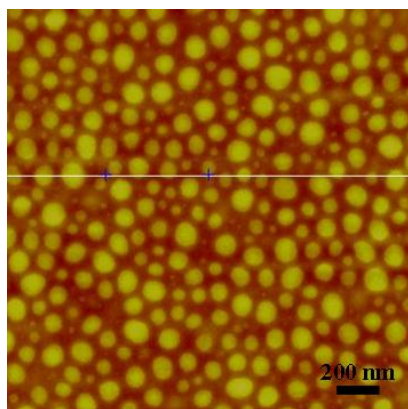
Figure 6.2. AFM height images of as-spun PS-b-P4VP/P4VP blend films as a function of P4VP weight fraction in the polymer solutions. P4VP weight fraction in the solutions was (a) 0.03, (b) 0.25, and (c) 0.45. (d) TEM image of PS-b-P4VP/P4VP film with 0.45 of P4VP weight fraction after iodine staining.

the AFM image of (c) film is comparable to those of darker domains in the TEM image of (d). These observations indicate that the P4VP homopolymer is solubilized in P4VP block domains during spincoating. It can be argued that the observed morphology of PS-b-P4VP/P4VP blend films is similar to that of PS-b-P4VP micelle films. To verify that nodules in PS-b-P4VP/P4VP blend films are formed due to the preferential affinity of THF for PS, similar to the blend films, we spincoated a PS-b-P4VP/P4VP solution with 0.45 of P4VP weight fraction at different levels of relative humidity (RH). RH during spincoating was controlled by adding water vapor to a glass chamber enclosing the spinning chuck on which the substrate was placed. RH was measured with a hydrometer inside the glass chamber. Figure 6.3 shows AFM height images of as-spun films depending on RH. For clarity, all three images are set to an identical height scale (30 nm). When RH during spincoating increased from 25% to 40%, the height of the nodules decreased. And, at 60% RH, the nodules were changed into pits. The observed behaviors are related to breath figure formation.<sup>102</sup> Generally, breath figures are ascribed to solvent-evaporative cooling on the surface of a polymer solution under humid conditions where water vapor is condensed into water droplets at the solution surface. The water droplets then interact with each other and become hexagonally packed. After complete evaporation of the solvent and water, traces of water droplets remain as a honeycomb structure in the polymer film.

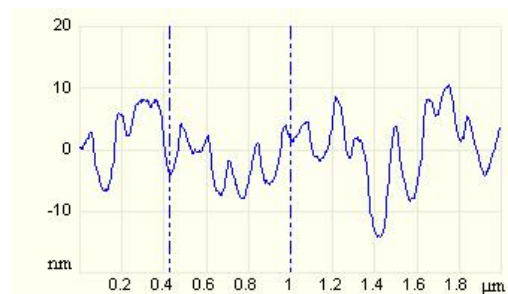
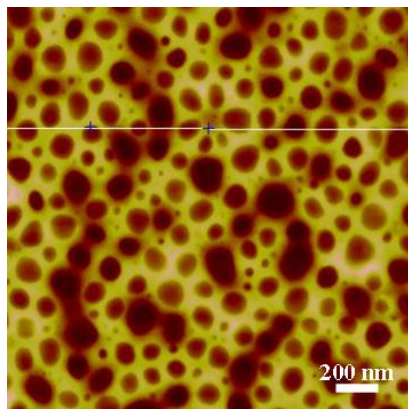
In our case, the fact that nodules, generated under dry conditions, were changed into pits at humid conditions indicates that THF evaporation rate was altered in the P4VP domains at humid conditions. Since THF evaporates faster in the P4VP domains than



(a)



(b)



(c)

Figure 6.3. AFM height images of as-spun PS-b-P4VP/P4VP blend films with 0.45 of P4VP weight fraction as a function of relative humidity (RH). RH : (a) 25%, (b) 40%, and (c) 60%.

in the PS matrix, at the early stage during spincoating at high humidity conditions this difference will cause the water vapor to condense preferentially on the P4VP domains. The condensed water will lower the THF evaporation rate significantly from the P4VP domains and lead to an elevated PS matrix since P4VP domains solidify last after the complete evaporation of the THF and condensed water.

Mean field calculations have shown that hexagonally packed P4VP cylinders embedded in PS can be expected for a volume fraction of P4VP block ranging from 0.12 to 0.31.<sup>21</sup> Therefore, as the concentration of added P4VP homopolymer increases, it can be expected that the PS-*b*-P4VP/P4VP blend films transition between sphere, cylinder and lamellar morphologies. Generally, in block copolymer melts, the morphology of the equilibrium microstructure is dependent on the volume fraction of minority block, the degree of polymerization and  $\chi$  between the blocks.<sup>84</sup> However, in block copolymer solutions, the phase behavior is more complicated and also depends on the polymer-solvent interaction parameters and the volume fraction of the polymer in the solution. During spincoating process, the solvent evaporates and the concentration of polymer solution varies from dilute to concentrated before formation of a thin film. Additionally, in our case, THF evaporates at different rates from the PS-rich phases compared to the P4VP-rich phases, depending on the preferential affinity. Therefore, the observed self-assembled structures of PS-*b*-P4VP/P4VP blend films, fabricated through spincoating, are far from thermodynamic equilibrium.

To confirm that the self-assembled structure can be utilized to generate nanoporous films, the P4VP homopolymer was removed from a PS-b-P4VP/P4VP film in ethanol. As a control experiment, a PS-b-P4VP film without P4VP homopolymer was also soaked in ethanol for 3 hours. After soaking, the nodules changed into holes. (Figure 6.4 (a)) Recently, Russell et al. found that PS-b-P4VP films, fabricated through spincoating of PS-b-P4VP solutions in toluene or toluene/THF mixtures, can be reconstructed by soaking the films in ethanol to leave P4VP on the surface, producing nanopores in the film.<sup>103, 104</sup> The same trend was observed after PS-b-P4VP/P4VP blend films were soaked in ethanol, while the size of holes increased as P4VP homopolymer amount in the polymer solutions increased, as shown in Figure 6.4 (b) and (c). The average size, calculated using ImageJ program<sup>105</sup>, was 88.5 nm<sup>2</sup>, 219.7 nm<sup>2</sup>, and 1452.6 nm<sup>2</sup> for each film (a), (b), and (c). Correspondingly, in each polymer film, the number density of pores decreased from 545/μm<sup>2</sup>, 388/μm<sup>2</sup>, to 141/μm<sup>2</sup> due to the increased pore size. It was confirmed that the nanopores penetrated through the entire films by measuring the cross-sectional image of the PS-b-P4VP/P4VP film with 0.45 P4VP weight fraction using SEM, as shown in Figure 6.4 (d). The film was chosen since the film was thickest among the polymer films studied.

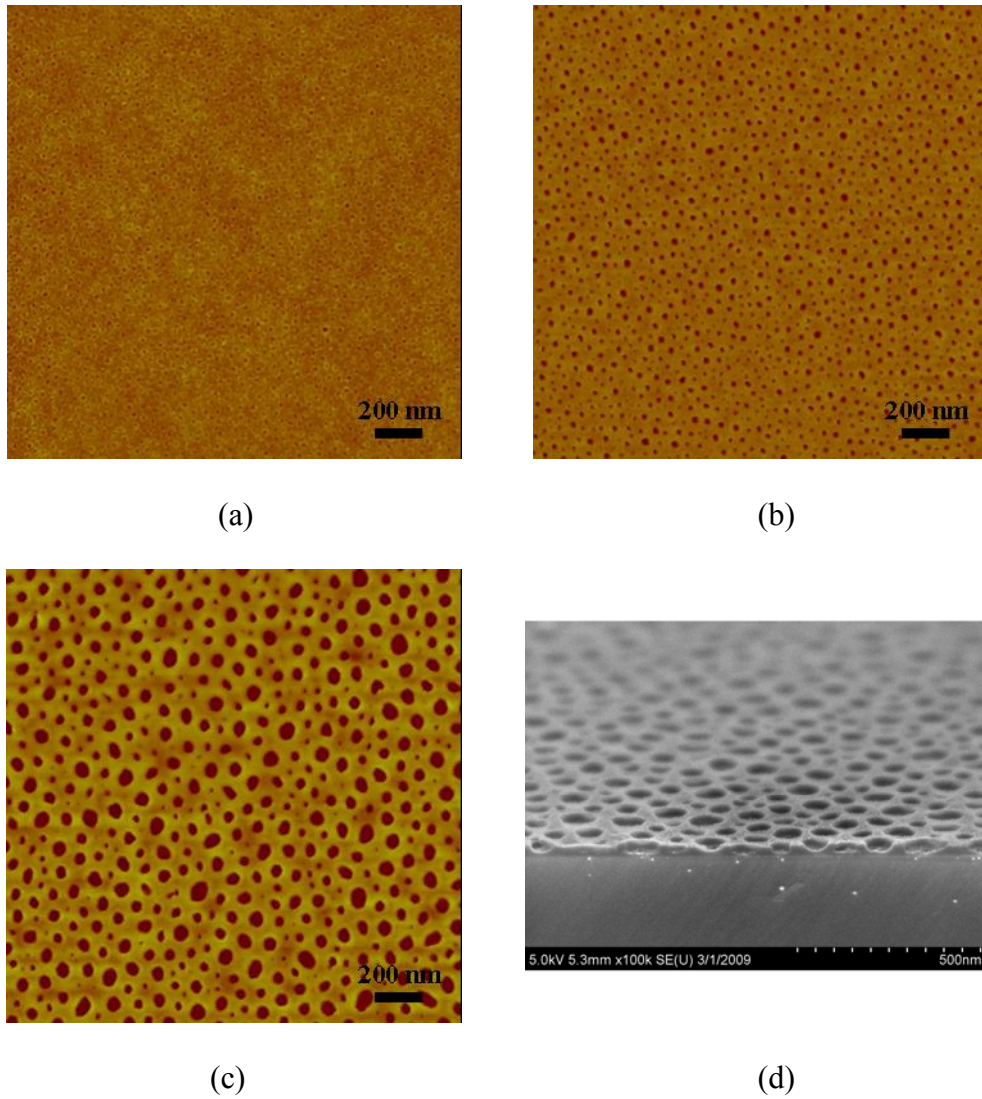


Figure 6.4. AFM height images of PS-b-P4VP/P4VP blend films after soaked in ethanol for 3 hours. P4VP weight fraction in the polymer solutions was (a) 0.03, (b) 0.25, and (c) 0.45. The cross-section of the film (c) was observed using SEM (d).

## 6.4 Conclusions

We have demonstrated using preferential solubility of PS in THF compared to P4VP, self-assembled structures can be generated in both PS/P4VP and PS-b-P4VP/P4VP blend films. In the resulting films P4VP domains protruded from the surface and their size was easily controlled by regulating the amount of P4VP homopolymer in the polymer solutions. Due to the large incompatibility of PS and P4VP, the added P4VP homopolymer was readily extracted from the as-spun films in with ethanol, which is a selective good solvent for P4VP, resulting in multiple length scale nanopores in the corresponding films. It is noteworthy that in our method, nanopores oriented normal to the substrate were generated without the requirement of a neutral surface and were formed using a relatively simple spin casting process and subsequent ethanol wash.

## Chapter 7: Conclusions and Suggestions for Future Work

### 7.1. Conclusions

Poly((2-dimethylamino)ethyl methacrylate) (PDMAEMA) with 60,000 g/mol and a narrow polydispersity, 1.12, was synthesized using group transfer polymerization. It was observed that when PDMAEMA was dissolved in D<sub>2</sub>O or in acidified D<sub>2</sub>O, the polymer shows polyelectrolyte behavior as the tertiary amines in the chain are charged. The polyelectrolyte behavior can be screened by adding 1.3 mM d-SDS or 3 mM NaCl in the solution. Above 3 mM deuterated sodium dodecylsulfate (d-SDS), small angle neutron scattering (SANS) intensity shows correlation peaks from charged micelles formed along the PDMAEMA chains. d-SDS micellization in the PDMAEMA solution starts below the normal SDS critical micelle concentration, which indicates that the PDMAEMA chains provide favorable interactions towards d-SDS micellization. As the d-SDS concentration is increased, the observed scattering peak position shifted to high  $q$ , indicating more charged micelles are associating per PDMAEMA chain. In spite of the unfavorable repulsive interactions, the charged micelles associate with the PDMAEMA chains in preference to forming free d-SDS micelles as the unfavorable interactions are relieved by stretching of the PDMAEMA chain.

A structural analysis of the d-SDS micelle/PDMAEMA mixture was performed at the condition where the PDMAEMA was contrast-matched with a mixture of 80% H<sub>2</sub>O and 20% D<sub>2</sub>O. From the model fit, it was found that the size of d-SDS micelle

decreased with increasing PDMAEMA concentration, while maintaining its spherical shape. The reduction in the aggregation number of d-SDS surfactant molecule per micelle lead to a smaller average distance between micelles as the PDMAEMA concentration increased. Although the smaller distance would be expected to be unfavorable due to the repulsive potential, from the form factors and the structure factors obtained from fitting the SANS data, it was found that the formation of smaller micelles with lower surface charge reduces the repulsive interaction potential between the micelles significantly.

Using the PDMAEMA/d-SDS complexes in solution, structured hydrogels with micelles were created by crosslinking the polymers with 1,2-bis(2-iodoethoxy)ethane (BIEE). Since each BIEE molecule generated two quaternized amines, the quaternized amines influenced d-SDS micellization similar to the effect of an electrolyte. From the model fits, it was found that the aggregation number of d-SDS surfactants per micelle increased to compensate for increased water contact due to the charge screening. The effect of the charge screening on the d-SDS micellization was confirmed from the reduced surface charges per micelle as the crosslinking ratio increased, disrupting the liquid-like order and eventually leading to a randomized distribution of the mixed micelles in hydrogel.

PDMAEMA of 60,000 g/mol with 1.12 PDI was quaternized using methyl iodide in THF. Using (quaternized) PDMAEMAs with different degrees of quaternization, it was attempted to control the micellization of d-SDS surfactants in the (quaternized) PDMAEMA solutions, and the structure was investigated using H/D contrast-

matching methods with SANS. From the model fits, it was found that spherical micelles in the PDMAEMA/d-SDS solution grew in radius and length and transformed to cylindrical micelles. A quaternized PDMAEMA hydrogel with cylindrical micelles was created by adding BIEE to a 290 mg/ml 51% quaternized PDMAEMA solution with 100 mM d-SDS. Since the crosslinking reaction generates quaternized monomers, the increased degree of quaternization in the hydrogel caused a change in the size of the micelles while the cylindrical shape was maintained.

We have demonstrated using preferential solubility of polystyrene (PS) in tetrahydrofuran (THF) compared to poly(4-vinylpyridine) (P4VP), self-assembled structures can be generated in both PS/P4VP and polystyrene-b-poly(4-vinylpyridine) (PS-b-P4VP)/P4VP blend films. Due to the large incompatibility of PS and P4VP, the added P4VP homopolymer was readily extracted from the as-spun films in with ethanol, which is a selective good solvent for P4VP, resulting in multiple length scale nanopores in the corresponding films. It is noteworthy that in our method, nanopores oriented normal to the substrate were generated without the requirement of a neutral surface and were formed using a relatively simple spin casting process and subsequent ethanol wash.

## **7.2. Suggestions for future work**

In this Section a suggestions are given for extension of the current work based on interesting behavior and ideas that were observed and developed during the experiments presented in this dissertation.

We have shown, using preferential solubility of PS in THF compared to P4VP, self-assembled structures can be generated in both PS/P4VP and PS-b-P4VP/P4VP blend films. Since the polymers form a glassy film during spincoating, the self-assembled structures are far from thermodynamic equilibrium. In general, equilibrium morphology of bulk diblock copolymer films is determined by a volume ratio between blocks, temperature and molecular weight. Although a surface and an interface have additional effects on equilibrium morphology in case of nano-thin diblock copolymers on substrates, several novel methods have been introduced to control nanostructures. Among those, controlling the rate of solvent evaporation in polystyrene-b-poly(ethylene oxide) (PS-b-PEO) and PS-b-PEO/(ethylene oxide) (PEO) films has critical advantages over others, such as no requirement of a neutral substrate, since a well-ordered self-assembly occurs at the air interface and ordering then propagates through the film.

We found that a well-ordered self-assembly in PS-b-P4VP or PS-b-P4VP/P4VP blend films could be induced using a solvent annealing, similar to PS-b-PEO or PS-b-PEO/PEO. Since P4VP homopolymers are solubilized in P4VP blocks in the films, the extraction of P4VP homopolymers in ethanol, which is a selective solvent for P4VP, from the blend films created a well-ordered nano-pores as well as reconstructed the films to leave P4VP blocks on the surface. The created pores are aligned to perpendicular to substrates, and it was possible to control the pore size by regulating the added amount of P4VP homopolymers in PS-b-P4VP/P4VP films.

Therefore, this method will give a convenient way to create nano-membranes with various pore sizes.

Although both P4VP and PEO have several similar chemical properties, such as hydrogen bonding formation and hydrophilicity, P4VP can be positively charged in acidic pH or through a quaternization using a chemical with a halide group. The resulting films can be utilized as smart membranes responding to electrolyte concentration in water. In pure water, charged P4VP blocks will swell due to the repulsive interactions between charged P4VP monomers, causing nanopores to be closed. On the other hand, in an excess electrolyte concentration, the screening of the repulsions between charged P4VP monomers will cause the nanopores to be open since the charged P4VP blocks will be deswelled.

## Bibliography

1. Hart, B. R.; Shea, K. J. *Macromolecules* **2002**, 35, (16), 6192-6201.
2. J. Wizeman, W.; Kofinas, P. *Biomaterials* **2001**, 22, (12), 1485-1491.
3. Piletsky, S. A.; Matuschewski, H.; Schedler, U.; Wilpert, A.; Piletska, E. V.; Thiele, T. A.; Ulbricht, M. *Macromolecules* **2000**, 33, (8), 3092-3098.
4. Piletsky, S. A.; Panasyuk, T. L.; Piletskaya, E. V.; Nicholls, I. A.; Ulbricht, M. *Journal of Membrane Science* **1999**, 157, (2), 263-278.
5. Shea, K. J.; Stoddard, G. J.; Shavelle, D. M.; Wakui, F.; Choate, R. M. *Macromolecules* **2002**, 23, (21), 4497-4507.
6. Spivak, D. A.; Shea, K. J. *Analytica Chimica Acta* **2001**, 435, (1), 65-74.
7. Spivak, D. A.; Shea, K. J. *Macromolecules* **1998**, 31, (7), 2160-2165.
8. Ulbricht, M. *Polymer* **2006**, 47, (7), 2217-2262.
9. Ye, L.; Weiss, R.; Mosbach, K. *Macromolecules* **2000**, 33, (22), 8239-8245.
10. Antonietti, M.; Caruso, R. A.; Hentze, H. P.; Goltner, C. In *Hydrophilic gels with new superstructures and their hybrids by nanocasting technologies*, 2000; 2000; pp 163-172.
11. Chakrapani, M.; Mitchell, S. J.; Van Winkle, D. H.; Rikvold, P. A. *Journal of Colloid and Interface Science* **2003**, 258, (1), 186-197.
12. Chakrapani, M.; Rill, R. L.; Van Winkle, D. H. *Macromolecules* **2003**, 36, (24), 9050-9059.
13. Chakrapani, M.; Van Winkle, D. H.; Patterson, B. C.; Rill, R. L. *Langmuir* **2002**, 18, (16), 6449-6452.

14. Glatter, O.; Kratky, O., *Small angle X-ray scattering*. Academic Press: 1982.
15. Higgins, J. S.; Benoit, H. C. **2002**.
16. Roe, R.-J., *Methods of X-Ray and Neutron Scattering in Polymer Science*. OXFORD UNIVERSITY PRESS: **2000**.
17. Webster, O. W.; Hertler, W. R.; Sogah, D. Y.; Farnham, W. B.; Rajanbabu, T. *V. J. Am. Chem. Soc.* **1983**, 105, (17), 5706-5708.
18. Hertler, W. R.; Sogah, D. Y.; Webster, O. W.; Trost, B. M. *Macromolecules* **1984**, 17, (7), 1415-1417.
19. Sogah, D. Y.; Hertler, W. R.; Webster, O. W.; Cohen, G. M. *Macromolecules* **1987**, 20, (7), 1473-1488.
20. Dicker, I. B.; Cohen, G. M.; Farnham, W. B.; Hertler, W. R.; Laganis, E. D.; Sogah, D. Y. *Macromolecules* **1990**, 23, (18), 4034-4041.
21. Matsen, M. W.; Bates, F. S. *Macromolecules* **1996**, 29, (4), 1091-1098.
22. Park, C.; Yoon, J.; Thomas, E. L. *Polymer* **2003**, 44, (22), 6725-6760.
23. Abetz, V.; Simon, P. F. W., Phase behaviour and morphologies of block copolymers. In *Block Copolymers I*, Springer-Verlag Berlin: Berlin, 2005; Vol. 189, pp 125-212.
24. Hillmyer, M. A., Nanoporous materials from block copolymer precursors. In *Block Copolymers II*, Springer-Verlag Berlin: Berlin, 2005; Vol. 190, pp 137-181.
25. Goddard, E. D. *Journal of the American Oil Chemists Society* **1994**, 71, (1), 1-16.
26. Magny, B.; Iliopoulos, I.; Zana, R.; Audebert, R. *Langmuir* **1994**, 10, (9), 3180-3187.

27. Goddard, E. D.; Leung, P. S.; Padmanabhan, K. P. A. *Journal of the Society of Cosmetic Chemists* **1991**, 42, (1), 19-34.
28. Leung, P. S.; Goddard, E. D. *Langmuir* **1991**, 7, (3), 608-609.
29. Goddard, E. D. *Colloids and Surfaces* **1986**, 19, (2-3), 255-300.
30. Goddard, E. D. *Colloids and Surfaces* **1986**, 19, (2-3), 301-329.
31. Goddard, E. D.; Ananthapadmanabhan, K. P., *Interactions of Surfactants with Polymers and Proteins*. CRC PRESS: **1993**.
32. Cabane, B. *Journal of Physical Chemistry* **1977**, 81, (17), 1639-1645.
33. Cabane, B.; Duplessix, R. *Journal De Physique* **1982**, 43, (10), 1529-1542.
34. Cabane, B.; Duplessix, R. *Journal De Physique* **1987**, 48, (4), 651-662.
35. Butun, V.; Armes, S. P.; Billingham, N. C. *Polymer* **2001**, 42, (14), 5993-6008.
36. Hoogeveen, N. G.; Stuart, M. A. C.; Fleer, G. J.; Frank, W.; Arnold, M. *Macromolecular Chemistry and Physics* **1996**, 197, (8), 2553-2564.
37. Butun, V.; Billingham, N. C.; Armes, S. P. *J. Am. Chem. Soc.* **1998**, 120, (46), 12135-12136.
38. Liu, S. Y.; Weaver, J. V. M.; Tang, Y. Q.; Billingham, N. C.; Armes, S. P.; Tribe, K. *Macromolecules* **2002**, 35, (16), 6121-6131.
39. Wesley, R. D.; Cosgrove, T.; Thompson, L.; Armes, S. P.; Baines, F. L. *Langmuir* **2002**, 18, (15), 5704-5707.
40. Chari, K.; Antalek, B.; Lin, M. Y.; Sinha, S. K. *Journal of Chemical Physics* **1994**, 100, (7), 5294-5300.

41. Glinka, C. J.; Barker, J. G.; Hammouda, B.; Krueger, S.; Moyer, J. J.; Orts, W. J. *Journal of Applied Crystallography* **1998**, 31, 430-445.
42. Baines, F. L.; Billingham, N. C.; Armes, S. P. *Macromolecules* **1996**, 29, (10), 3416-3420.
43. Couderc-Azouani, S.; Sidhu, J.; Georgiou, T. K.; Charalambous, D. C.; Vamvakaki, M.; Patrickios, C. S.; Bloor, D. M.; Penfold, J.; Holzwarth, J. F.; Wyn-Jones, E. *Langmuir* **2004**, 20, (15), 6458-6469.
44. BROWN, T. L.; H. EUGENE LeMAY, J., *CHEMISTRY*. Prentice-Hall, Inc.: **1991**.
45. RUBINSTEIN, M.; COLBY, R. H., *Polymer Physics*. OXFORD UNIVERSITY PRESS: **2004**.
46. Yun, S. I.; Briber, R. M.; Kee, R. A.; Gauthier, M. *Polymer* **2006**, 47, (8), 2750-2759.
47. Ermi, B. D.; Amis, E. J. *Macromolecules* **1996**, 29, (7), 2701-2703.
48. Ermi, B. D.; Amis, E. J. *Macromolecules* **1997**, 30, (22), 6937-6942.
49. Bergstrom, L. M.; Kjellin, U. R. M.; Claesson, P. M.; Grillo, I. *Journal of Physical Chemistry B* **2004**, 108, (6), 1874-1881.
50. Josson, B.; Lindaman, B.; Holmberg, K.; Kronberg, B., *SURFACTANTS AND POLYMERS IN AQUEOUS SOLUTION*. John Wiley & Sons Ltd: **1998**.
51. Nagarajan, R. *Chem. Phys. Lett.* **1980**, 76, (2), 282-286.
52. Nagarajan, R. *Colloids and Surfaces* **1985**, 13, (1), 1-17.
53. Nagarajan, R. *Journal of Chemical Physics* **1989**, 90, (3), 1980-1994.

54. Cabane, B.; Duplessix, R.; Zemb, T. *Journal De Physique* **1985**, 46, (12), 2161-2178.
55. Wesley, R. D.; Cosgrove, T.; Thompson, L. *Langmuir* **1999**, 15, (24), 8376-8382.
56. Jean, B.; Lee, L. T.; Cabane, B. *Colloid and Polymer Science* **2000**, 278, (8), 764-770.
57. Matsuoka, H.; Ise, N.; Okubo, T.; Kunugi, S.; Tomiyama, H.; Yoshikawa, Y. *The Journal of Chemical Physics* **1985**, 83, (1), 378-387.
58. Nisato, G.; Ivkov, R.; Amis, E. J., Structure of Charged Dendrimer Solutions As Seen by Small-Angle Neutron Scattering. In 1999; Vol. 32, pp 5895-5900.
59. Ramzi, A.; Scherrenberg, R.; Joosten, J.; Lemstra, P.; Mortensen, K. *Macromolecules* **2002**, 35, (3), 827-833.
60. Hansen, J. P.; Hayter, J. B. *Molecular Physics* **1982**, 46, (3), 651-656.
61. Hayter, J. B.; Penfold, J. *Journal of the Chemical Society-Faraday Transactions I* **1981**, 77, 1851-1863.
62. Hayter, J. B.; Penfold, J. *Molecular Physics* **1981**, 42, (1), 109-118.
63. Hiemenz, P. C.; Rajagopalan, R., *Principles of Colloid and Surface Chemistry*. MARCEL DEKKER, Inc.: **1997**.
64. Chari, K.; Kowalczyk, J.; Lal, J. *Journal of Physical Chemistry B* **2004**, 108, (9), 2857-2861.
65. Mya, K. Y.; Jamieson, A. M.; Sirivat, A. *Langmuir* **2000**, 16, (15), 6131-6135.
66. Aswal, V. K.; Goyal, P. S. *Physical Review E* **2000**, 61, (3), 2947-2953.

67. Kumar, S.; David, S. L.; Aswal, V. K.; Goyal, P. S.; KabirudDin. *Langmuir* **1997**, 13, (24), 6461-6464.
68. Hayter, J. B.; Penfold, J. *Colloid and Polymer Science* **1983**, 261, (12), 1022-1030.
69. Bastardo, L. A.; Garamus, V. M.; Bergstrom, M.; Claesson, P. M. *Journal of Physical Chemistry B* **2005**, 109, (1), 167-174.
70. Bastiat, G.; Grassl, B.; Borisov, O.; Lapp, A.; Francois, J. *Journal of Colloid and Interface Science* **2006**, 295, (2), 417-426.
71. Bastiat, G.; Grassl, B.; Khoukh, A.; Francois, J. *Langmuir* **2004**, 20, (14), 5759-5769.
72. Claesson, P. M.; Bergstrom, M.; Dedinaite, A.; Kjellin, M.; Legrand, J. F.; Grillo, I. *Journal of Physical Chemistry B* **2000**, 104, (49), 11689-11694.
73. Hassan, P. A.; Fritz, G.; Kaler, E. W. *Journal of Colloid and Interface Science* **2003**, 257, (1), 154-162.
74. Hassan, P. A.; Raghavan, S. R.; Kaler, E. W. *Langmuir* **2002**, 18, (7), 2543-2548.
75. Hayter, J. B.; Zemb, T. *Chem. Phys. Lett.* **1982**, 93, (1), 91-94.
76. An, S. W.; Su, T. J.; Thomas, R. K.; Baines, F. L.; Billingham, N. C.; Armes, S. P.; Penfold, J. *The Journal of Physical Chemistry B* **1998**, 102, (2), 387.
77. Haupt, K.; Mosbach, K. *Chem. Rev.* **2000**, 100, (7), 2495-2504.
78. Wulff, G. *Angew. Chem.-Int. Edit. Engl.* **1995**, 34, (17), 1812-1832.
79. Sellergren, B. *Angew. Chem.-Int. Edit.* **2000**, 39, (6), 1031-+.

80. Hammouda, B.; Ho, D. L. *Journal of Polymer Science Part B-Polymer Physics* **2007**, 45, (16), 2196-2200.
81. Hammouda, B.; Ho, D. L.; Kline, S. *Macromolecules* **2004**, 37, (18), 6932-6937.
82. Zheng Fang; Joseph P. Kennedy. *Journal of Polymer Science Part A: Polymer Chemistry* **2002**, 40, (21), 3679-3691.
83. Livsey, I. *Journal of the Chemical Society-Faraday Transactions II* **1987**, 83, 1445-1452.
84. Bates, F. S.; Fredrickson, G. H. *Annu. Rev. Phys. Chem.* **1990**, 41, 525-557.
85. M. Lazzari, M. A. L.-Q. *Advanced Materials* **2003**, 15, (19), 1583-1594.
86. Thurn-Albrecht, T.; Schotter, J.; Kastle, C. A.; Emley, N.; Shibauchi, T.; Krusin-Elbaum, L.; Guarini, K.; Black, C. T.; Tuominen, M. T.; Russell, T. P. *Science* **2000**, 290, (5499), 2126-2129.
87. Mansky, P.; Liu, Y.; Huang, E.; Russell, T. P.; Hawker, C. J. *Science* **1997**, 275, (5305), 1458-1460.
88. Morkved, T. L.; Lu, M.; Urbas, A. M.; Ehrichs, E. E.; Jaeger, H. M.; Mansky, P.; Russell, T. P. *Science* **1996**, 273, (5277), 931-933.
89. Kim, S. H.; Misner, M. J.; Xu, T.; Kimura, M.; Russell, T. P. *Advanced Materials* **2004**, 16, (3), 226-231.
90. Jeong, U.; Ryu, D. Y.; Kho, D. H.; Lee, D. H.; Kim, J. K.; Russell, T. P. *Macromolecules* **2003**, 36, (10), 3626-3634.
91. Kim, S. H.; Misner, M. J.; Russell, T. P. *Advanced Materials* **2004**, 16, (23-24), 2119-2123.

92. Colfen, H. *Macromol. Rapid Commun.* **2001**, 22, (4), 219-252.
93. Antonietti, M.; Heinz, S.; Schmidt, M.; Rosenauer, C. *Macromolecules* **1994**, 27, (12), 3276-3281.
94. Ali, N.; Park, S.-Y. *Langmuir* **2008**, 24, (17), 9279-9285.
95. Boltau, M.; Walheim, S.; Mlynek, J.; Krausch, G.; Steiner, U. *Nature* **1998**, 391, (6670), 877-879.
96. Cui, L.; Peng, J.; Ding, Y.; Li, X.; Han, Y. *Polymer* **2005**, 46, (14), 5334-5340.
97. Li, X.; Xing, R.; Zhang, Y.; Han, Y.; An, L. *Polymer* **2004**, 45, (5), 1637-1646.
98. Tanaka, K.; Takahara, A.; Kajiyama, T. *Macromolecules* **1996**, 29, (9), 3232-3239.
99. Walheim, S.; Boltau, M.; Mlynek, J.; Krausch, G.; Steiner, U. *Macromolecules* **1997**, 30, (17), 4995-5003.
100. Clarke, C. J.; Eisenberg, A.; La Scala, J.; Rafailovich, M. H.; Sokolov, J.; Li, Z.; Qu, S.; Nguyen, D.; Schwarz, S. A.; Strzhemechny, Y.; Sauer, B. B. *Macromolecules* **1997**, 30, (14), 4184-4188.
101. Zha, W.; Han, C. D.; Lee, D. H.; Han, S. H.; Kim, J. K.; Kang, J. H.; Park, C. *Macromolecules* **2007**, 40, (6), 2109-2119.
102. Srinivasarao, M.; Collings, D.; Philips, A.; Patel, S., Three-Dimensionally Ordered Array of Air Bubbles in a Polymer Film. In 2001; Vol. 292, pp 79-83.
103. Park, S.; Kim, B.; Wang, J. Y.; Russell, T. P. *Advanced Materials* **2008**, 20, (4), 681-685.

104. Park, S.; Wang, J.-Y.; Kim, B.; Russell, T. P. *Nano Letters* **2008**, 8, (6), 1667-1672.
105. Abramoff, M. D., Magelhaes, P.J., Ram, S.J. *Biophotonics International* **2004**, 11, (7), 36-42.